# Spectral Minutiae Representations for Fingerprint Recognition

**Haiyun Xu**

# SPECTRAL MINUTIAE REPRESENTATIONS FOR FINGERPRINT RECOGNITION

Haiyun Xu

De promotiecommissie:

*voorzitter en secretaris:*

    Prof.dr.ir. A.J. Mouthaan        Universiteit Twente

*promotor:*

    Prof.dr.ir. C.H. Slump            Universiteit Twente

*assistent promotor:*

    Dr.ir. R.N.J. Veldhuis           Universiteit Twente

*referenten:*

    Dr.ir. A.M. Bazen              Dermalog Identification Systems GmbH

    Dr.ir. T.A.M. Kevenaar         priv-ID B.V.

*leden:*

    Prof.dr. A.A. Stoorvogel       Universiteit Twente

    Prof.dr. S. Etalle             Universiteit Twente

    Prof.dr. C. Busch              Hochschule Darmstadt

    Prof.dr.ir. J. Ortega-Garcia    Universidad Autonoma de Madrid

SPECTRAL MINUTIAE REPRESENTATIONS FOR FINGERPRINT
RECOGNITION


PROEFSCHRIFT


ter verkrijging van
de graad van doctor aan de Universiteit Twente,
op gezag van de rector magnificus,
prof. dr. H. Brinksma,
volgens besluit van het College voor Promoties
in het openbaar te verdedigen
op donderdag 30 september 2010 om 16.45 uur


door


Haiyun Xu
geboren op 12 februari 1977
te Shanghai, China

Dit proefschrift is goedgekeurd door:

De promotor:            Prof.dr.ir. C.H. Slump

De assistent promotor:  Dr.ir. R.N.J. Veldhuis

*This thesis is dedicated to my family:*
*Marco, Leon and Rick*

# Contents

# List of Abbreviations

**AFIS**       Automated Fingerprint Identification System

**CPCA**       Column Principal Component Analysis

**DET**        Detection Error Trade-off curve

**DFT**        Discrete Fourier Transform

**ECC**        Error Correcting Code

**EER**        Equal Error Rate

**EM-LCS**     Enrollment Mask only with Largest Components Selection

**EM-RCS**     Enrollment Mask only with Reliable Components Selection

**FAR**        False Acceptance Rate

**FFT**        Fast Fourier Transform

**FHD**        Fractional Hamming Distance

**FMR**        False Match Rate

**FNMR**       False Non-Match Rate

**FRR**        False Rejection Rate

**FTCR**       Failure to Capture Rate

**GAR**        Genuine Acceptance Rate

**HD**         Hamming Distance

**LCS**        Largest Components Selection

**LDFT**       Line Discrete Fourier Transform

**PCA**        Principal Component Analysis

**PIN**        Personal Identification Number

**RCS**        Reliable Components Selection

**ROC**        Receiver Operating Characteristic curve

**ROI**        Region of Interest

**SM**         Spectral Minutiae Representation

**SMC**        Complex Spectral Minutiae Representation

**SML**        Location-based Spectral Minutiae Representation

**SMO**        Orientation-based Spectral Minutiae Representation

**SP**         Singular Point

**STD**        Standard Deviation

**SVD**        Singular Value Decomposition

**VM-LCS**     Verification Mask only with Largest Components Selection

**WSC**        Weighted Sum Correlation

# Chapter 1

# Introduction

The term biometrics refers to the technologies that measure and analyze human intrinsic physical (such as fingerprints, face, iris) or behavioral (such as signature, voice, gait) characteristics for authenticating individuals.

Nowadays, biometric technology is increasingly deployed in civil and commercial applications. The growing use of biometrics is raising security and privacy concerns about the biometric technology. Storing biometric data, known as biometric templates, in a database leads to several privacy risks such as identity fraud and cross matching. A solution is to apply *biometric template protection* techniques, which aim to make it impossible to recover the biometric data from the templates.

The goal of our research is to combine biometric systems with template protection. Aimed at fingerprint recognition, this thesis introduces the *Spectral Minutiae Representation* method, which enables the combination of a minutiae-based fingerprint recognition system with template protection schemes based on fuzzy commitment or helper data schemes.

## 1.1 Biometrics and Fingerprints

Recognition of individuals by means of biometric characteristics is gaining importance because of several reasons: first, unlike passwords, PIN codes or tokens, biometric identifiers cannot be forgotten or lost, and they add to user convenience since they are always at hand; second, a biometric identifier is tightly linked to an individual, therefore, it cannot easily be forged or shared.

When constructing a biometric system, there are several issues that need to be considered when selecting a biometric characteristic, including universality, distinctiveness, permanence, performance, acceptability and so on [1]. Currently, fingerprint is the

most commonly used biometric modality. Compared with various biometric charac-
teristics, such as face, signature and voice, the fingerprint has high levels of distinc-
tiveness, permanence and performance and at the same time it has the advantages of
both ease of use and low cost. The biometric revenues estimated by International Bio-
metric Group in 2009 [2] shows that fingerprint continues to be the leading biometric
technology in terms of market share. Concerning the user acceptance of biometrics,
the report by Unisys Security Index in December 2008 reveals that biometric technolo-
gies are becoming increasingly familiar and accepted, and among various biometric
modalities, fingerprint is the most acceptable biometric technology [3].

### 1.1.1 Fingerprint features

Maltoni et al. [1] put fingerprint features into three categories: *Global level*, *Local level*
and *Very-fine level*. The features at the global level are based on the fingerprint ridge
flow pattern, such as directional field, singular points and frequency image. These fea-
tures are not discriminative enough for very accurate recognition, but they are more
robust to quality degradation, and they are also very useful for fingerprint classifica-
tion and indexing [4,5]. They can also be used as auxiliary data to assist fingerprint
recognition. The features at the local level are the local ridge characteristics. *Minu-
tiae* are the most prominent ridge characteristics. They are very discriminative and
suitable for accurate recognition. The features at the very-fine level are intra-ridge
details, such as sweat pores. Extracting such features is only feasible for good quality,
high-resolution fingerprints, which are not available in most practical applications.
We summarize the characteristics of each category in Table 1.1.

Table 1.1: Fingerprint features and their characteristics.

| Types | Scale | Examples | Characteristics |
|---|---|---|---|
| Level 1 | Global level | singular points directional field | +Robust to low-quality fingerprints −Moderately discriminative |
| Level 2 | Local level | minutiae | +High discriminative +Mature techniques −Unreliable automatic minutiae extraction for low-quality fingerprints |
| Level 3 | Very-fine level | sweat pores | +Enhance individuality −Require high resolution sensor |

The research in this thesis is mainly based on the fingerprint minutiae features. Minu-
tiae are the endpoints and bifurcations of fingerprint ridges, see Figure 1.1. Each
minutia can be described by several attributes, such as type (e.g., ridge ending or
ridge bifurcation), its location in the fingerprint image and orientation. The most
commonly used parameters for minutiae comparison algorithms are $(x, y, \theta)$, where
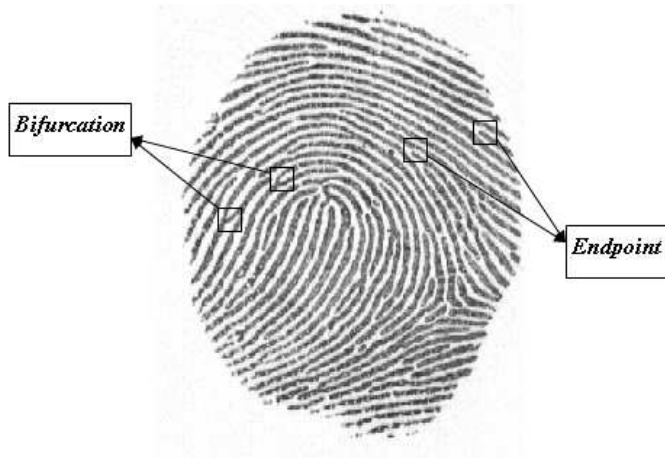
Fig. 1.1: *Minutiae of a fingerprint.*

$(x, y)$ is the location of the minutia and $\theta$ its orientation [1]. They are known to remain unchanged over an individual's lifetime and allow a very discriminative classification of fingerprints. There are a large number of academic research activities and commercial applications on fingerprint minutiae extraction and comparison (matching) [6–17].

## 1.1.2 Applications characteristics of biometric systems

When designing a biometric recognition system, analyzing the application characteristics is very important. Wayman et al. [18] suggest that a biometric recognition application can be understood by following characteristics:

1. Cooperative vs. non-cooperative. This property can also be referred to as 'positive' and 'negative' recognition application. In a cooperative application, the individual needs to prove that he/she is someone known to the system, while in a non-cooperative application, the individual needs to prove that he/she is not someone known to the system. For example, a company's employee entrance control using biometrics is a cooperative application, whereas an airport application for detecting terrorists is a non-cooperative application.
2. Overt vs. covert. If the subject is aware that his/her biometric characteristic is being measured for authentication, such application is overt. Otherwise, it is an covert application.
3. Habituated vs. non-habituated. This property indicates how often the individuals in the application will interact with the biometric system. 'Habituated' individuals imply that the individuals are familiar with the system, and this will give a positive effect on the recognition performance.

4. Attended vs. non-attended. This property indicates whether the process of biometric data acquisition will be observed and guided by system management (for example, a system administrator).
5. Standard vs. non-standard environment. This property indicates whether the application is operated in a controlled environment (such as temperature, pressure, moisture, lighting conditions). Generally, an indoor application is in a standard environment, whereas an outdoor application is considered as a non-standard environment application.
6. Public vs. private. This property indicates whether the individuals of the system are customers (public) or employees (private) of the system management.
7. Open vs. closed. This property indicates whether the biometric data are used by a single (closed) or multiple (open) applications. In an open application, the interoperability is an important issue and data and processing standards are required.

### 1.1.3  Terms and definitions

In this section, we will list some relevant terms and definitions of biometrics. For comprehensive background knowledge and a broader biometric vocabulary, we recommend the readers references [1, 19, 20].

#### 1.1.3.1  Biometric Applications

Depending on the application context, a biometric system can operate in either *verification* or *identification* mode.

*Verification*: the verification process is to confirm (or verify) a biometric claim through biometric comparisons. A verification system implements a one-to-one comparison.

*Identification*: in the identification process, the system compares the feature extracted from the live-scanned biometric sample against all the templates in the database. An identification system implements a one-to-many comparison.

*Recognition*: biometric recognition is a general term for both biometric verification and biometric identification.

The structure diagram of a fingerprint verification system is shown in Figure 1.2, which includes several important parts:

*Biometric Database*: the database of biometric data record(s). Depending on the application, the biometric database can be a very large database (e.g., for the US-VISIT system [21]), a normal size database (e.g., for a building's access control system), or a single subject database (e.g., a cardholder's biometric template(s) stored on a smart card).

*Enrollment*: the process for registering individuals in a biometric system. During the enrollment process, the individual's biometric characteristics will be captured by a sensor, and the biometric template will be finally created and stored into the
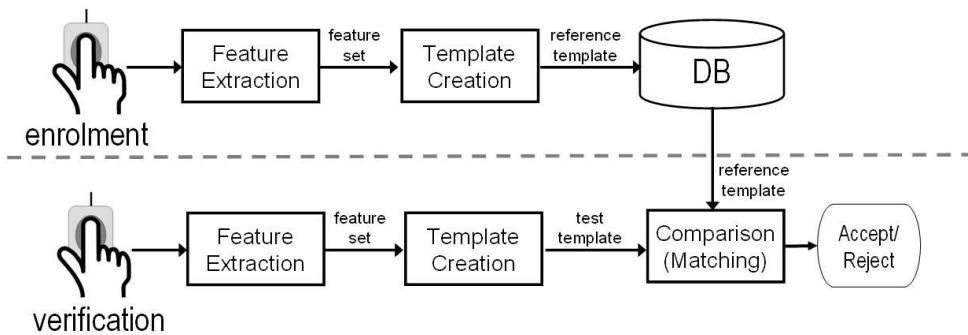
Fig. 1.2: *The structure diagram of a fingerprint verification system.*

database. The template created during enrollment is called *reference* template and it will be compared later with a *test* template during verification or identification process.

*Feature extraction*: in order to facilitate comparison, the biometric features (such as fingerprint minutiae) will be extracted from the raw digital sample (such as a fingerprint image). This process is called feature extraction.

*Comparison*: during verification or identification, the *test* template will be compared with the *reference* template. Normally, in this process, the system will first compute a number (called *similarity/dissimilarity score* or *matching score*), which corresponds to the degree of similarity/dissimilarity between the reference and test templates. Finally, by using a *system threshold*, the final decisions (accept/reject or match/non-match) will be made.

#### 1.1.3.2 Performance indicators

The recognition performance of a fingerprint verification system can be evaluated by means of several measures. During the comparison process, a fingerprint verification system can make two types of errors: *false match*, accepting the fingerprints from two individuals; *false non-match*, rejecting the fingerprints from the same individual. For a positive biometric verification system, these two types of errors are often denoted as *false acceptance* and *false rejection*. In this thesis, we will use the following performance indicators to evaluate the recognition performance of our system[1].

The *False Acceptance Rate* (FAR) is the probability that the system outputs a 'match' decision for fingerprints that are not from the same finger.

---

[1]According to *ISO/IEC 19795-1, Information technology - Biometric performance testing and reporting - Part 1: Principles and framework* [22], the terms false match and false non-match refer to the errors of the algorithm. The terms false acceptance and false rejection refer to the errors made by the entire system. In many publications, including this thesis, the terms false acceptance and false rejection are also used to evaluate the algorithm.

The *False Rejection Rate* (FRR) is the probability that the system outputs a 'non-match' decision for the fingerprints from the same finger.

The *Equal Error Rate* (EER): when the decision threshold of a biometric verification system is set such that the FAR and FRR are equal, the common value of FAR and FRR is referred to as the EER.

The *Genuine Acceptance Rate* (GAR), GAR= 1−FRR, is the probability that the system outputs a 'match' decision for fingerprints that are from the same finger.

The *GAR/FRR given at a certain FAR*: for different applications, the required FAR or FRR are different. For example, a home network application may require low FRR for user convenience. For high security applications, a low FAR is very important. In this thesis, we will use the GAR@FAR=0.1% as a performance measure.

The *Receiver Operating Characteristics* (ROC) curve: in signal detection theory, a ROC curve is a graphical plot of false positives against true positives. For biometrics, the ROC curve plots the FAR against the GAR. The ROC curve is threshold independent and it presents the performance of a biometric system under different threshold settings. The ROC curves also allow a flexible performance comparison of different systems.

The *Detection Error Trade-off* (DET) curve: the DET curve is a variant of the ROC curve. It plots the FAR against the FRR. It gives a visual characterization of the trade-off between the FAR and the FRR.

## 1.2   Biometric Template Protection

In the previous section, we introduced the advantages of using biometrics to enhance security. Nowadays, biometric technology is increasingly deployed in civil and commercial applications. For example, in October 2001, the Dutch airport Schiphol launched an automated border passage system using iris recognition for safer and faster border control. Now this system has become a permanent facility at Schiphol. In 2004, the U.S. immigration and border management system US-VISIT, involving the collection and analysis of biometric data, became operational [21]. Later in Europe, in order to detect counterfeit or manipulated documents and to confirm the identification of the individual, the Council of the European Union (EU) adopted the Biometric Passports Regulation. It states that the Schengen regime and Schengen-affiliated third countries like Norway are obliged to include two biometric identifers (face and fingerprints) into their citizen's passports by the end of June 2009 [23].

The growing use of biometrics in various cases, especially in civil applications, is raising privacy concerns about the biometric technology. There are several privacy threats to biometrics: (1) Impersonation: when an attacker steals a biometric template, he might construct artificial biometric identifiers that pass authentication. (2) Irrevocability: unlike passwords, biometric characteristics cannot be updated, reissued or destroyed. Thus, once lost, lost forever. (3) Privacy: since biometric data is sensitive

personal information, in many countries, protecting the stored personal information, including biometric data, is regulated by legislation. (4) Cross-matching: the biometric templates can be used by an attacker to perform cross-matching between databases and track people's behavior.

A solution to solve the above-mentioned problems is to apply template protection techniques. ISO is supporting this strategy with a new standard on privacy compliant biometric systems: in 2010, a completed final committee draft *ISO/IEC 24745 - Information technology - Security techniques - Biometric information protection* has been issued [24, 25]. In this draft standard, several requirements to protect an individual's privacy in a biometric context are described:

**Renewability.** Once a biometric template is compromised, it should be possible to generate a new template from the same biometric characteristic. Renewability, also referred to as *revocability* or *cancelable*[2], is an important property to deal with identity theft. It should be noted that the renewability property may also be needed for other reasons: for example, a biometric reference may only be valid for a limited period for higher security. In this case, the system should be able to renew, revoke or replace the reference.

**Unlinkability.** The biometric references used in different applications shall not be linkable. This is to prevent the attacker to trace a person's behavior by using the biometric reference as a unique identifier to link across different applications (i.e., cross-matching threats).

**Irreversibility.** To prevent the unauthorized use of biometric data for any purpose other than originally intended, it should be computationally infeasible to obtain the unprotected biometric template from the protected template. Generally the original biometric features need to be transformed to satisfy this requirement. Thus, it results in a biometric comparison of the protected templates in a transformed space.

Biometric template protection, defined as protecting the biometric data stored in a database, has received significant attention from the research community. To have an overview of the existing template protection schemes, the readers can refer to [26] and [27].

## 1.3 Purpose of the Research

In the previous sections, we discussed the importance of deploying biometric technology to enhance security and user convenience, and the necessity of biometric template protection due to privacy concerns. The research described in this thesis is done in the context of two projects: the *Protection of Biometric Template* (ProBiTe) project [3]

---

[2]There are trivial differences between the concepts of 'renewability' and 'revocability'. In this thesis, we will not give emphasis on their differences.

[3]The ProBiTe project is supported by the Dutch Technology Foundation STW (http://www.stw.nl) and the research program Sentinels (http://www.sentinels.nl).

and the *TrUsted Revocable Biometric IdeNtitiEs* (TURBINE) project [4]. Both projects
concern the integration of biometric recognition in security systems and target on the
privacy enhancing technology solution for biometric recognition systems.

The goal of our research is to solve the problems of combining biometric recognition
and template protection. Template protection techniques can be applied to all sorts of
biometric data. In both ProBiTe and TURBINE, the research on biometrics focuses on
the fingerprint recognition system, because fingerprint is the most accepted biometric
characteristic and it combines ease of use with a good recognition performance. From
the biometric aspect, the main research question is:

**How can we combine a fingerprint recognition system with template protection schemes?**

To answer this research question, we need to first consider three aspects:

**Aspect I: Selection of the target application.** First of all, we need to understand the application. What is the target application of the ProBiTe and TURBINE projects? The design of our algorithms should focus on the application requirements.

**Aspect II: Selection of a template protection scheme.** There are different template protection schemes on noisy data (including biometric templates) [26] and [27]. *Which template protection scheme should we choose?*

**Aspect III: Selection of fingerprint features.** In Section 1.1.1, we introduced different fingerprint features. We now have to decide on which features we should focus our research.

Next, we will discuss these three aspects.

## 1.3.1   Selection of the target application

The target application of the ProBiTe project is using biometrics in a home network
to enhance the ease of use. Besides the applications in a home network, the results
of this project can also be applied in financial domains, border control, ICT and consumer electronics. Compared with ProBiTe, TURBINE addresses a broader scope
of application domains, including eGovernment, eHealth, eID, eBanking, physical access control, and mobile telecommunications, but the main focus is border control.
The target of both projects is to cope with the privacy risks in biometric systems.
Based on the application characteristics introduced in 1.1.2, our application characteristics can be summarized as: cooperative, overt, habituated, attended enrollment
and non-attended recognition, standard environment, both public and private, closed.

Based on our application characteristics, in our research, we can assume that the
target biometric data subjects are cooperative to the system, and they are familiar
with how to interact with the system. Since the target application is operated in a

---

[4]The TURBINE research project (http://www.turbine-project.eu) is financed by the European
Community's 7th Framework Programme.

standard environment, coping with very poor quality fingerprints due to extremely wet/dry fingers will not be our main concern.

### 1.3.2 Selection of a template protection scheme

We will first present a brief review of several existing fingerprint template protection schemes. Ratha et al. [28] proposed the *Cancelable Fingerprint Template* by applying non-invertible transforms on fingerprint features. The challenges of their work are both designing 'non-invertibility' transforms and preventing losing recognition performance in the transformed space as well. Boult et al. [29] introduced the *Revocable Fingerprint Biotokens* that separates fingerprint data into two parts: the encrypted part to enhance the privacy, and the unencrypted part to assist the fingerprint recognition. The initial attempt of this algorithm received promising results. However, this method need to be changed or adjusted when applied to other biometric features, and some template protection requirements (such as 'unlinkability') still need to be analyzed. Another popular method is the *Fuzzy Vault* scheme, proposed by Juels and Sudan [30]. It has been implemented for fingerprints [31, 32]. However, these implementations require an absolute pre-alignment of fingerprints, which is error-prone. And both the recognition performance and the comparison speed from these attempts are also not satisfying.

In this thesis, our algorithms target on combining fingerprint recognition systems with template protection schemes based on *Fuzzy Commitment* and the *Helper Data* scheme, such as [5] and [33]. These two schemes are equivalent. The helper data scheme can be regarded as fuzzy commitment together with a quantization scheme using helper data. Figure 1.3 shows the architecture of a helper data scheme. The reader is referred to [33] for an explanation of this figure.

In both ProBiTe and TURBINE, the helper data scheme was chosen as the template protection solution. The helper data scheme is one of the simplest constructions for cryptography over noisy data, thus, it is not restricted to certain biometric characteristics or feature formats. Furthermore, this approach is tolerant to within-class variance in biometric data and this tolerance is determined by the error correcting capability of the underlying error correcting code.

The template protection based on the helper data scheme puts several constraints to the fingerprint recognition system. (1) It requires a fixed-length feature vector, which is ordered, as input. This means that the symbols $\vec{X}_i$ and $\vec{X}_i{}'$ in Figure 1.3 must represent fixed-length feature vectors. (2) When combining biometric systems with template protection schemes, the biometric features will be compared in a protected domain. Therefore, applying template protection schemes also requires an alignment-free feature representation. (3) From Figure 1.3, we can also see that in the helper data scheme, the real-valued features need to be quantized to a binary string. Therefore, a fixed-length binary string that is alignment-free is required as an input of the helper data scheme.
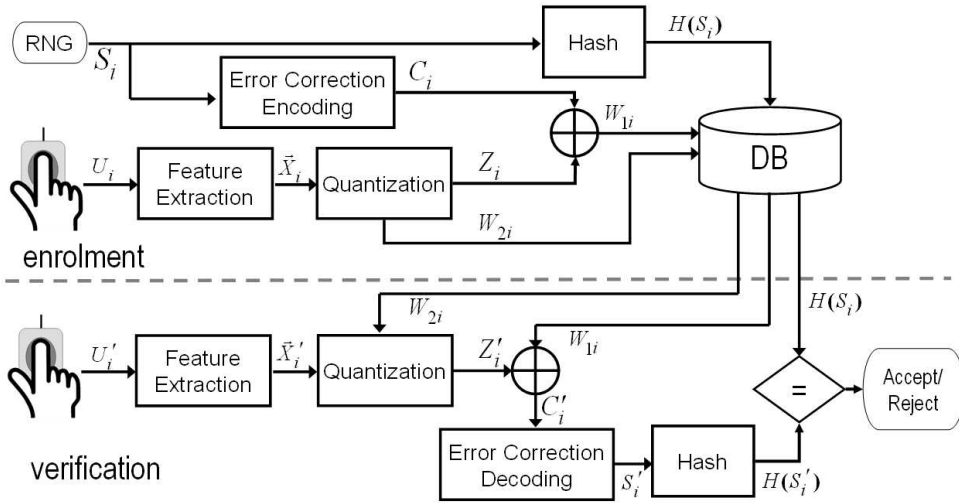
Fig. 1.3: *The structure diagram of the helper data scheme.*

### 1.3.3   Selection of fingerprint features

In order to select fingerprint features, we first list the desired properties for fingerprint recognition systems and template protection schemes (based on the helper data scheme) in Table 1.2 (columns "Shape"and "Minutiae"). We compare the two main fingerprint recognition techniques: the *shape-based* method, which uses image-based features such as directional field and Gabor filter responses [4,5], and the minutiae-based method [9–11]. Their features are illustrated in Figure 1.4 respectively.

First, template protection based on the helper data scheme requires a fixed-length feature vector as input. The shape method satisfies this requirement, while minutiae features are with variable length and unordered. Next, when applying template protection, the two fingerprints or two minutiae sets are compared in a protected domain. Thus, a relative alignment between two fingerprints or minutiae sets are not possible. Therefore, we need a translation and rotation invariant feature. For both shape and minutiae features, the translation and rotation invariance can only be obtained via pre-alignment or minutiae pair descriptor, which is not directly available. Furthermore, in the helper data scheme, the real-valued feature vector need to be quantized to a binary string. For both shape and minutiae features, a direct binary representation is not available.

For all the biometric systems, recognition performance is a very important factor. A high comparison speed is another important factor, and it is especially crucial for a biometric identification system with a very large database. Minutiae-based methods have a very good recognition performance (especially for good quality fingerprints), however, its comparison speed is relatively slow. When designing a biometric system,

(a)                                                             (b)
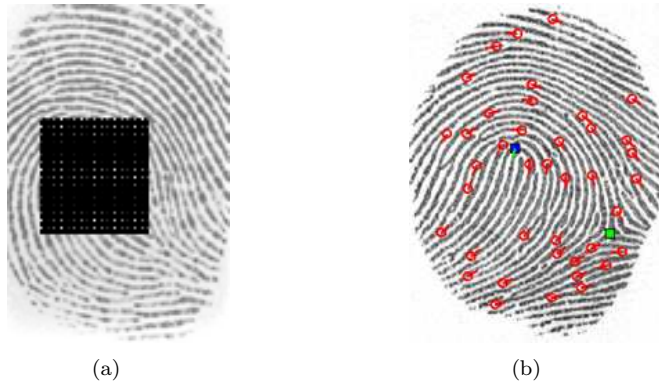
Fig. 1.4: Illustration of the fingerprint features.  (a) Shape-based features; (b) Minutiae (marked as red points).

Table 1.2: Desired Properties for Biometric Template Protection.

| Methods<br>Properties | Shape | Minutiae | Our target method |
|---|---|---|---|
| Fixed-length feature vector | 🙂 | ☹️ | 🙂 |
| Translation rotation invariance | 😐 | 😐 | 🙂 |
| Binarization | ☹️ | ☹️ | 🙂 |
| Recognition performance | 😐 | 🙂🙂 | 🙂 |
| Comparison speed | 🙂 | ☹️ | 🙂 |
| Market penetration | 😐 | 🙂🙂 | 🙂 |

another important factor to take into account is the market penetration. Minutiae-based techniques are most commonly used in fingerprint recognition systems and they have high market penetration.

Based on our application characteristics, we choose minutiae features for our investigations for several reasons. (1) Minutiae are very discriminative features, and the automatic minutiae extraction technique is relatively mature. (2) We target our application in a high security scenario and we expect reasonable good quality fingerprints in our applications. In this case, minutiae features can result in high recognition performance. (3) Minutiae-based techniques are most commonly used. A large amount of existing fingerprint recognition systems are based on the minutiae techniques. In the algorithms that we will introduce in this thesis, we also use some features at the global level (e.g., singular points) to enhance the recognition performance.

### 1.3.4   Refined research question

After discussing Aspects I-III, we now further refine our research question to:

**How can we combine a minutiae-based fingerprint recognition system with template protection based on the helper data scheme?**

In Table 1.2 (column "Our target method"), we have listed the goals of our target method: we want to keep the high recognition performance and the market advantage of the minutiae-based algorithms; in addition, we will transform a minutiae set into a fixed-length feature vector (eventually, a fixed-length binary string), which is translation and rotation invariant (thus, alignment-free). By achieving an alignment-free fixed-length binary string from a minutiae set, we can also greatly improve the comparison speed of minutiae-based methods.

Given the research question of this thesis, we specify five targets for achieving the desired properties of our target fingerprint recognition system:

- Target I: Fixed-length feature vector;
- Target II: Translation and rotation invariance;
- Target III: Binarization;
- Target IV: High recognition performance;
- Target V: High comparison speed.

It should be noted that for achieving Targets I, II and III, which are required by template protection based on the helper data schemes, we are willing to sacrifice a little bit recognition performance when we design our algorithms.

## 1.4   Overview of the Thesis

This thesis is based on published papers. The main chapters are Chapters 2-7. Chapters 2-6 present the main contributions of this thesis and each of them consists of

one or more papers in their original published format[5]. Chapter 7 is not based on published papers, but it evaluates the techniques that have been presented in Chapters 2-6 on the same fingerprint database, aiming to give a clear presentation of the progress of the spectral minutiae representation scheme.

### 1.4.1   Chapters overview

The thesis is organized as follows:

In Chapter 2, the basic idea of the spectral minutiae representation is introduced. The spectral minutiae representation is a novel method to represent a minutiae set as a fixed-length feature vector, which is invariant to translation, and in which rotation and scaling become translations that they can be easily compensated for. In this chapter, we will introduce two spectral minutiae representations: the *location-based spectral minutiae representation* (SML) and the *orientation-based spectral minutiae representation* (SMO). SML encodes fingerprint minutiae location information, while SMO encodes both minutiae location and orientation information.

Based on the spectral minutiae representations SML and SMO introduced in Chapter 2, we will propose several enhancements in Chapter 3. First, the spectral minutiae matching algorithms are improved by applying the *weighted sum correlation matching* and *fast rotation shift searching*. Second, we explore the method to enhance the recognition performance by incorporating two types of *minutiae quality information* in the spectral minutiae representations. Third, we use fingerprint minutiae subsets to cope with the limited overlap problem between the reference and test fingerprints.

In Chapter 4, we will explore feature reduction methods to reduce the spectral minutiae feature set. First, we introduce the *Column Principle Component Analysis* (CPCA) feature reduction algorithm, which reduces the spectral minutiae feature in the vertical direction. Next, the *Line Discrete Fourier Transform* (LDFT) feature reduction algorithm is proposed to reduce the feature in the horizontal direction. The CPCA and LDFT feature reduction algorithms can be applied independently or in conjunction. Both methods are applied to the SML and SMO features.

In Chapter 5, we will present a new version of the spectral minutiae representations called the *Complex Spectral Minutiae Representation*, denoted as SMC. Compared with SMO, SMC improves the recognition performance significantly by incorporating the minutiae orientation in a different way. In this chapter, the CPCA and LDFT feature reduction algorithms that introduced in Chapter 4 are also applied to SMC.

In Chapter 6, we will propose two methods to quantize the real-valued spectral minutiae features into binary strings: the *Spectral Bits* and the *Phase Bits*. In this chapter, we also investigate the multi-sample fusion algorithms to improve the recognition performance. Furthermore, we will propose different schemes to mask out unreliable bits.

---

[5]Only trivial corrections have been applied for the consistency of the whole thesis, which do not influence the contents of the paper.
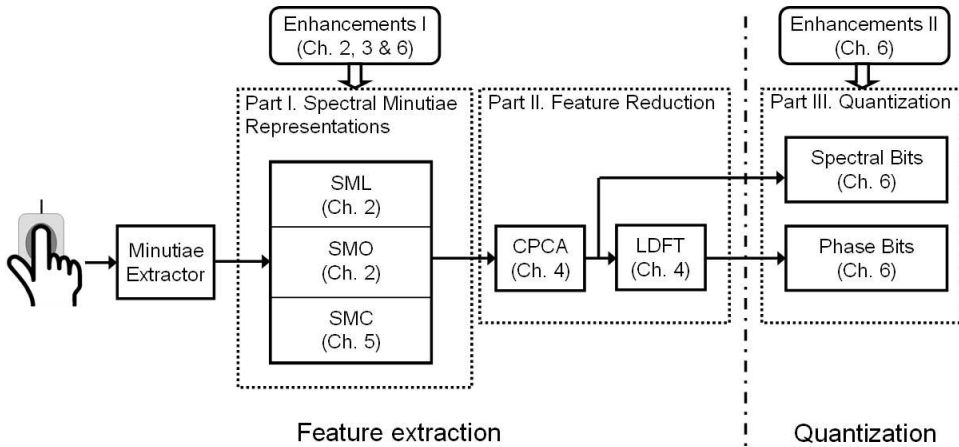
Fig. 1.5: *Block diagram of our designed system, focussing on the main contributions of this thesis.*

Since SMC outperformed SML and SMO, the binary representations will be investigated for the SMC features.

In Chapter 7, we will give an evaluation of the techniques that have been presented in Chapters 2-6, in order to have a clear comparison of each technique and to make the progress of the spectral minutiae representation scheme explicit.

Finally, we will give conclusions and recommendations in Chapter 8.

### 1.4.2   Main contributions

In Figure 1.3, we show the diagram of our target biometric template protection system, the helper data scheme. From the biometric aspect, the blocks "Feature Extraction"and "Quantization"are our research topics. Based on the system operating processes, we divide our research into three parts: I. Spectral Minutiae Representations; II. Feature Reduction; III. Quantization. In Figure 1.5, we present the block diagram of the contributions of this thesis in the context of a system diagram. In addition, we list the main contributions of this thesis in association with the system diagram and thesis chapters in Table 1.3.

### 1.4.3   Viewpoints of the thesis

In Section 1.3, we brought forward the research question of this thesis, and specified five targets for our research on fingerprint recognition systems. In Table 1.4, we associate each main chapter of this thesis with its achieved target(s). In this table, we also list the related system blocks from each chapter.

Table 1.3: Main Contributions of this thesis.

| System Diagram | Thesis | Main Contributions |
|---|---|---|
| Part I. Spectral Minutiae Representations | Chapter 2 | Location-based Spectral Minutiae Representation (SML) |
| | | Orientation-based Spectral Minutiae Representation (SMO) |
| | Chapter 5 | Complex Spectral Minutiae Representation (SMC) |
| Part II. Feature Reduction | Chapter 4 | Column Principle Component Analysis (CPCA) |
| | | Line Discrete Fourier Transform (LDFT) |
| Part III. Quantization | Chapter 6 | Spectral Bits |
| | | Phase Bits |

Table 1.4: Associated system blocks and targets of main chapters.

| Thesis | System Block(s) | Target(s) |
|---|---|---|
| Chapter 2 | SML | Target I: Fixed-length feature vector |
| | SMO | Target II: Translation and rotation invariance |
| | Enhancements I | Target IV: High recognition performance |
| Chapter 3 | Enhancements I | Target IV: High recognition performance |
| Chapter 4 | Feature Reduction | Target V: High comparison speed |
| Chapter 5 | SMC | Target I: Fixed-length feature vector |
| | | Target II: Translation and rotation invariance |
| | | Target IV: High recognition performance |
| Chapter 6 | Quantization | Target III: Binarization; |
| | | Target V: High comparison speed |
| | Enhancements I Enhancements II | Target IV: High recognition performance |
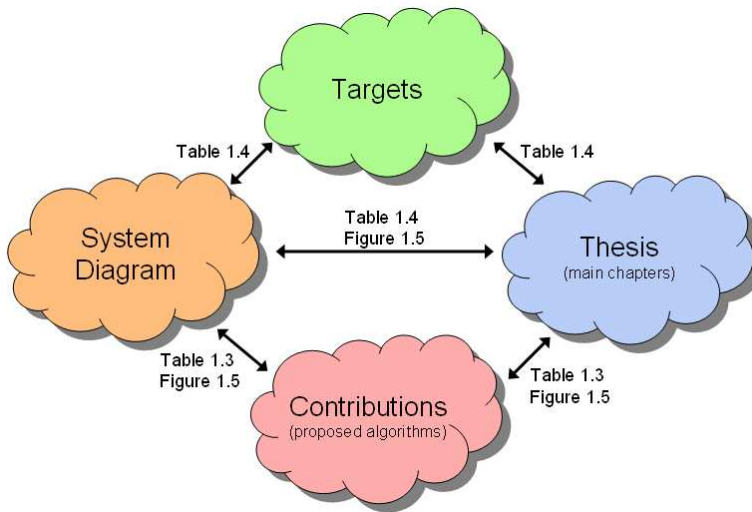
Fig. 1.6: *Four viewpoints of this thesis and their relations.*

Up to now, we have already looked at this thesis from four different viewpoints: targets, system diagram, thesis structure and contributions:

- Targets: given the research question, we specified five targets to achieve the desired properties of our fingerprint recognition system;
- System Diagram: our designed fingerprint recognition system, focussing on the feature extraction and quantization parts;
- Thesis structure: the main chapters of this thesis;
- Contributions: our proposed algorithms to achieve our research goal.

We have already presented the relations of these four viewpoints via Figure 1.5 and Tables 1.3, 1.4. The overview of these aspects and their relations are illustrated in Figure 1.6. These four viewpoints can help the readers understand the thesis and our research targets.

# Chapter 2

# Spectral Minutiae Representations of Fingerprints

## 2.1 Chapter Introduction

PURPOSE. This chapter introduces the basic concept of the *Spectral Minutiae Representations*. The spectral minutiae representation is a novel method to represent a fingerprint minutiae set as a fixed-length feature vector, which is invariant to translation, and in which rotation and scaling become translations that can be easily compensated for. These characteristics enable the combination of fingerprint recognition systems with template protection schemes that require a fixed-length feature vector and allow for faster matching as well.

CONTENTS. First, we introduce two spectral minutiae representations: the *location-based spectral minutiae representation* (SML) and the *orientation-based spectral minutiae representation* (SMO). SML encodes minutiae location information, while SMO encodes both minutiae location and orientation information. Second, based on the spectral minutiae features, two correlation-based matching algorithms for spectral minutiae are presented: the *direct matching* and the *Fourier-Mellin matching*. Third, we evaluate the algorithms on three fingerprint databases: FVC2000-DB2, FVC2002-DB2 and MCYT. In addition, we proposed two methods to enhance the recognition performance: score-level fusion on SML and SMO, denoted as *SM Fusion*, and incorporating the singular points, denoted as *Enhancement by SP*. Finally, we analyse the spectral minutiae algorithms in three cases: (a) limited overlap between two fingerprints; (b) missing and spurious minutiae; (c) minutiae errors on location and orientation. This chapter presents the basic concept of the spectral minutiae representations and is constructed as the foundation of the following chapters in this thesis. In the context of the system diagram, the content of this chapter is highlighted in
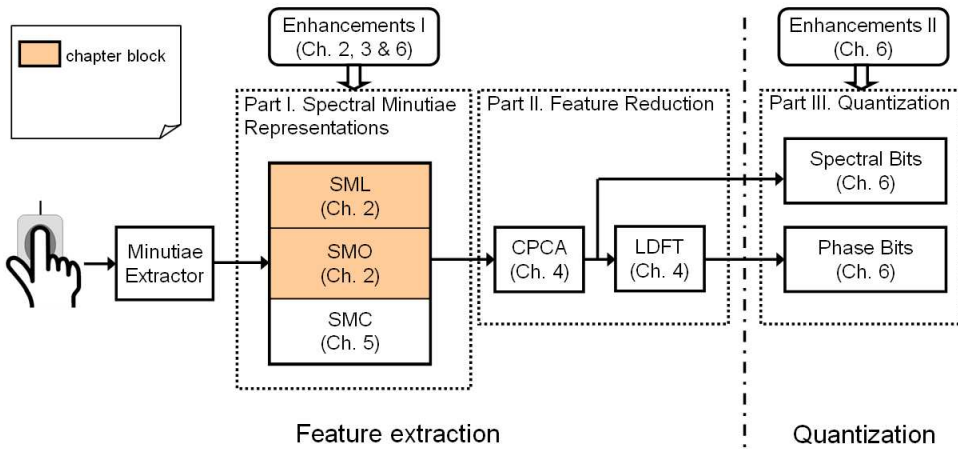
Fig. 2.1: *Block diagram of our designed system, highlighting the content of Chapter 2.*

Figure 2.1. Later, a new version called the *Complex Spectral Minutiae Representation*, denoted as SMC, was developed and will be presented in Chapter 5.

PUBLICATION(S). The content of Section 2.2 of this chapter has been published in [34].

## 2.2    Fingerprint Verification Using Spectral Minutiae Representations

**Abstract**

Most fingerprint recognition systems are based on the use of a minutiae set, which is an unordered collection of minutiae locations and orientations suffering from various deformations such as translation, rotation and scaling. The spectral minutiae representation introduced in this paper is a novel method to represent a minutiae set as a fixed-length feature vector, which is invariant to translation, and in which rotation and scaling become translations, so that they can be easily compensated for. These characteristics enable the combination of fingerprint recognition systems with template protection schemes that require a fixed-length feature vector. This chapter introduces the concept of and algorithms for two representation methods: the location-based spectral minutiae representation (SML) and the orientation-based spectral minutiae representation (SMO). Both algorithms are evaluated using two correlation-based spectral minutiae matching algorithms. We present the performance of our algorithms on three fingerprint databases. We also show how the performance can be improved by using a fusion scheme and singular points.

## 2.2.1   Introduction

Among various biometric characteristics, such as face, signature and voice, fingerprint has one of the highest levels of distinctiveness and performance [35] and it is the most commonly used biometric modality. Compared with most other biometric techniques, fingerprint recognition systems also have the advantages of both ease of use and low cost. All these reasons explain the popularity of fingerprint recognition systems.

Minutiae are the endpoints and bifurcations of fingerprint ridges. They are known to remain unchanged over an individual's lifetime [35] and allow a very discriminative classification of fingerprints. Each minutia can be described by parameters $(x, y, \theta)$, where $(x, y)$ is the location of the minutia and $\theta$ its orientation [36].

Nowadays, many fingerprint recognition systems are based on minutiae matching [7], [9]. However, minutiae-based fingerprint matching algorithms have some drawbacks that limit their application. First, due to the fact that minutiae sets are unordered, the correspondence between individual minutia in two minutiae sets is unknown before matching and this makes it difficult to find the geometric transformation (consisting of translation, rotation, scaling, and optionally non-linear deformations [9]) that optimally registers (or aligns) two sets. For fingerprint identification systems with very large databases [21], in which a fast comparison algorithm is necessary, minutiae-based matching algorithms will fail to meet the high performance speed requirements. Secondly, a minutiae representation of a fingerprint cannot be applied directly in recently developed template protection schemes based on fuzzy commitment and helper data schemes, such as [5] and [33], that require as an input a fixed-length feature vector representation of a biometric modality[1].

The spectral minutiae representation as proposed in this paper overcomes the above drawbacks of the minutiae sets, thus broadening the application of minutiae-based algorithms. Our method is inspired by the Fourier-Mellin transform, which allows a representation of images in a way that is invariant to translation, rotation and scaling [37–39]. By representing minutiae as a magnitude spectrum, we transform a minutiae set into a fixed-length feature vector that at the same time does not need registration to compensate for translation, rotation and scaling. Our algorithm does not distinguish between endpoints and bifurcations, because the type of a minutia can be easily confused due to acquisition noises or pressure differences during acquisition. However, the orientation remains the same when this occurs. By using a spectral minutiae representation instead of minutiae sets, we meet the requirements of a template protection system and allow for faster matching as well.

The spectral minutiae representation method can be easily integrated into a minutiae-based fingerprint recognition system. Minutiae sets can be directly transformed to this new representation, which makes this method compatible with the large amount of existing minutiae databases.

---

[1]Other template protection systems exist [32] that do not pose this fixed-length feature vector requirement.

This paper is organized as follows. First, the concept of spectral minutiae representation is explained in detail in Section 2.2.2. Next, in Section 2.2.3, two spectral minutiae matching algorithms are proposed. Then, Section 2.2.4 and Section 2.2.5 present the experimental results and discussions. Finally, we draw conclusions in Section 2.2.6.

## 2.2.2    Spectral Minutiae Representation

The spectral minutiae representation is based on the shift, scale and rotation properties of the two-dimensional continuous Fourier transform. If we have an input signal $f(\vec{x})$, $\vec{x} = (x, y)^{\mathrm{T}}$ (we denote the transpose of a vector $\vec{v}$ as $\vec{v}^{\mathrm{T}}$), its continuous Fourier transform is

$$\mathscr{F}\{f(\vec{x})\} = F(\vec{\omega}) = \int_{\vec{x} \in \mathbb{R}} f(\vec{x}) \exp(-\mathrm{j}\vec{\omega}^{\mathrm{T}}\vec{x}) \mathrm{d}\vec{x}, \tag{2.1}$$

with $\vec{\omega} = (\omega_{\mathrm{x}}, \omega_{\mathrm{y}})^{\mathrm{T}}$. The Fourier transform of a translated $f(\vec{x})$ is

$$\mathscr{F}\{f(\vec{x} - \vec{x}_0)\} = \exp(-\mathrm{j}\vec{\omega}^{\mathrm{T}}\vec{x}_0) F(\vec{\omega}), \tag{2.2}$$

with $\vec{x}_0 = (x_0, y_0)^{\mathrm{T}}$ the translation vector. The Fourier transform of an isotropically scaled $f(\vec{x})$ is

$$\mathscr{F}\{f(a\vec{x})\} = a^{-2} F(a^{-1}\vec{\omega}), \tag{2.3}$$

with $a$ $(a > 0)$ the isotropic scaling factor. The Fourier transform of a rotated $f(\vec{x})$ is

$$\mathscr{F}\{f(\Phi\vec{x})\} = F(\Phi\vec{\omega}), \tag{2.4}$$

with

$$\Phi = \begin{pmatrix} \cos\phi & -\sin\phi \\ \sin\phi & \cos\phi \end{pmatrix}. \tag{2.5}$$

Here $\Phi$ is the (orthonormal) rotation matrix, and $\phi$ is the (anticlockwise) rotation angle of $f(\vec{x})$.

It can be seen from (2.2) that if only the magnitude of the Fourier spectrum is retained, this results in a translation invariant representation of the input signal. Furthermore, from (2.3) and (2.4) it follows that scaling and rotation of the input signal results in a scaled and rotated Fourier spectrum.

In order to exploit the above properties of the two-dimensional Fourier transform, we re-map the Fourier spectral magnitude onto a polar-logarithmic coordinate system, such that the rotation and scaling become translations along the angular and radial axes, respectively. The detailed steps are as follows. Consider a signal $t(\vec{x})$ that is a translated, scaled and rotated replica of $r(\vec{x})$,

$$t(\vec{x}) = r(a\Phi\vec{x} - \vec{x}_0), \tag{2.6}$$

then the magnitude of the Fourier transforms of $t(\vec{x})$ and $r(\vec{x})$ are related by,

$$|T(\vec{\omega})| = a^{-2}|R(a^{-1}\Phi\vec{\omega})|, \tag{2.7}$$

which is a translation invariant representation of the input signal. If we re-map the Fourier spectral magnitude onto a polar-logarithmic coordinate system as,

$$\lambda = \log\sqrt{\omega_{\mathrm{x}}^2 + \omega_{\mathrm{y}}^2}, \qquad \beta = \mathrm{angle}(\omega_{\mathrm{x}}, \omega_{\mathrm{y}}), \tag{2.8}$$

$$R_{\mathrm{pl}}(\lambda, \beta) = |R(\mathrm{e}^\lambda \cos\beta, \mathrm{e}^\lambda \sin\beta)|, \tag{2.9}$$

$$T_{\mathrm{pl}}(\lambda, \beta) = |T(\mathrm{e}^\lambda \cos\beta, \mathrm{e}^\lambda \sin\beta)|, \tag{2.10}$$

then we have the Fourier spectral magnitude of $t(\vec{x})$ and $r(\vec{x})$ on the polar-logarithmic coordinates,

$$T_{\mathrm{pl}}(\lambda, \beta) = a^{-2} R_{\mathrm{pl}}(\beta + \phi, \lambda - \log a). \tag{2.11}$$

Equation (2.11) is a translation invariant description of the input signal, while the rotation and scaling have become translations along the new coordinate system axes. If we would perform a second Fourier transform on $T_{\mathrm{pl}}(\lambda, \beta)$, this is called a Fourier-Mellin transform [40], [41]. By retaining the magnitude of this Fourier-Mellin spectrum, we can obtain a translation, rotation and scaling invariant representation of the input signal.

We will introduce a similar procedure as shown in equations (2.7) to (2.11), which can be applied to minutiae sets in order to find a representation that is invariant to translation and where rotation and scaling are translations.

### 2.2.2.1  Location-based spectral minutiae representation (SML)

When implementing the Fourier transform there are two important issues that should be considered. First, when a discrete Fourier transform is taken of an image, this

results in a representation of a periodic repetition of the original image. This is undesirable because it introduces errors due to discontinuities at the image boundaries. Second, the re-mapping onto a polar-logarithmic coordinate system after using a discrete Fourier transform introduces interpolation artifacts. Therefore, we introduce an *analytical* representation of the input minutiae, and then use *analytical* expressions of a continuous Fourier transform that are evaluated on a grid in the polar-logarithmic plane. These analytical expressions are obtained as follows. Assume we have a fingerprint with $Z$ minutiae. With every minutia, a function $m_i(x, y) = \delta(x - x_i, y - y_i), i = 1, \ldots, Z$ is associated where $(x_i, y_i)$ represents the location of the $i$-th minutia in the fingerprint image. Thus, in the spatial domain, every minutia is represented by a Dirac pulse. The Fourier transform of $m_i(x, y)$ is given by:

$$\mathscr{F}\{m_i(x, y)\} = \exp(-\mathrm{j}(\omega_\mathrm{x} x_i + \omega_\mathrm{y} y_i)), \qquad (2.12)$$

and the location-based spectral minutiae representation is defined as

$$\mathcal{M}_\mathrm{L}(\omega_\mathrm{x}, \omega_\mathrm{y}) = \sum_{i=1}^{Z} \exp(-\mathrm{j}(\omega_\mathrm{x} x_i + \omega_\mathrm{y} y_i)). \qquad (2.13)$$

In order to reduce the sensitivity to small variations in minutiae locations in the spatial domain, we use a Gaussian low-pass filter to attenuate the higher frequencies. This multiplication in the frequency domain corresponds to a convolution in the spatial domain where every minutia is now represented by a Gaussian pulse. A 2D Gaussian $g(x, y)$ in the space domain and its Fourier transform $G(\omega_\mathrm{x}, \omega_\mathrm{y})$ are

$$g(x, y) = \frac{1}{2\pi\sigma^2} \exp(-\frac{x^2 + y^2}{2\sigma^2}) \overset{\mathscr{F}}{\longleftrightarrow} G(\omega_\mathrm{x}, \omega_\mathrm{y}) = \exp(-\frac{\omega_\mathrm{x}^2 + \omega_\mathrm{y}^2}{2\sigma^{-2}}). \qquad (2.14)$$

Equation (2.14) shows that the parameter $\sigma$ of the Gaussian in the space domain appears as its reciprocal in the Gaussian in the frequency domain.

Following the shift property of the Fourier transform, the magnitude of $\mathcal{M}$ is taken in order to make the spectrum invariant to translation of the input and we obtain

$$\left| \mathcal{M}_\mathrm{L}(\omega_\mathrm{x}, \omega_\mathrm{y}; \sigma_\mathrm{L}^2) \right| = \left| \exp\left( -\frac{\omega_\mathrm{x}^2 + \omega_\mathrm{y}^2}{2\sigma_\mathrm{L}^{-2}} \right) \sum_{i=1}^{Z} \exp(-\mathrm{j}(\omega_\mathrm{x} x_i + \omega_\mathrm{y} y_i)) \right|. \qquad (2.15)$$

Equation (2.15) is the analytical expression for the spectrum, which can directly be evaluated on a polar-logarithmic grid. The resulting representation in the polar-logarithmic domain is invariant to translation, while rotation and scaling of the input have become translations along the polar-logarithmic coordinates.

### 2.2.2.2 Orientation-based spectral minutiae representation (SMO)

The location-based spectral minutiae representation (SML) only uses the minutiae location information. However, including the minutiae orientation as well may give better discrimination. Therefore, it can be beneficial to also include the orientation information in our spectral representation. The orientation $\theta$ of a minutia can be incorporated by using the spatial derivative of $m(x, y)$ in the direction of the minutia orientation. Thus, to every minutia in a fingerprint, a function $m_i(x, y, \theta)$ is assigned being the derivative of $m_i(x, y)$ in the direction $\theta_i$, such that

$$\mathscr{F}\{m_i(x, y, \theta)\} = \mathrm{j}(\omega_{\mathrm{x}} \cos \theta_i + \omega_{\mathrm{y}} \sin \theta_i) \cdot \exp(-\mathrm{j}(\omega_{\mathrm{x}} x_i + \omega_{\mathrm{y}} y_i)). \tag{2.16}$$

As in the SML algorithm, using a Gaussian filter and taking the magnitude of the spectrum yields

$$\left| \mathcal{M}_{\mathrm{O}}(\omega_{\mathrm{x}}, \omega_{\mathrm{y}}; \sigma_{\mathrm{O}}^2) \right| = \left| \exp\left( -\frac{\omega_{\mathrm{x}}^2 + \omega_{\mathrm{y}}^2}{2\sigma_{\mathrm{O}}^{-2}} \right) \right.$$
$$\left. \sum_{i=1}^{Z} \mathrm{j}(\omega_{\mathrm{x}} \cos \theta_i + \omega_{\mathrm{y}} \sin \theta_i) \cdot \exp(-\mathrm{j}(\omega_{\mathrm{x}} x_i + \omega_{\mathrm{y}} y_i)) \right|. \tag{2.17}$$

### 2.2.2.3 Implementation

In the previous sections we introduced analytical expressions for the spectral minutiae representations of a fingerprint. In order to obtain our final spectral representations, the continuous spectra (2.15) and (2.17) are sampled on a polar-logarithmic grid. In the radial direction $\lambda$, we use $M = 128$ samples between $\lambda_{\mathrm{l}} = 0.1$ and $\lambda_{\mathrm{h}} = 0.6$. In the angular direction $\beta$, we use $N = 256$ samples uniformly distributed between $\beta = 0$ and $\beta = \pi$. Because of the symmetry of the Fourier transform for real-valued functions, using the interval between 0 and $\pi$ is sufficient. This polar-logarithmic sampling process is illustrated in Figures 2.2 and 2.3.

The sampled spectra (2.15) and (2.17) will be denoted by $S_{\mathrm{L}}(m, n; \sigma_{\mathrm{L}})$ and $S_{\mathrm{O}}(m, n; \sigma_{\mathrm{O}})$, respectively, with $m = 1, \ldots, M, n = 1, \ldots, N$. When no confusion can arise, the parameter $\sigma$ and the subscripts L and O will be omitted.

Examples of the minutiae spectra achieved with SML are shown in Figure 2.4, and those achieved with SMO are shown in Figure 2.5. In these figures, $\sigma_{\mathrm{L}} = 0.32$ (2.15) and $\sigma_{\mathrm{O}} = 3.87$ (2.17). For each spectrum, the horizontal axis represents the rotation angle of the spectral magnitude (from 0 to $\pi$); the vertical axis represents the frequency of the spectral magnitude (the frequency increases from top to bottom). It should be noted that the minutiae spectrum is periodic on the horizontal axis.

(a)                                              (b)
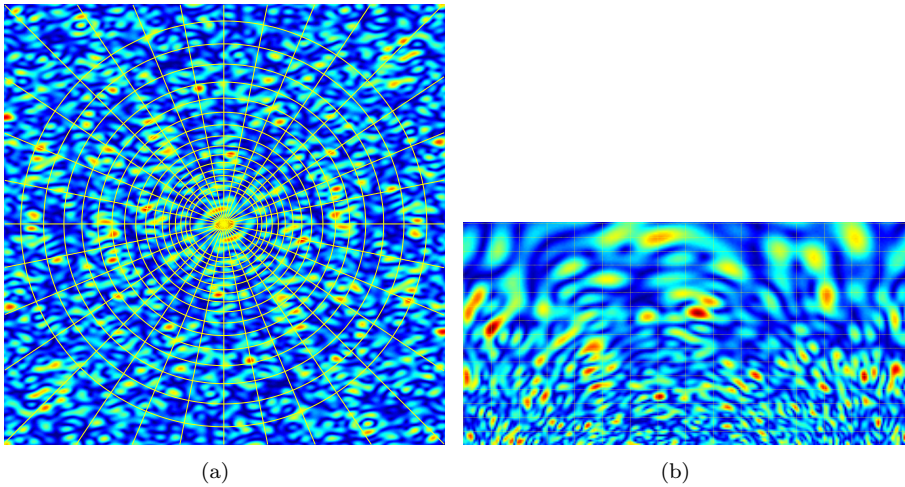
Fig. 2.2: Illustration of the polar-logarithmic sampling (SML spectra). (a) the Fourier spectrum in a Cartesian coordinate and a polar-logarithmic sampling grid; (b) the Fourier spectrum sampled on a polar-logarithmic grid.





(a)                                              (b)

Fig. 2.3: Illustration of the polar-logarithmic sampling (SMO spectra). (a) the Fourier spectrum in a Cartesian coordinate and a polar-logarithmic sampling grid; (b) the Fourier spectrum sampled on a polar-logarithmic grid.

(a)



(b) Minutiae spectrum of (a)



(c)



(d) Minutiae spectrum of (c)



(e)



(f) Minutiae spectrum of (e)



(g)



(h) Minutiae spectrum of (g)
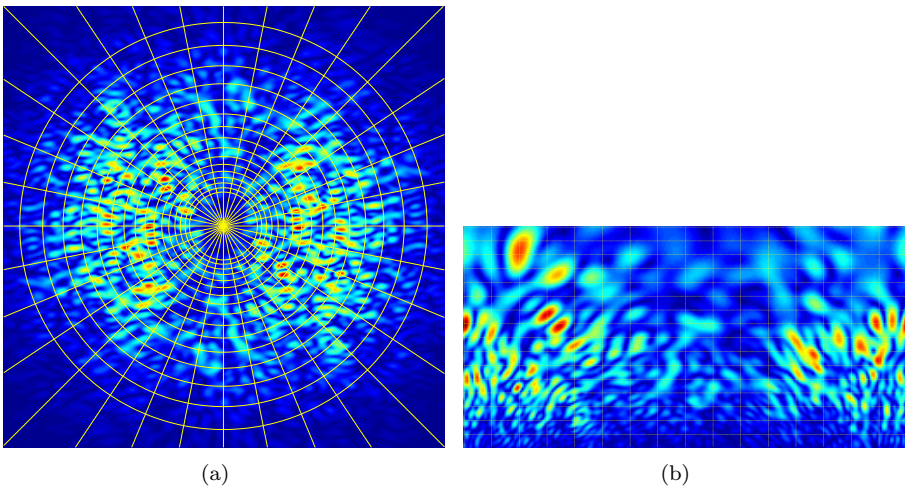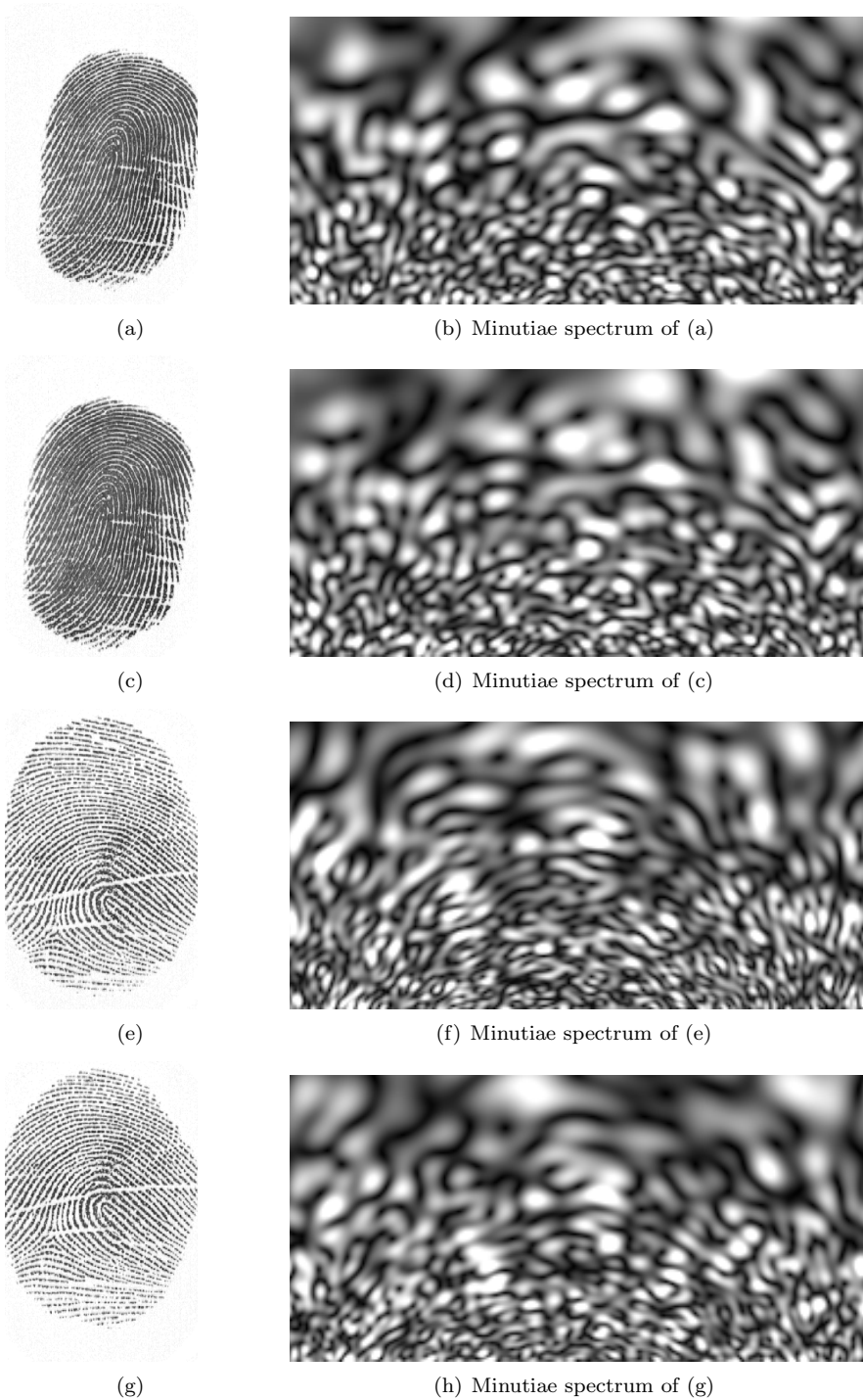
Fig. 2.4: Examples of minutiae spectra using SML. (a) and (c) are fingerprints from the same finger; (e) and (g) are fingerprints from the same finger.

(a)



(b) Minutiae spectrum of (a)



(c)



(d) Minutiae spectrum of (c)



(e)



(f) Minutiae spectrum of (e)



(g)



(h) Minutiae spectrum of (g)
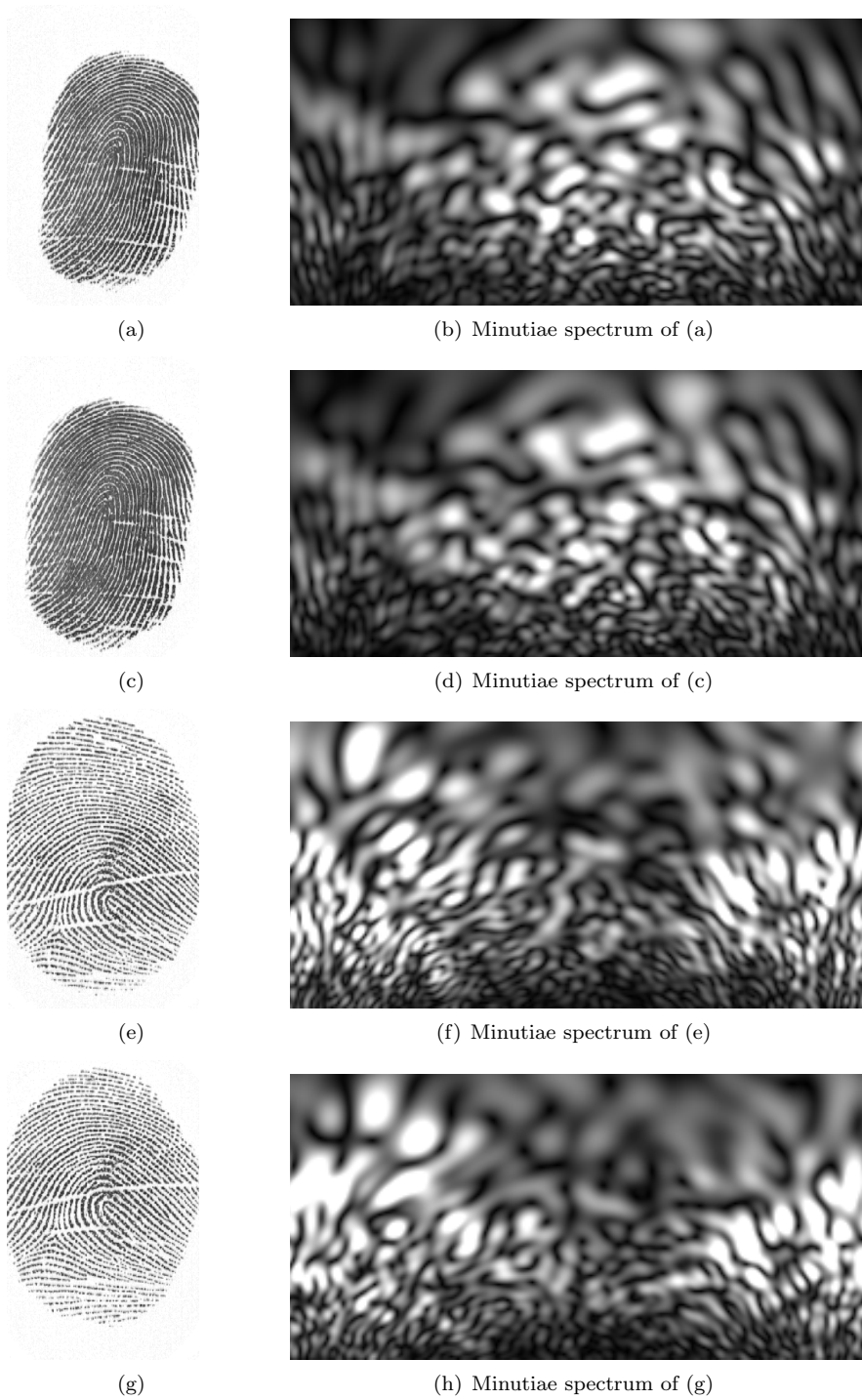
Fig. 2.5: Examples of minutiae spectra using SMO. (a) and (c) are fingerprints from the same finger; (e) and (g) are fingerprints from the same finger.

### 2.2.3   Spectral Minutiae Matching

After representing fingerprints by minutiae spectra, the next step is matching: the comparison of two minutiae spectra. The result of matching is either a 'match' (the two spectra appear to be from the same finger) or a 'non-match' (the two spectra appear to be from different fingers). Normally, in this step, we will first compute a number (similarity score), which corresponds to the degree of similarity. Then, by using a threshold, we can make a match/non-match decision [42].

In this paper, two matching algorithms are presented. In the first algorithm (direct matching), the correlation of two spectral images was chosen as a similarity score, which is a common similarity measure in image processing. The second algorithm is the Fourier-Mellin matching, in which the Fourier transform of the minutiae spectrum is taken, and only the magnitude is retained. This will generate a completely translation, rotation and scaling invariant descriptor of the minutiae set, and then a correlation-based method is used to calculate the similarity score of the Fourier-Mellin spectra.

#### 2.2.3.1   Direct Matching

Let $R(m, n)$ and $T(m, n)$ be the two sampled minutiae spectra in the polar-logarithmic domain respectively achieved from the *reference* fingerprint and *test* fingerprint. Both $R(m, n)$ and $T(m, n)$ are normalized to have zero mean and unit energy. We use the two-dimensional correlation coefficient between $R$ and $T$ as a measure of their similarity.

In practice, the input fingerprint images are rotated and might be scaled (for example, depending on the sensor that is used to acquire an image). Since the minutiae spectra are translation invariant, but not rotation and scaling invariant, this method has to test a few different combinations of rotation and scaling, which are translations in the minutiae spectra. To be specific, the scaling becomes the shift (or translation) in the vertical direction, and the rotation becomes the circular shift in the horizontal direction. We denote $T(m - i, n - j)$ as a shifted version of $T(m, n)$, with a shift of $i$ in the vertical direction and a circular shift $j$ in the horizontal direction. Then, the correlation coefficient between $R$ and $T$ is defined as:

$$C^{(R,T)}(i, j) = \frac{1}{MN} \sum_{m,n} R(m, n)T(m - i, n - j).  \qquad (2.18)$$

In most fingerprint databases, there is no scaling difference between the fingerprints, or the scaling can be compensated for on the level of the minutiae sets [43]. Therefore, in practice only a few rotations need to be tested. We chose to test rotations from -15 units to +15 units in steps of 3 units, which corresponds to a range from $-10\,^\circ$ to $+10\,^\circ$ in steps of $2°$. The maximum score from the different combinations is the final matching score between $R$ and $T$,

$$S^{(R,T)} = \max_j \{C^{(R,T)}(0,j)\}, \tag{2.19}$$

with

$$j = 3k \quad \text{for } k = -5...5. \tag{2.20}$$

### 2.2.3.2   Fourier-Mellin Matching

The Fourier-Mellin transform is often used to obtain a completely translation, rotation and scaling invariant descriptor. It is based on the scale-invariance property of the Mellin transform. The Mellin transform [44] is defined for complex $s = \sigma + j\omega$ as

$$\mathscr{M}\{f(x)\} = F_{\mathrm{M}}(s) = \int_0^\infty f(x)x^{s-1}\mathrm{d}x. \tag{2.21}$$

If we define the Mellin transform on the imaginary axis, thus $s = j\omega$, then the Mellin transform becomes

$$F_{\mathrm{M}}(\omega) = \int_0^\infty f(x)x^{j\omega-1}\mathrm{d}x. \tag{2.22}$$

The Mellin transform of a scaled $f(x)$ with a scaling factor $a$ is

$$\mathscr{M}\{f(ax)\} = F_{\mathrm{M}}^a(\omega) = \int_0^\infty f(ax)x^{j\omega-1}\mathrm{d}x. \tag{2.23}$$

If we make a change of variable $y = ax$, thus $x = y/a$, then (2.23) becomes

$$
\begin{aligned}
F_{\mathrm{M}}^a(\omega) &= \int_0^\infty f(y)(\frac{y}{a})^{j\omega-1}\frac{1}{a}\mathrm{d}y \\
&= a^{-j\omega}\int_0^\infty f(y)y^{j\omega-1}\mathrm{d}y \\
&= a^{-j\omega}F_{\mathrm{M}}(\omega) \\
&= \exp(-j\omega \ln a)F_{\mathrm{M}}(\omega).
\end{aligned}
\tag{2.24}
$$

Equation (2.24) shows that the scale change in the time domain just becomes a phase change in the Mellin domain. Therefore, the magnitude of the Mellin transform is scale-invariant,

$$|F_{\mathrm{M}}^a(\omega)| = |F_{\mathrm{M}}(\omega)|. \tag{2.25}$$

A standard Fourier-Mellin transform, sometimes called a circular Fourier and radial Mellin transform [45], is written as

$$\mathscr{M}_{\mathrm{f}}\{f(r,\beta)\} = M_{\mathrm{f}}(s,\omega_\beta) = \int_0^{2\pi} \int_0^\infty r^{s-1} f(r,\beta) \exp(-\mathrm{j}\omega_\beta \beta) \mathrm{d}r \mathrm{d}\beta. \tag{2.26}$$

If we make a change of variable $r = \mathrm{e}^\lambda$, thus $\lambda = \ln r$, and let $s = -\mathrm{j}\omega_\lambda$, thus define the radial Mellin transform on the imaginary axis, then the Fourier-Mellin transform becomes

$$\mathscr{M}_{\mathrm{f}}\{f(r,\beta)\} = M_{\mathrm{f}}(\omega_\lambda,\omega_\beta) = \int_0^{2\pi} \int_{-\infty}^\infty f(\lambda,\beta) \exp(-\mathrm{j}\omega_\lambda \lambda) \exp(-\mathrm{j}\omega_\beta \beta) \mathrm{d}\lambda \mathrm{d}\beta. \tag{2.27}$$

This is a 2D Fourier transform of the function $f(\lambda,\theta)$. Equation (2.27) shows that the Fourier-Mellin transform can be implemented by a polar-logarithmic transform of the original signal, and then using a 2D Fourier transform. Therefore, by performing a 2D Fourier transform on the minutiae spectra, we implement a Fourier-Mellin transform, and we can obtain a Fourier-Mellin descriptor by only retaining the magnitude. We denote $R_{\mathrm{FM}}(m,n)$ and $T_{\mathrm{FM}}(m,n)$ as the magnitude of the 2D Fourier transform of the spectral minutiae spectra $R(m,n)$ and $T(m,n)$. In the Fourier-Mellin matching algorithm, the correlation of two Fourier-Mellin magnitude $R_{\mathrm{FM}}(m,n)$ and $T_{\mathrm{FM}}(m,n)$ was chosen as a similarity score,

$$S_{\mathrm{FM}}^{(R,T)} = \frac{1}{MN} \sum_{m,n} R_{\mathrm{FM}}(m,n) T_{\mathrm{FM}}(m,n). \tag{2.28}$$

## 2.2.4   Experiments

### 2.2.4.1   Measurements

We test the spectral minutiae representation in a verification setting. A verification system authenticates a person's identity by comparing the captured biometric characteristic with the corresponding biometric template(s) pre-stored in the system. It conducts a one-to-one comparison to determine whether the identity claimed by the individual is true [35].

The matching performance of a fingerprint verification system can be evaluated by means of several measures. Commonly used are the *false acceptance rate* (FAR),

|      |      |      |      |
| :--: | :--: | :--: | :--: |
| (a)  | (b)  | (c)  | (d)  |

Fig. 2.6: Examples of fingerprint samples in MCYT: (a) and (b) are the fingerprints that we accepted from MCYT;(c) and (d) are fingerprints that we rejected from MCYT because of the low quality.

the *false rejection rate* (FRR), and the *equal error rate* (EER). When the decision threshold of a biometric security system is set such that the FAR and FRR are equal, the common value of FAR and FRR is referred to as the EER. In this paper, we use FAR, EER and the *genuine acceptance rate* (GAR), GAR= 1−FRR, as performance indicators of our scheme.

### 2.2.4.2   Experimental settings

The proposed algorithms have been evaluated on MCYT [46], FVC2000-DB2 [47] and FVC2002-DB2 [48] fingerprint databases.  The fingerprint data that we used from MCYT are obtained from 10 individuals.  Each individual contributed data from 10 different fingers with 10 samples per finger. We also tested our algorithms on two FVC fingerprint databases because they are public-domain fingerprint databases. Compared with MCYT, the fingerprints in FVC have lower quality and bigger displacements.  For the FVC databases, we used the same experimental protocol as in the FVC competition. Both FVC databases contain 100 fingers, with 8 samples per finger.  In FVC2002-DB2, we only used four samples (samples 1, 2, 7 and 8) in our experiments[2], while in FVC2000-DB2, we used all the 8 samples from each finger. The characteristics of the databases are summarized in Table 2.1.

We generated two minutiae sets from MCYT. The first minutiae set contains manually extracted minutiae, which serves as a high quality minutiae set. The second minutiae set is obtained by the VeriFinger minutiae extractor [11] and will be called 'VeriFinger minutiae'. In order to be able to manually extract reliable minutiae from fingerprint samples, we chose the 10 individuals from MCYT that have reasonably good quality fingerprints.  The quality measurement that we used here is based on fingerprint's

---

[2]In FVC2002 databases, samples 3, 4, 5 and 6 were obtained by requesting the biometric data subjects to provide fingerprints with exaggerated displacement and rotation [32].  In a security scenario where the biometric data subject is aware that cooperation is crucial for security reasons, he will be cooperative. Therefore, only samples 1, 2, 7 and 8 are chosen.

Table 2.1: Characteristics of databases used in our experiments.

|  | MCYT | FVC2000-DB2 | FVC2002-DB2 |
|---|---|---|---|
| Sensor | U.are.U (Digital Persona) | TouchChip (ST Microelectronics) | FX2000 (Biometrika) |
| Sensor type | optical | capacitive | optical |
| Image size | 256x400 | 256x364 | 296x560 |
| Resolution | 500 dpi | 500 dpi | 569 dpi |

variance and coherence [49]. The variance and the coherence of a fingerprint reflect the clarity of its ridge-valley structures. In general, good quality fingerprints have higher variance and coherence than low quality fingerprints. Some samples that we accepted and rejected from MCYT are shown in Figure 2.6. For FVC databases, we only used the minutiae sets that are obtained by the VeriFinger minutiae extractor.

For each comparison, we chose two fingerprints from the data set: one as a *reference* fingerprint, another as a *test* fingerprint. For matching genuine pairs, we used all the possible combinations. For matching imposter pairs, we chose one sample from each identity. Therefore, we have 4500, 2800 and 600 genuine scores for MCYT, FVC2000-DB2 and FVC2002-DB2, respectively. For each database, we have 4950 imposter scores.

In the spectral minutiae representation, we used a Gaussian low-pass filter on the spectrum to attenuate the higher frequencies, see Equations (2.15) and (2.17). From our experiments, we noticed that for SML and SMO, we need to choose different Gaussian parameters ($\sigma_L$ and $\sigma_O$) to achieve the best performances. Figure 2.7 and 2.8 show the influence of the Gaussian parameter $\sigma$ to the performances on MCYT VeriFinger minutiae set (using direct matching algorithm). We noticed that the Gaussian parameter has larger effects on SML than on SMO. Moreover, a Gaussian kernel is needed for SMO for achieving a better performance, while for SML it is not. The reason is that because the minutiae orientation is incorporated as a derivative of the delta function (see Equation (2.16)), this will amplify the noise (both in minutiae location and orientation) in the high frequency part in SMO. Therefore, a Gaussian kernel is needed for SMO to attenuate the higher frequencies. In SML, the high frequency part contains discriminative information, while the noise is evenly distributed in all frequencies, therefore, a Gaussian kernel does not help for a better performance. In our experiments, we finally chose $\sigma = 0$ for SML (in this case, no multiplication with Gaussian in the frequency domain) and $\sigma = 4.24$ for SMO. In case the fingerprint resolution is 500dpi, the Gaussian parameter $\sigma = 4.24$(pixel) in the spacial domain is about 0.21(mm) in reality.

From our experiments, we also noticed that the careful selection of frequency ranges ($\lambda_l$ and $\lambda_h$) of spectral minutiae are essential for a high performance, especially for SMO. For low quality fingerprints or an unreliable minutiae extractor (where the
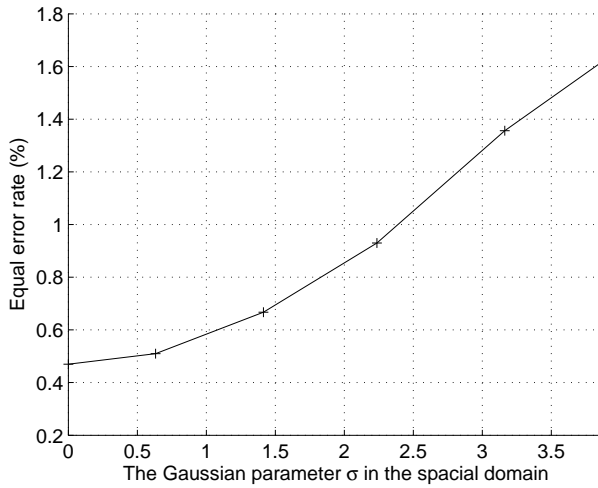
Fig. 2.7: Relation of the Gaussian $\sigma$ (in the spacial domain) and SML performances (MCYT VeriFinger minutiae set, using direct matching algorithm).
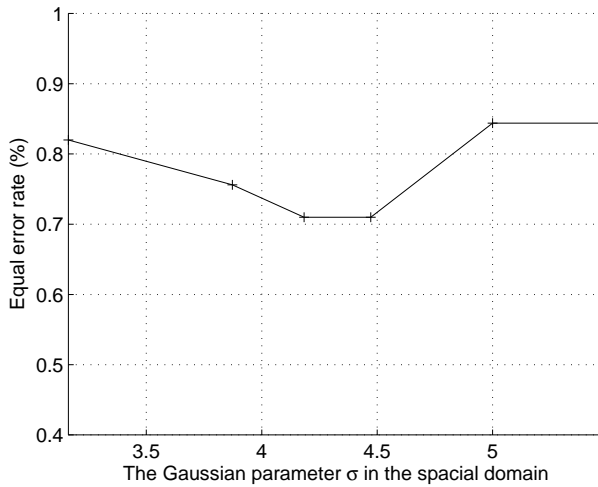


Fig. 2.8: Relation of the Gaussian $\sigma$ (in the spacial domain) and SMO performances (MCYT VeriFinger minutiae set, using direct matching algorithm).

Table 2.2: Settings of the frequency range.

| Databases | SML | | SMO | |
|---|---|---|---|---|
| | $\lambda_l$ | $\lambda_h$ | $\lambda_l$ | $\lambda_h$ |
| MCYT (Manual minutiae) | 0.1 | 0.6 | 0.05 | 0.6 |
| MCYT (VeriFinger minutiae) | 0.1 | 0.6 | 0.01 | 0.56 |
| FVC2000-DB2 and FVC2002-DB2 | 0.08 | 0.62 | 0.001 | 0.53 |

errors on minutiae location and orientation are higher), we need to use the lower frequencies that are more robust to noise. The final settings of $\lambda_l$ and $\lambda_h$ for the databases are shown in Table 2.2.

### 2.2.4.3   Results of SML and SMO

We tested both SML and SMO representation methods. The EERs we achieved are shown in Tables 2.3, 2.4 and 2.5, and the ROC (*receiver operating characteristic*) curves are shown in Figures 2.9, 2.10 and 2.11. For MCYT VeriFinger minutiae sets, the genuine and imposter distributions (resulting from direct matching) are shown in Figure 2.12.

From Tables 2.3-2.5, we can see that the direct matching algorithm received better results than the Fourier-Mellin matching algorithm. The Fourier-Mellin matching algorithm first implemented a 2D Fourier transform, and then achieved a rotation and scaling invariant descriptor by only retaining the magnitude. In this step, the phase information was discarded. However, in our application, the spectral minutiae do not suffer from the scaling problem, and the rotation range is also limited. From the result we can see that by discarding phase to achieve this rotation and scaling invariant degraded the performance. For direct matching algorithm, SML received better results if the minutiae are with high quality (MCYT manual minutiae case). When using automatically extracted minutiae sets (in which the minutiae suffer more noise), SMO performed better.

From the results, we can also see that for both SMO and SML, the manually extracted minutiae received better results than the VeriFinger minutiae for MCYT. Also, MCYT received much better results than the two FVC databases. These show that our algorithms are sensitive to the minutiae quality and fingerprint quality. In Section 2.2.5, we will present a further discussion about the factors that can influence the performance of our algorithms.

### 2.2.4.4   Fusion results of SML and SMO

In Section 2.2.4.3 we showed the recognition results for both SML and SMO. To illustrate the relation of the SML and SMO results, we made a scatter plot for the

Table 2.3: MCYT: Direct matching results.

| Minutiae sets | EERs (SML) | EERs (SMO) |
|---|---|---|
| Manual minutiae | 0.09% | 0.12% |
| VeriFinger minutiae | 0.47% | 0.42% |

Table 2.4: MCYT: Fourier-Mellin matching results.

| Minutiae sets | EERs (SML) | EERs (SMO) |
|---|---|---|
| Manual minutiae | 3.16% | 1.96% |
| VeriFinger minutiae | 6.56% | 3.29% |

Table 2.5: FVC: Direct matching results.

| Databases | EERs (SML) | EERs (SMO) |
|---|---|---|
| FVC2000-DB2 | 9.8% | 8.4% |
| FVC2002-DB2 | 6.4% | 6.1% |
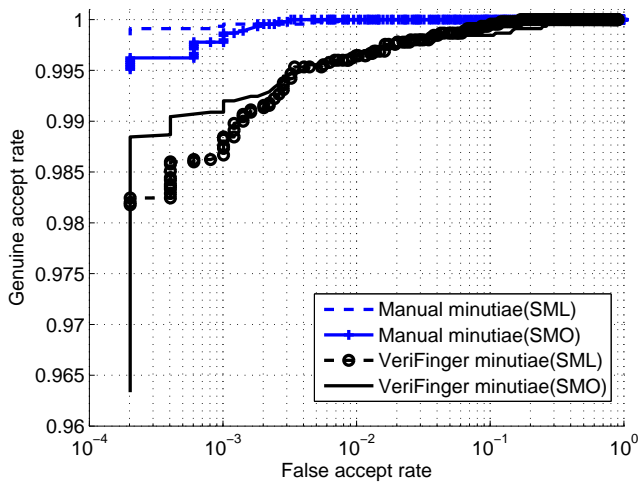


Fig. 2.9: ROC curves (MCYT: using direct matching).
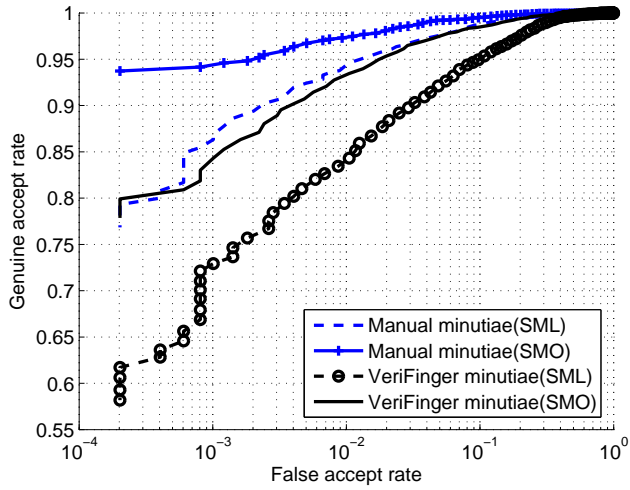
Fig. 2.10: ROC curves (MCYT: using Fourier-Mellin matching).
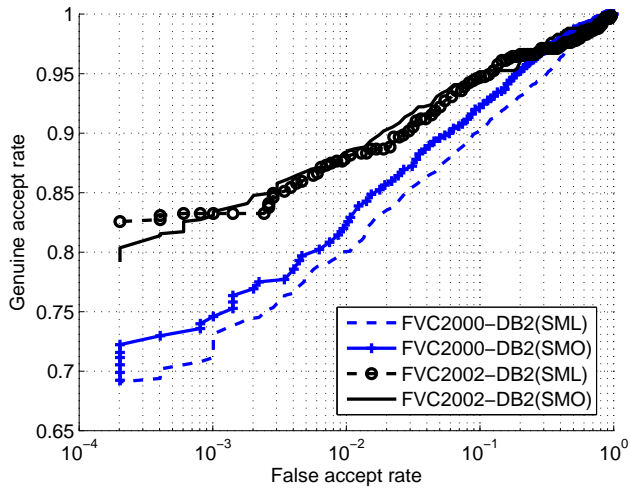


Fig. 2.11: ROC curves (FVC2000-DB2 and FVC2002-DB2: using direct matching).
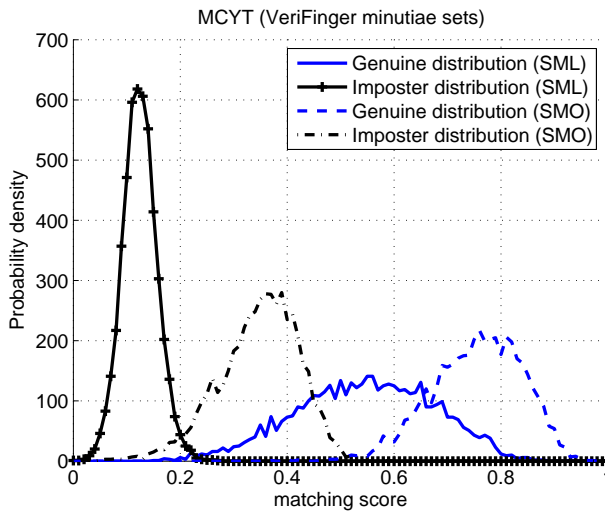
Fig. 2.12: Genuine and imposter distributions (VeriFinger minutiae sets, using direct matching).
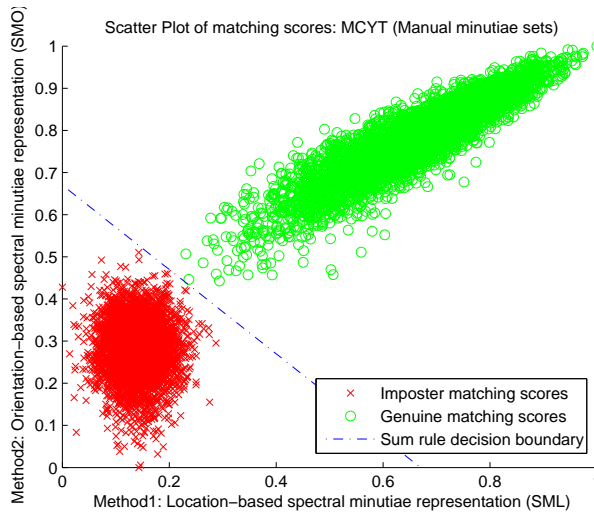


Fig. 2.13: Scatter plot of scores in MCYT manual minutiae case.

Table 2.6: MCYT: Fusion results of SML and SMO (direct matching).

| Minutiae sets | EERs (SML) | EERs (SMO) | EERs (fusion) |
|---|---|---|---|
| Manual minutiae | 0.09% | 0.12% | 0% |
| VeriFinger minutiae | 0.47% | 0.42% | 0.22% |

Table 2.7: MCYT: Fusion results of SML and SMO (Fourier-Mellin matching).

| Minutiae sets | EERs (SML) | EERs (SMO) | EERs (fusion) |
|---|---|---|---|
| Manual minutiae | 3.16% | 1.96% | 1.0% |
| VeriFinger minutiae | 6.56% | 3.29% | 1.86% |

Table 2.8: FVC: Fusion results of SML and SMO (direct matching).

| Databases | EERs (SML) | EERs (SMO) | EERs (fusion) |
|---|---|---|---|
| FVC2000-DB2 | 9.8% | 8.4% | 6.2% |
| FVC2002-DB2 | 6.4% | 6.1% | 4.8% |

genuine and imposter scores in the MCYT manual minutiae case (direct matching results), shown in Figure 2.13.

From Figure 2.13, we can see that the genuine scores from SML and SMO are correlated. At the same time, the imposter scores seem relatively uncorrelated. From the picture it can also be seen that the genuine and imposter distribution can be better separated using a fusion approach [50]. For this reason, we use the matching score based fusion to improve the performance. A sum rule with equal weights for SML and SMO is used [51], whose decision boundary is shown as the dashed line in Figure 2.13. The fusion results are shown in Tables 2.6, 2.7 and 2.8 (for comparison, the results of SML and SMO are also listed). The ROC curves are shown in Figures 2.14 and 2.15 (using the direct matching algorithm). We can see that the fusion results are much better than the SML and SMO results.

For fingerprint identification systems with very large databases, the matching speed is crucial. Because our algorithms use a fixed-length feature vector and avoid fingerprint alignment, the matching speed is promising. For both SML and SMO using the direction matching algorithm, we need to implement 360,448 real multiplications and 360,437 real additions. We tested the matching speed for the fusion case of SML and SMO and we can implement 8,000 comparisons (or matchings) per second using optimized C language programming on a PC with Intel Pentium D processor 2.80 GHz and 1 GB of RAM.
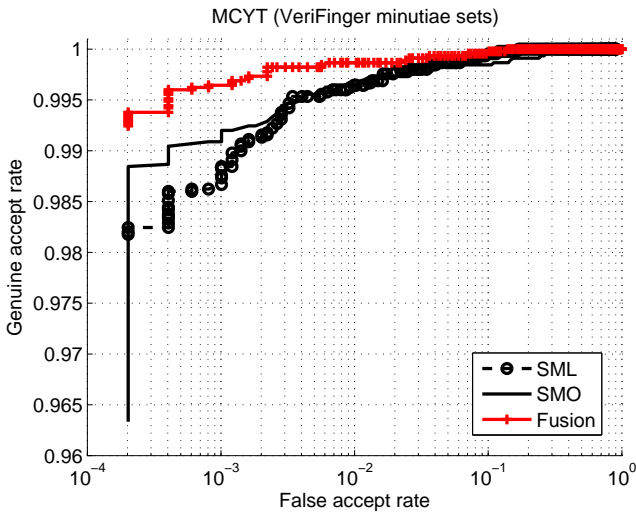
Fig. 2.14: ROC curves (MCYT: using direct matching).
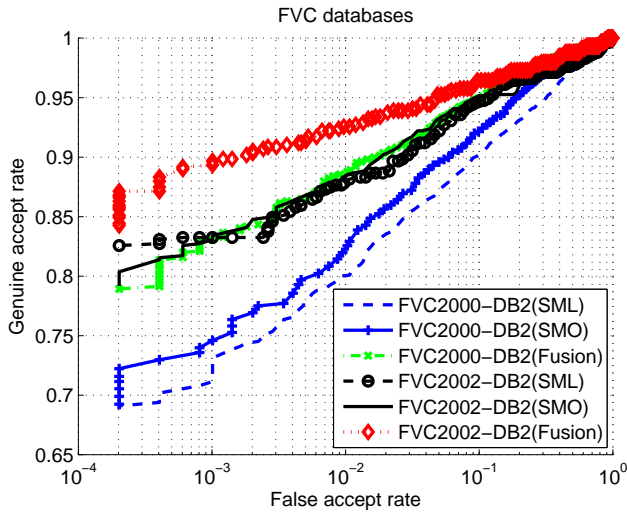


Fig. 2.15: ROC curves (FVC: using direct matching).

Table 2.9: The percentages of fingerprints without SPs.

| Databases | No core | No delta | No core and no delta |
|-----------|---------|----------|----------------------|
| MCYT | 4.8% | 73% | 3.6% |
| FVC2000-DB2 | 18% | 81.5% | 16.25% |
| FVC2002-DB2 | 7.75% | 66% | 7.75% |

### 2.2.4.5 Improvements by using singular points of fingerprints

In a fingerprint, *singular points* (SPs) can be identified. Henry [52] defined two types of singular points, the *core* and the *delta*. One fingerprint contains 0-2 cores and 0-2 deltas. Some methods used SPs to pre-align the fingerprints [4, 5]. However, some fingerprints do not contain SPs. Therefore, using SPs for pre-alignment is not reliable. In Table 2.9, we show the percentages of fingerprints in which SPs are not detected by the VeriFinger minutiae extractor. There are three cases for the failure of SPs detection: (1) the finger does not contain SPs; (2) SPs are not present in the fingerprint image because of a big displacement; (3) the extractor fails to find the SPs. If we only accept the fingerprints containing SPs, it will cause a high *failure to capture rate* (FTCR). Therefore, we have designed an algorithm in which SPs can assist the verification, while they will not cause FTCR.

In our algorithm, SPs are used to avoid the limited-overlap problems between the reference and test fingerprints. We use the direct matching algorithm for the experiment and the matching score without SPs information is denoted as $S_{\mathrm{DM}}$. Taking SML as example, the procedure is as follows.

(1) In a minutiae set, only take the minutiae within distance $D$ from the SPs as a new minutiae set to generate a subset spectral minutiae representation (Sub-SM). Thus, depending on the number of SPs, each fingerprint can generate 0-4 different Sub-SMs.

(2) During matching, if both the reference and test fingerprints have the same type of SPs (both having at least 1 core or 1 delta), 1-4 comparisons (the matching scores are denoted as $S_{\mathrm{SP}1-4}$) will be generated. For example, if the reference fingerprint has 1 core, while the test fingerprint has 2, the Sub-SM from the reference fingerprint will be compared with each of the Sub-SMs from the test fingerprint. If the reference and test fingerprints have both 2 cores, 2 comparisons will be generated by comparing the Sub-SMs from the upper-left core, and the Sub-SMs from the lower-right core, respectively.

(3) The largest score among $S_{\mathrm{DM}}$ and $S_{\mathrm{SP}1-4}$ is chosen as the new matching score, denoted as $S_{\mathrm{SP}}$.

(4) A sum-rule fusion as presented in Section 2.2.4.4 for $S_{\mathrm{DM}}$ and $S_{\mathrm{SP}}$ is used as the final result for SML.

Finally, the steps (1)-(4) are also applied to SMO, and a sum-rule fusion as presented in Section 2.2.4.4 for SML and SMO is used for a final result using SPs. We performed

Table 2.10: Results using Singular Points (Direct Matching).

| Databases | EER | GAR | | |
|---|---|---|---|---|
| | | FAR = 1% | FAR = 0.1% | FAR = 0% |
| MCYT | 0.13% | 99.9% | 99.8% | 99.5% |
| FVC2000-DB2 | 5.19% | 91.7% | 88.1% | 85.5% |
| FVC2002-DB2 | 3.86% | 95.5% | 92.7% | 89.7% |
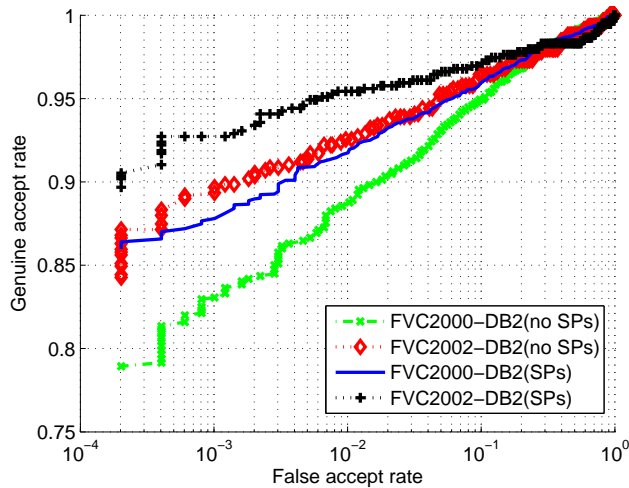


Fig. 2.16: ROC curves using SPs.

the experiments on the three databases (using VeriFinger minutiae sets). Considering the resolution and image size of fingerprints from each databases (see Table 2.1), we chose the distance $D = 120$(pixel) for MCYT and FVC2000-DB2, and $D = 130$(pixel) for FVC2002-DB2. The results are shown in Table 2.10 and the ROC curves of FVC databases are shown in Figure 2.16 (for comparison, the ROC curves without SPs improvement are also shown).

### 2.2.4.6   Comparison

We compared our results with other well-known minutiae matchers on the FVC2002-DB2 database: VeriFinger[3] and Fuzzy Vault according to the protocol in [32]. The results are shown in Table 2.11. We notice that the commercial minutiae matcher VeriFinger received much better results than ours. One reason is that the VeriFinger

---

[3]VeriFinger Extractor Version 5.0.2.0 and VeriFinger Matcher version 5.0.2.1 are used.

Table 2.11: Results comparison on FVC2002-DB2.

| Methods | EER | GAR | | |
|---------|-----|-----------|--------------|------------|
|         |     | FAR = 1% | FAR = 0.1% | FAR = 0% |
| Our method | 3.86% | 95.5% | 92.7% | 89.7% |
| VeriFinger | 1.0% | 99% | 98.8% | 98.6% |
| Fuzzy Vault | – | – | 91% | 86% |

matcher uses some fingerprint features that are not defined in ISO minutiae template [43]. Another reason is that, with our global representation, we cannot perform minutiae pair searching, which is a crucial step for minutiae-based matching. These two reasons may cause the degradation of our algorithm compared with VeriFinger.

We also compared the performance of our method with a minutiae based fingerprint recognition system combined with a template protection scheme based on fuzzy vault, which is presented in [32]. The reason of this comparison is that in [32] an alignment between a fingerprint pair using minutiae information is also not possible. Please note that [32] includes a template protection scheme, whereas our system does not. Moreover, because [32] implemented an alignment using high curvature points derived from the fingerprint orientation field, this caused a 2% *failure to capture rate* (FTCR), while our method does not suffer from this.

### 2.2.5   Discussion

The spectral minutiae representations are minutiae-based algorithms. A false rejection from a minutiae-based fingerprint recognition system can be caused by several factors: (1) translation, rotation and scaling deformations of minutiae; (2) non-linear distortions of minutiae; (3) limited overlap between the reference and test fingerprints; (4) missing minutiae (the minutiae extractor fails to detect the existing minutiae) and spurious minutiae (the minutiae extractor falsely identifies a minutia); (5) Errors on minutiae location and orientation.

The spectral minutiae matching algorithms have been designed to cope with the minutiae translation, rotation and scaling deformations, factor (1). Table 2.6 shows that the manually extracted minutiae receive a better recognition accuracy than the automatically extracted minutiae (VeriFinger minutiae sets). We assume that the manual extraction is accurate to detect the true minutia and obtain its location and orientation, then the performance degradation of the automatically extracted minutiae is mainly caused by factors (4) and (5). However, the manual minutiae cannot avoid errors related to limited overlap and non-linear distortions, factors (2) and (3). Therefore, we will analyse our algorithms' sensitivity to factors (3) to (5) in this section. The non-linear distortions (factor (2)) can be included into minutiae errors (factor (5)). To measure the influences of these three factors, we simulated them on the 1000

Fig. 2.17: Creation of limited overlap between a fingerprint pair.

minutiae sets that we manually extracted from MCYT. We used the parameter setting in Section 2.2.2.3 and the direct matching algorithm to perform the simulations.

### 2.2.5.1   Limited overlap between the reference and test fingerprints

During the verification phase, the finger may be placed at different locations and in different angles on the sensor, which results in a limited overlap between the reference and test fingerprints. In both the SML and SMO algorithms, all the extracted minutiae are used in the fingerprint representation, therefore, a limited overlap between a fingerprint pair will cause an insufficient percentage of matching minutiae, and will lead to a reduced performance.

In order to study this effect, we performed simulations where minutiae in a certain area were removed from the extracted minutia set. During the simulation, based on the minutiae location, we removed a fraction of $p$ minutiae at the top of a fingerprint to obtain the reference minutia set. For the test minutiae set, we removed a fraction of $p$ minutiae from *the same fingerprint* at the bottom (see Figure 2.17). All the corresponding minutiae are without any errors on both location and orientation. After the minutiae removals, the corresponding minutiae fraction $P_{\mathrm{corr}}$ between the reference and test fingerprints is:

$$P_{\mathrm{corr}} = \frac{1 - 2p}{1 - p} \tag{2.29}$$

The matching results for different percentage $p$ are shown in Figure 2.18.

From the results we can see that when the removal percentage is below 20% (in which case the corresponding minutiae percentage $P_{\mathrm{corr}}$ is above 75%), it will hardly cause any error recognition in both the SML and SMO algorithms. When $p$ increases, the
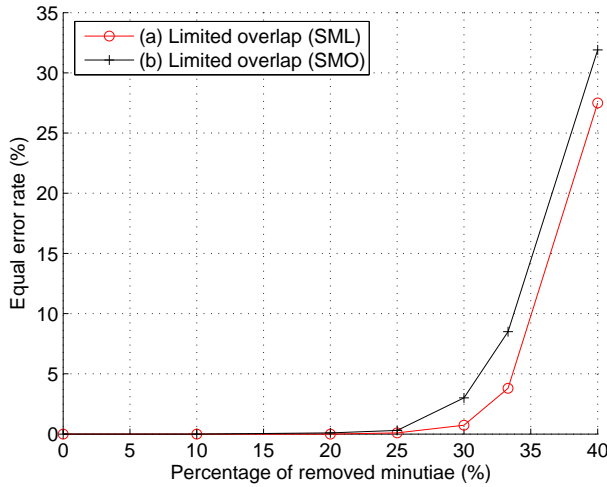
Fig. 2.18: Simulation of limited overlap between the reference and test fingerprints.

performances of both algorithms degrade. Compared with SMO, SML is more robust to the limited overlap between a fingerprint pair.

### 2.2.5.2 Missing and spurious minutiae

An unreliable minutiae extractor or bad quality fingerprints can bring a great number of missing and spurious minutiae, which will lead to an insufficient number of corresponding minutiae, and then lead to a reduced performance. During the simulation, we first discarded a fraction of $p$ randomly chosen minutiae from a minutiae set to obtain a reference minutiae set. Next, we discarded another fraction of $p$ minutiae from the original minutiae set to obtain the test minutiae set. The matching results for different $p$ are shown in Figure 2.19.

Similar as the simulation results from the limited overlap case, missing and spurious minutiae do not influence the equal error rates if the removed fraction is below 20%. When $p$ increases, the performances of both algorithms degrade. When $p$ is relatively small (below to 35%), SML performs better than SMO. When $p$ is bigger, SML degrades faster than SMO, which leads to a worse performance.

### 2.2.5.3 Errors on minutiae location and orientation

Many factors can cause errors on minutiae location and orientation, such as an unreliable minutiae extractor, noisy fingerprint images and elastic deformations of fingerprints. The latter one is even unavoidable for manually extracted minutiae. During the simulation, the original minutiae sets are used as reference minutiae sets. Then we
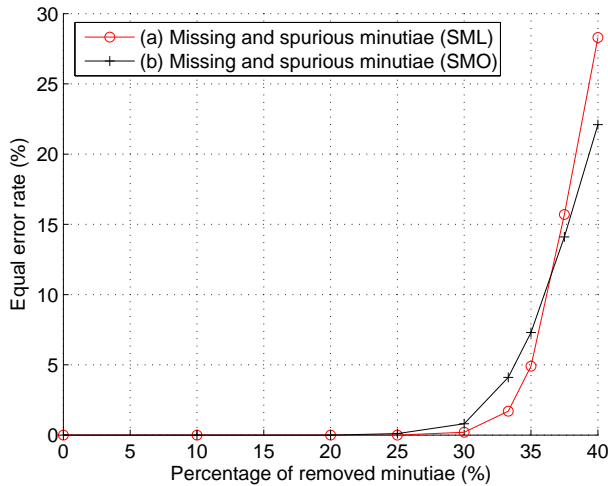
Fig. 2.19: Simulation of missing and spurious minutiae.

add zero-mean Gaussian distributed noise to the minutiae location or/and orientation to build test minutiae sets.

For the SML algorithm, we simulated the case of errors on the minutiae location. For the SMO algorithm, we simulated three cases: (a) errors only on the minutiae location; (b) errors only on the minutiae orientation; (c) errors on both the minutiae location and orientation.

Figure 2.20 shows the influence of minutiae location errors to SML and SMO (the errors that we added are measured by pixels, for our fingerprints, 1 pixel is about 0.05mm distance in reality). We can see that if the location errors are relatively small (the standard deviation $\sigma$ is smaller than 3 pixels), this will not cause any false recognition. When the errors increase, the performances of both SML and SMO degrade. When $\sigma$ is smaller than 7, SML performances better than SMO. When $\sigma$ is bigger than 7, SML degrades faster than SMO, and finally leads to a worse performance.

Figure 2.21 shows the influence of different error cases to SMO. To simulate a similar error scale on minutiae location and orientation, we scaled to orientation such that 1 pixel error on the location corresponds to 0.04 rad error on the orientation. Compared with case (a) and (b), we can see that the errors on minutiae orientation cause much less performance degradation than the errors on minutiae location. The case (a) and (c) show that adding errors on orientation does not degrade the result greatly.

From Figure 2.20 and 2.21, we also notice that when the errors become bigger (for example, $\sigma$ changes from 6 to 7), the equal error rates can degrade with 6%. That is a big influence which cannot be ignored.
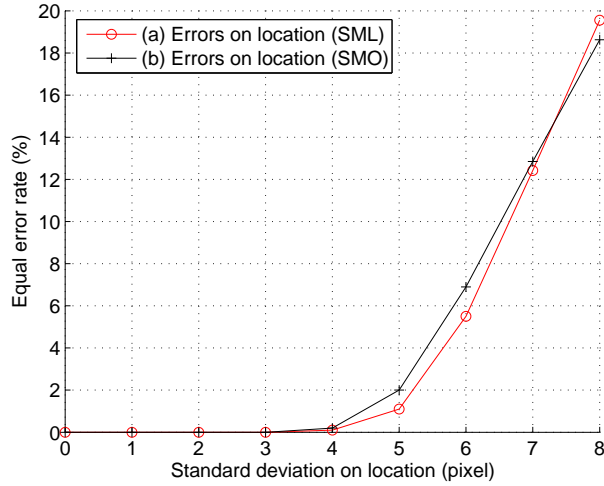
Fig. 2.20: Simulation of errors on the minutiae location (SML and SMO).
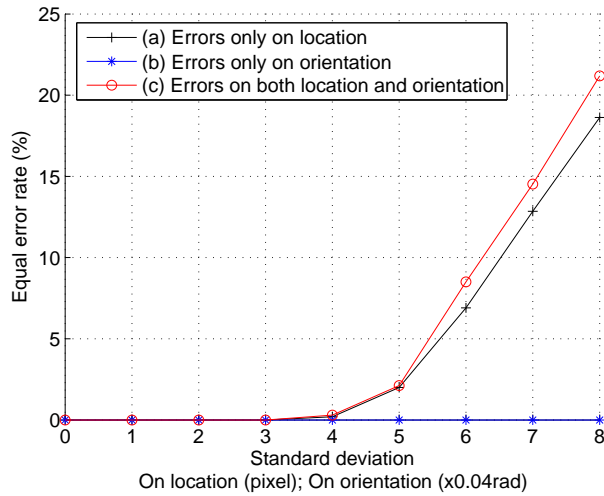


Fig. 2.21: Simulation of errors on the minutiae location and orientation (SMO).

### 2.2.6    Conclusions

The spectral minutiae representation is a novel method to represent a minutiae set as a fixed-length feature vector, which enables the combination of fingerprint recognition systems and template protection schemes. In order to be able to apply the spectral minutiae representation with a template protection scheme, for example based on a fuzzy extractor [53], the next step would be to extract bits that are stable for the genuine user and completely random for an arbitrary user. For example, we can apply 2D Gabor filters for bit extraction, which has been used in iris codes [54]. Another possibility is to first apply additional dimensionality reduction by a combination of PCA and LDA and then apply single bit extraction according to the reliable component scheme or multi bit extraction [55].

The spectral minutiae representation avoids the difficulties of minutiae registration by representing a minutiae set as a translation-invariant spectrum, in which rotation and scaling become translations, which can be easily compensated for. Moreover, this method is compatible with the large number of existing minutiae databases and the additional cost to integrate this new scheme is relatively low.

This paper introduces two spectral minutiae representation methods: the location-based spectral minutiae representation (SML) and the orientation-based spectral minutiae representation (SMO). Both algorithms are evaluated using a correlation based spectral minutiae matching algorithm (direct matching) and a Fourier-Mellin matching algorithm. From the experiments, the direct matching algorithm gives a better performance. Comparing SML and SMO, SML shows better results if the fingerprints are of good quality and the minutiae extractor is reliable, while SMO is more robust against the minutiae noise. After investigating the relation between the SML and SMO results, a matching score based fusion is applied, which obtains better results. Finally, a method using singular points showing a better performance is presented.

In this paper, we also discussed three factors that can degrade our algorithms' performances: limited overlap between the reference and test fingerprints; missing and spurious minutiae; errors on minutiae location and orientation. It shows that in general SML is more robust to all these three factors. However, if the percentage of missing and spurious minutiae is too high ($p > 35\%$), or the errors on minutiae location are too big (standard deviation $\sigma > 7$ (pixel)), then SMO shows a better performance. Therefore, in case the fingerprints have good quality and/or the minutiae extractor is reliable, SML shows a better recognition performance. Overall, the performance can be improved by implementing fusion of SML and SMO. However, these three factors are unavoidable in a fingerprint recognition system. To cope with the limited overlaps and to be more robust against the minutiae errors are topics of further research.

## 2.3    Chapter Conclusions

In this chapter, we introduced the basic idea of the spectral minutiae representation. Two spectral minutiae representation methods have been proposed and analyzed: the *location-based spectral minutiae representation* (SML) and the *orientation-based spectral minutiae representation* (SMO). We also proposed two methods to enhance the recognition performance of SML and SMO: one is the score-level fusion on SML and SMO, denoted as *SM Fusion*; another is incorporating singular points, denoted as *Enhancement by SP*.

The spectral minutiae representation method proposed in this chapter showed promising results, which motivate us to further investigate and optimize this method.

Table 2.12: The contributions of Chapter 2 and their achieved targets.

| Contribution(s) | Target(s) |
|---|---|
| SML | Target I: Fixed-length feature vector |
| SMO | Target II: Translation and rotation invariance |
| SM Fusion | Target IV: High recognition performance |
| Enhancement by SP | |

With regard to the research question and the targets of this thesis that are formulated in Section 1.3, this chapter addressed Target I, fixed-length feature vector, Target II, translation and rotation invariance, and Target IV, high recognition performance. With the spectral minutiae representation algorithm proposed in this chapter, Targets I and II have been achieved. The two enhancement methods "SM Fusion" and "Enhancement by SP" contributed to Target IV. The contributions of this chapter together with their achieved targets are summarized in Table 2.12.

# Chapter 3

# Enhancements to Spectral Minutiae Representations

## 3.1 Chapter Introduction

PURPOSE. In Chapter 2, we presented two spectral minutiae representations, SML and SMO. The analysis in Section 2.2.5 shows that the performance of the spectral minutiae algorithms can be degraded by the limited overlap between two fingerprints, missing and spurious minutiae, and minutiae errors. To cope with the above problems, we explore several methods to enhance the recognition performance of the spectral minutiae representations.

CONTENTS. Based on the spectral minutiae representations SML and SMO introduced in Chapter 2, we propose several enhancements. First, in Section 3.2, the spectral minutiae matching algorithms are improved by applying the *weighted sum correlation matching* and *fast rotation shift searching*. The algorithms are evaluated on the MCYT database. In this section, the enhancements are only applied to the SML features. Second, in Section 3.3, we explore the performance enhancement by including two types of *minutiae quality information* in both the SML and SMO features. We evaluated the performance on the FVC2002-DB2 database. Third, in Section 3.4, we use fingerprint minutiae subsets to cope with the limited overlap problem between the reference and test fingerprints. The algorithm is evaluated on the MCYT database. In the context of the system diagram, the content of this chapter and its referred blocks are highlighted in Figure 3.1. The fast rotation shift searching algorithm will be used in Chapters 4 and 5, and the minutiae quality data enhancement will be applied to the complex spectral minutiae feature in Chapter 6.

PUBLICATION(S). Section 3.2 has been published in [56]. Section 3.3 has been
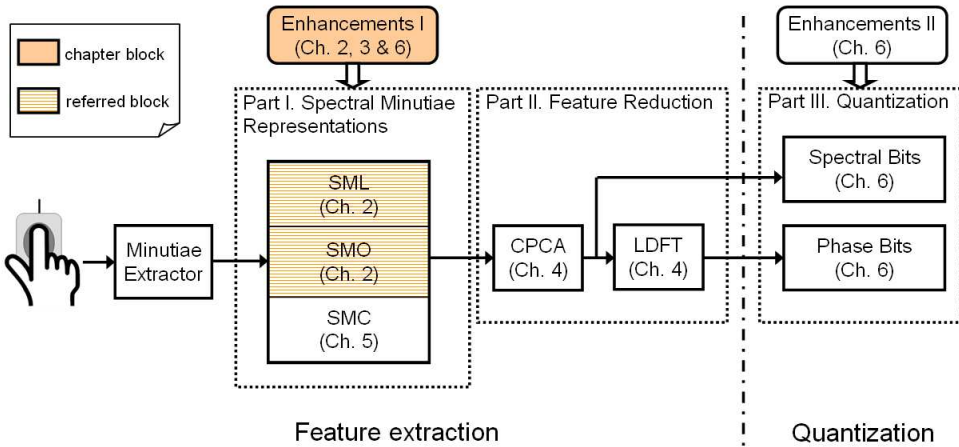
Fig. 3.1: *Block diagram of our designed system, highlighting the content of Chapter 3 and its referred blocks.*

published in [57]. Section 3.4 has been published in [58].

A NOTE TO READERS. The readers can focus on the following subsections: (1) 3.2.3 introduces the weighted sum correlation matching and the fast rotation shift searching; (2) 3.3.3 introduces how to incorporate minutiae quality data to improve the recognition performance; (3) 3.4.3 uses minutiae subsets to cope with the limited overlap problem. Subsections 3.2.2, 3.3.2 and 3.4.2 give the background that have already been introduced in Chapter 2. The readers can skip these parts.

## 3.2 Spectral Minutiae: A Fixed-length Representation of a Minutiae Set

**Abstract**

Minutiae, which are the endpoints and bifurcations of fingerprint ridges, allow a very discriminative classification of fingerprints. However, a minutiae set is an unordered set and the minutiae locations suffer from various deformations such as translation, rotation and scaling. In this paper, we introduce a novel method to represent a minutiae set as a fixed-length feature vector, which is invariant to translation, and in which rotation and scaling become translations, so that they can be easily compensated for. By applying the spectral minutiae representation, we can combine the fingerprint recognition system with a template protection scheme, which requires a fixed-length feature vector. This paper also presents two spectral minutiae matching algorithms and shows experimental results.

### 3.2.1   Introduction

A fingerprint consists of a pattern of line structures, which are called ridges. The most prominent ridge characteristics are minutiae, which are the ridge endpoints and bifurcations. They are known to remain unchanged over an individual's lifetime [35]. Minutiae-based fingerprint recognition techniques are popular and widely used [7,9]. However, they have some drawbacks, which limit their application. First, due to the fact that minutiae sets are unordered, the correspondence between individual minutia in two minutiae sets is unknown before matching and this makes it difficult to find the geometric transformation (consisting of translation, rotation, scaling, and optionally non-linear deformations [9]) that optimally registers (or aligns) two sets. For fingerprint identification systems with very large databases [59], in which a fast comparison algorithm is necessary, minutiae-based matching algorithms will fail to meet the high speed requirements. Secondly, a minutiae representation of a fingerprint cannot be applied directly in recently developed template protection schemes, such as [5] and [26] (chapter 3), which require as an input a fixed-length feature vector representation of a biometric modality. The spectral minutiae representation as proposed in this paper overcomes the above drawbacks of the minutiae sets, thus broadening the application of minutiae-based algorithms.

There are several algorithms to extract a fixed-length feature vector from fingerprints. The FingerCode as presented in [4] is based on ridge features. The author concluded that FingerCodes are not as distinctive as minutiae and they can be used as complementary information for fingerprint matching. Willis and Myers brought forward a fixed-length minutiae wedge-ring feature [60], which recorded the minutiae numbers on a pattern of wedges and rings. However, this method can only perform a coarse fingerprint authentication, and cannot handle big translations and rotations. Recently, a feature vector based on the distribution of the pairwise distances between minutiae is proposed by Park et al. [61]. However, this algorithm is only evaluated on the manually labeled minutiae and the performance is not satisfying.

Our method is inspired by the Fourier-Mellin transform, which was first introduced by the optical research community [37]. It was often used in image processing to obtain a translation, rotation and scaling invariant descriptor of the image [39,45]. However, the implementation of the Fourier-Mellin transform requires a Fourier transform and a polar-logarithmic mapping. When applying those on a digital image, a resampling and interpolation process is normally unavoidable. To avoid the interpolation errors, we introduce an *analytical* representation of the minutiae set, and then use *analytical* expressions of a continuous Fourier transform that can be evaluated on polar-logarithmic coordinates. By representing minutiae in the spectral domain, we transform a minutiae set into a fixed-length feature vector, which at the same time does not need registration to compensate for translation, rotation and scaling. By using a spectral minutiae representation instead of minutiae sets, we meet the requirements of template protection and allow for faster matching as well.

The spectral minutiae representation method can be easily integrated into a minutiae-based fingerprint recognition system. Minutiae sets can be directly transformed to

this new representation, which makes this method compatible with the large amount of existing minutiae databases.

This paper is organized as follows. First, in Section 3.2.2, the concept of spectral minutiae representation is explained in detail. Next, two correlation-based spectral minutiae matching algorithms are proposed in Section 3.2.3. Then, Section 3.2.4 will present the experimental results. Finally, we will draw conclusions in Section 3.2.5.

## 3.2.2   Spectral Minutiae Representation

### 3.2.2.1   Background

The spectral minutiae representation is based on the shift, scale and rotation properties of the two-dimensional continuous Fourier transform. If we have an input signal $f(\vec{x})$, $\vec{x} = (x, y)^{\mathrm{T}}$ (we denote the transpose of a vector $\vec{v}$ as $\vec{v}^{\mathrm{T}}$), its continuous Fourier transform is

$$\mathscr{F}\{f(\vec{x})\} = F(\vec{\omega}) = \int_{-\infty}^{\infty} \int_{-\infty}^{\infty} f(\vec{x}) \exp(-\mathrm{j}\vec{w}^{\mathrm{T}}\vec{x}) \mathrm{d}\vec{x}, \qquad (3.1)$$

with $\vec{\omega} = (\omega_x, \omega_y)^{\mathrm{T}}$. The Fourier transform of a translated $f(\vec{x})$ is

$$\mathscr{F}\{f(\vec{x} - \vec{x}_0)\} = \exp(-\mathrm{j}\vec{\omega}^{\mathrm{T}}\vec{x}_0) F(\vec{\omega}), \qquad (3.2)$$

with $\vec{x}_0 = (x_0, y_0)^{\mathrm{T}}$ the translation vector. The Fourier transform of an isotropically scaled $f(\vec{x})$ is

$$\mathscr{F}\{f(a\vec{x})\} = a^{-2} F(a^{-1}\vec{\omega}), \qquad (3.3)$$

with $a$ $(a > 0)$ the isotropic scaling factor. The Fourier transform of a rotated $f(\vec{x})$ is

$$\mathscr{F}\{f(\Phi\vec{x})\} = F(\Phi\vec{\omega}), \qquad (3.4)$$

with

$$\Phi = \begin{pmatrix} \cos\phi & -\sin\phi \\ \sin\phi & \cos\phi \end{pmatrix}. \qquad (3.5)$$

Here $\Phi$ is the (orthonormal) rotation matrix and $\phi$ is the (anticlockwise) rotation angle of $f(\vec{x})$.

It can be seen from (3.2) that if only the magnitude of the Fourier spectrum is retained, this results in a translation invariant representation of the input signal. Furthermore,

from (3.3) and (3.4) it follows that scaling and rotation of the input signal results in a scaled and rotated Fourier spectrum.

Based on the above properties of the two-dimensional Fourier transform, we can re-map the Fourier spectral magnitude onto a polar-logarithmic coordinate system with respect to an origin, such that the rotation and scaling become translations along the angular and radial axes, respectively. The detailed steps are as follows. Consider a signal $t(\vec{x})$ that is translated, scaled and rotated replica of $r(\vec{x})$,

$$t(\vec{x}) = r(a\Phi\vec{x} - \vec{x}_0),\qquad(3.6)$$

then the magnitude of the Fourier transforms of $t(\vec{x})$ and $r(\vec{x})$ are related by,

$$|T(\vec{\omega})| = a^{-2}|R(a^{-1}\Phi\vec{\omega})|,\qquad(3.7)$$

which is a translation invariant representation of the input signal. If we re-map the Fourier spectral magnitude onto a polar-logarithmic coordinate system as,

$$\lambda = \log\sqrt{\omega_{\mathrm{x}}^2 + \omega_{\mathrm{y}}^2},\qquad \beta = \arctan(\frac{\omega_{\mathrm{y}}}{\omega_{\mathrm{x}}}),\qquad(3.8)$$

$$R_{\mathrm{pl}}(\lambda, \beta) = |R(\mathrm{e}^\lambda\cos\beta, \mathrm{e}^\lambda\sin\beta)|,\qquad(3.9)$$

$$T_{\mathrm{pl}}(\lambda, \beta) = |T(\mathrm{e}^\lambda\cos\beta, \mathrm{e}^\lambda\sin\beta)|,\qquad(3.10)$$

then we have the Fourier spectral magnitude of $t(\vec{x})$ and $r(\vec{x})$ on the polar-logarithmic coordinates,

$$T_{\mathrm{pl}}(\lambda, \beta) = a^{-2}R_{\mathrm{pl}}(\beta + \phi, \lambda - \log a).\qquad(3.11)$$

Equation (3.11) is a translation invariant description of the input signal, while the rotation and scaling have become translations along the new coordinate system axes. If we would perform a Fourier transform on $T_{\mathrm{pl}}(\lambda, \beta)$, this is called a Fourier-Mellin transform.

We will introduce a similar procedure as we showed from equations (3.7) to (3.11) that can be applied to minutiae sets in order to find a representation which is invariant to translation and where rotation and scaling are translations.

### 3.2.2.2   An analytical spectral minutiae representation

When implementing the Fourier transform there are two important issues that should be considered. First, when a discrete Fourier transform is taken of a continuous

image, this results in a description of a periodic repetition of the original image. This is undesirable because it introduces errors. Second, the re-mapping onto a polar-logarithmic coordinate system after using a discrete Fourier transform introduces interpolation artifacts. Therefore we introduce an *analytical* representation of the input minutiae, and then use *analytical* expressions of a continuous Fourier transform that are evaluated on every grid point in the polar-logarithmic plane. These analytical expressions are obtained as follows. Assume we have a fingerprint with $Z$ minutiae. With every minutia, a function $m_i(x, y) = \delta(x - x_i, y - y_i), i = 1, \ldots, Z$ is associated where $(x_i, y_i)$ represents the location of the $i$-th minutia in the fingerprint image. Thus, in the spatial domain, every minutia is represented by a Dirac pulse. The Fourier transform of $m_i(x, y)$ is given by:

$$\mathscr{F}\{m_i(x, y)\} = \exp(-\mathrm{j}(\omega_{\mathrm{x}} x_i + \omega_{\mathrm{y}} y_i)), \tag{3.12}$$

and the spectral representation of the minutiae is defined as

$$\mathcal{M}(\omega_{\mathrm{x}}, \omega_{\mathrm{y}}) = \sum_{i=1}^{Z} \exp(-\mathrm{j}(\omega_{\mathrm{x}} x_i + \omega_{\mathrm{y}} y_i)). \tag{3.13}$$

This is the analytical expression for the spectrum which can be directly evaluated on a polar-logarithmic grid. The resulting representation in the polar-logarithmic domain is invariant to translation, while rotation and scaling of the input have become translations along the polar-logarithmic coordinates.

### 3.2.2.3    Implementation

In order to obtain our final spectral representation, the continuous spectrum (3.13) is sampled on a polar-logarithmic grid. In the radial direction $\lambda$ we use $M = 128$ samples logarithmically distributed between $\lambda = 0.1$ and $\lambda = 0.6$. In the angular direction $\beta$, we use $N = 256$ samples uniformly distributed between $\beta = 0$ and $\beta = \pi$. Because of the symmetry of the Fourier transform for real-valued functions, using the interval between 0 and $\pi$ is sufficient. This polar-logarithmic sampling process is illustrated in Figure 3.2.

The examples of the minutiae spectra are shown in Figure 3.3. For each spectrum, the horizontal axis represents the rotation angle of the spectral magnitude (from 0 to $\pi$); the vertical axis represents the frequency of the spectral magnitude (the frequency increases from top to bottom). We can notice that the minutiae spectrum is periodic on the horizontal axis.

## 3.2.3    Spectral Minutiae Matching

After representing fingerprints in the form of minutiae spectra, the next step is matching: the comparison of two minutiae spectra. The result of matching is either a 'match'
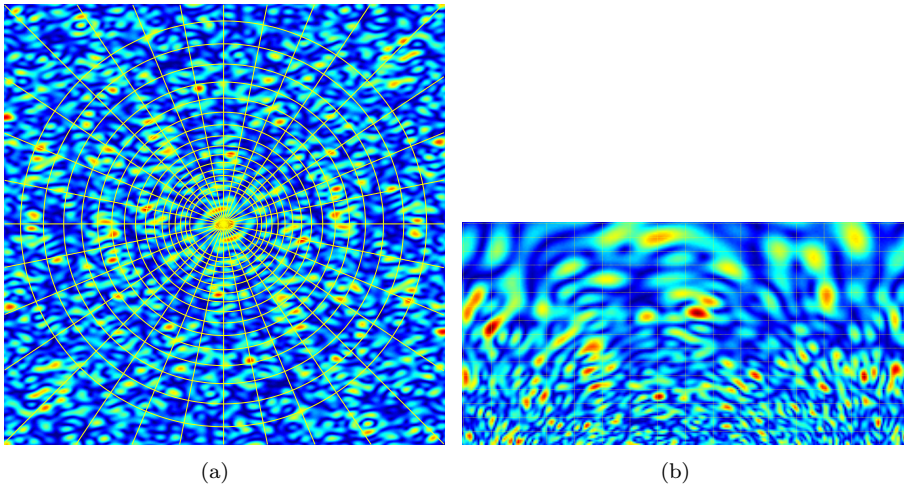
Fig. 3.2: Illustration of the polar-logarithmic sampling. (a) the Fourier spectrum in a Cartesian coordinate and a polar-logarithmic sampling grid; (b) the Fourier spectrum sampled on a polar-logarithmic grid.

(the two spectra appear to be from the same finger) or a 'non-match' (the two spectra appear to be from different fingers). Normally, in this step, we will first compute a number (similarity score) which corresponds to the degree of similarity. Then, by using a threshold, we can make a match/non-match decision [42].

### 3.2.3.1 Direct matching

Let $R(m, n)$ and $T(m, n)$ be the two sampled minutiae spectra in the polar-logarithmic domain respectively achieved from the *reference* fingerprint and *test* fingerprint. Both $R(m, n)$ and $T(m, n)$ are normalized to have zero mean and unit energy. As a similarity score, the correlation of two minutiae spectra was chosen, which is a common similarity measure in image processing. Therefore, the matching score between $R$ and $T$ is defined as:

$$S_{\mathrm{DM}}^{(R,T)} = \frac{1}{MN} \sum_{m,n} R(m,n)T(m,n). \qquad (3.14)$$

(a)


(b) Minutiae spectrum of (a)


(c)


(d) Minutiae spectrum of (c)


(e)


(f) Minutiae spectrum of (e)


(g)


(h) Minutiae spectrum of (g)
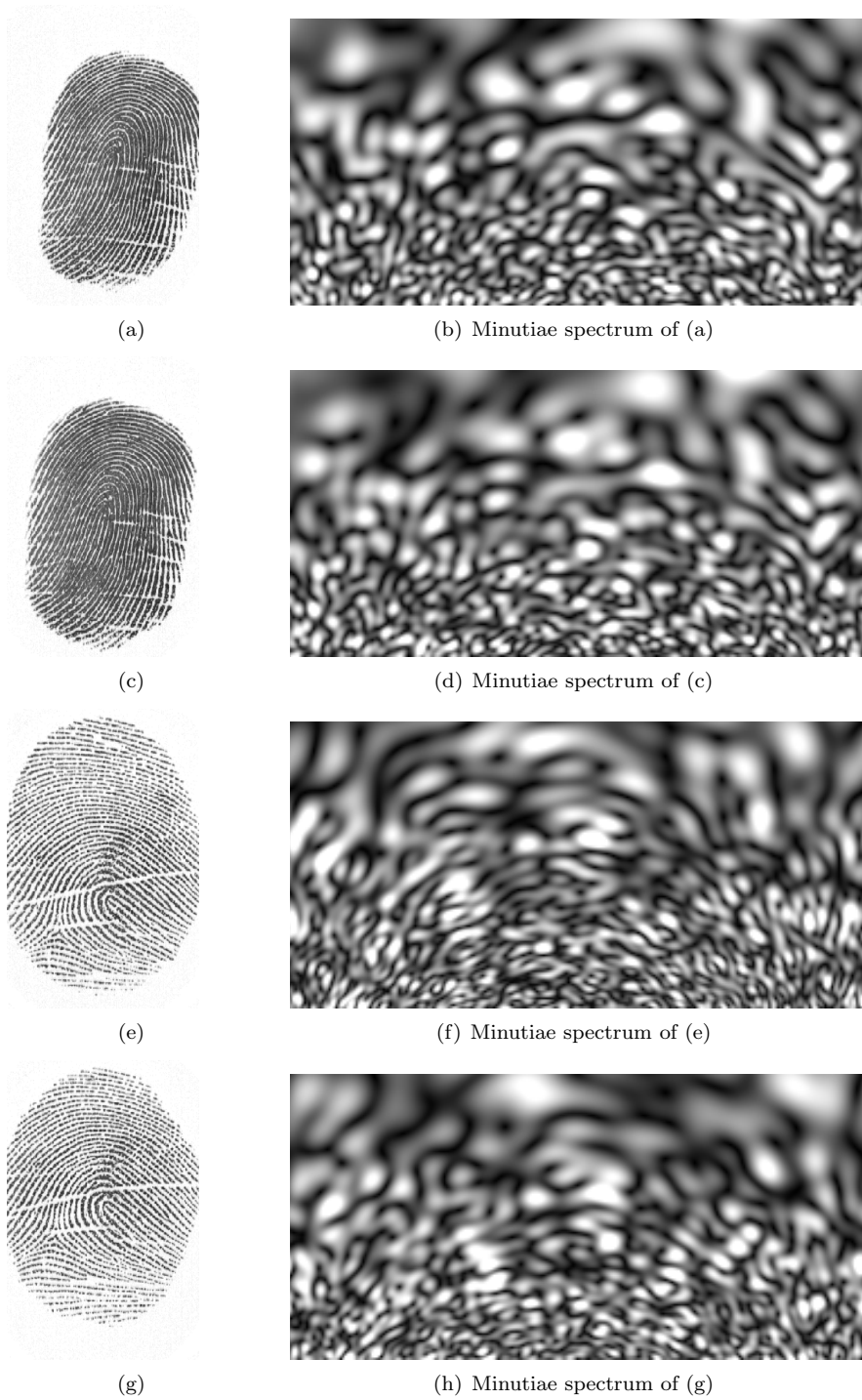
Fig. 3.3: Examples of minutiae spectra. (a) and (c) are fingerprints from the same finger; (e) and (g) are fingerprints from the same finger.

### 3.2.3.2    Weighted sum correlation matching

Let $R(m,n)$ and $T(m,n)$ be as defined in the previous subsection. The *line correlation* $C^{(R,T)}(m)$ of $R(m,n)$ and $T(m,n)$ is defined as

$$C^{(R,T)}(m) = \frac{1}{N} \sum_{n=1}^{N} R(m,n)T(m,n), \tag{3.15}$$

for $m = 1...M$, where $M = 128, N = 256$.

During matching, a weighted sum rule for the line correlation values is chosen as the similarity score of $R(m,n)$ and $T(m,n)$, which is defined as:

$$S_{\text{WSC}}^{(R,T)} = \frac{1}{M} \sum_{m=1}^{M} w(m)C^{(R,T)}(m), \tag{3.16}$$

with $w(m)$ the sum rule weight for the correlation value $C^{(R,T)}(m)$. The weights $w(m)$ need to be obtained by training. It is chosen as:

$$w(m) = \frac{\mu_G(m) - \mu_I(m)}{\sqrt{\sigma_G(m)\sigma_I(m)}}, \tag{3.17}$$

which is related to the detection index used in communication theory [62]. In (3.17), $\mu_G(m)$ and $\sigma_G(m)$ are the mean and the standard deviation of $C^{(R,T)}(m)$ in case $R$ and $T$ are from the same finger (a genuine pair), and $\mu_I(m)$ and $\sigma_I(m)$ are the mean and the standard deviation of $C^{(R,T)}(m)$ in case $R$ and $T$ are from different fingers (an imposter pair).

### 3.2.3.3    Fast rotation shift searching

In most fingerprint databases, there is no scaling difference between the fingerprints, or the scaling can be compensated for on the level of the minutiae sets [43]. Therefore, in practice only rotations have to be compensated for. This is done by testing a few rotations. Because we applied the polar-logarithmic transform to the Fourier spectra, the rotation becomes the circular shift in the horizontal direction in our minutiae spectra. We chose to test rotation from $-10°$ to $+10°$, which corresponds circular shifts from -15 units to +15 units in the polar-logarithmic domain. This rotation range is fingerprint data dependent. If big rotations appeared often in fingerprint samples, then a larger rotation range should be applied. Let $T_k(m,n)$ be defined as $T(m,n)$ with a circular shift $k$ in the horizontal direction. For each shift trial, a new similarity score $S^{(R,T_k)}$ is calculated using (3.14) or (3.16). Finally, the highest score is chosen as the final matching score and the corresponding shift $k$ is recorded as the best shift (that is, the best rotation).

We applied a fast search for the best shift. This algorithm consists of the following steps:

(1) 5 circular shifts ($k = -12, -6, 0, 6, 12$) are applied to $T(m, n)$ and the similarity scores $S^{(R,T_k)}$ are calculated. The maximum value of $S^{(R,T_k)}$ is denoted as $S_1$ and its corresponding shift $k$ is denoted as $k_1$;

(2) 2 circular shifts ($k = k_1 - 2, k_1 + 2$) are applied to $T(m, n)$, and the similarity scores $S^{(R,T_k)}$ are calculated. The maximum value of $S^{(R,T_k)}$ and $S_1$ is denoted as $S_2$, and its corresponding shift $k$ is denoted as $k_2$;

(3) 2 circular shifts ($k = k_2 - 1, k_2 + 1$) are applied to $T(m, n)$, and the similarity scores $S^{(R,T_k)}$ are calculated. The maximum value of $S^{(R,T_k)}$ and $S_2$ is denoted as $S_{\text{final}}$.

Using this fast rotation shift search algorithm, only 9 shift trials need to be tested, instead of 31 shift trials for an exhaustive search. After these steps, the value $S_{\text{final}}$ is recorded as the final matching score between $R$ and $T$. We tested both fast search and exhaustive search methods, and gained similar results. But, theoretically, this fast search solution is heuristic and may not give optimal results.

### 3.2.4　Results

#### 3.2.4.1　Measurements

We test the spectral minutiae representation in a verification setting. A verification system authenticates a person's identity by comparing the captured biometric characteristic with her own biometric template(s) pre-stored in the system. It conducts a one-to-one comparison to determine whether the identity claimed by the individual is true [35].

The matching performance of a fingerprint verification system is evaluated by means of several measures. The most commonly used are *the false acceptance rate* (FAR), *the false rejection rate* (FRR), and *the equal error rate* (EER). FAR is the probability that the system gives a 'match' decision for fingerprints that are not from the same finger. FRR is the probability that the system gives a 'non-match' decision for fingerprints that are from the same finger. When the decision threshold of a biometric security system is set so that the FAR and FRR are equal, the common value of FAR and FRR is referred to as the EER. For simplicity, we use EER as a performance indicator of our scheme.

The proposed algorithms have been evaluated by applying them to the MCYT Biometric Database [46]. We used the fingerprint data containing 3600 fingerprints. They were obtained from the first 30 individuals (person ID from 0000 to 0029 in MCYT). Each individual contributed data from 10 different fingers, and from each finger, 12 samples were collected using the optical sensor U.are.U from Digital Persona [63], with a resolution of 500dpi. The minutiae sets were obtained by the VeriFinger minutiae extractor [11].
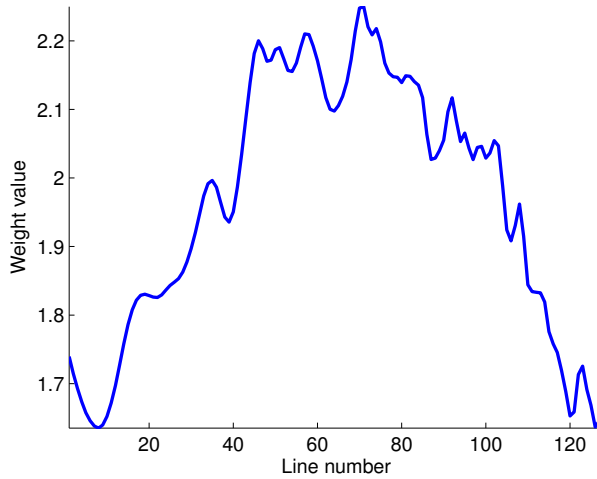
Fig. 3.4: The weights for each line correlation.

Among our fingerprint dataset, we used 1200 fingerprint samples from 10 individuals (person ID from 0020 to 0029 in MCYT) as a training set to calculate the weighted sum correlation weights (3.17), and 2400 fingerprint samples from 20 individuals (person ID from 0000 to 0019) as the test set.

For each comparison, we chose two fingerprints from the data set: one as a *reference* fingerprint, another one as a *test* fingerprint. For matching verification (genuine pairs), we used all the possible combinations, thus we have in total $10 \times 10 \times \binom{12}{2} = 6600$ genuine scores in the training set, and $20 \times 10 \times \binom{12}{2} = 13200$ genuine scores in the test set. For non-matching verification (imposter pairs), we compared each fingerprint with 10 randomly chosen samples from other individuals, thus we have in total $1200 \times 10 = 12000$ imposter scores in the training set, and $2400 \times 10 = 24000$ imposter scores in the test set.

The weights (3.17) for the weighted sum correlation matching that we obtained from the training set are shown in Figure 3.4. The EERs we achieved from the test dataset are shown in Table 3.1. The genuine and imposter distributions are shown in Figure 3.5. The FAR, FRR and DET (*Detection Error Trade-off*) curves are shown in Figure 3.6 and 3.7 respectively. In these figures, the matching scores are normalized to the interval [0,1] for a better comparison.

From Table 3.1, we can see that the weighted sum correlation matching (WSC) received a small improvement compared with the direct matching (DM). From Figure 3.5, the genuine score distributions for the two matching algorithms are almost overlapping, while the imposter scores from WSC are slightly lower. However, based on the very small difference in EERs, we cannot state that WSC is a better matching algorithm.

Table 3.1: Matching results (the test dataset).

| Matching method | EER |
|---|---|
| Direct matching (DM) | 3.21% |
| Weighted sum correlation (WSC) | 3.13% |
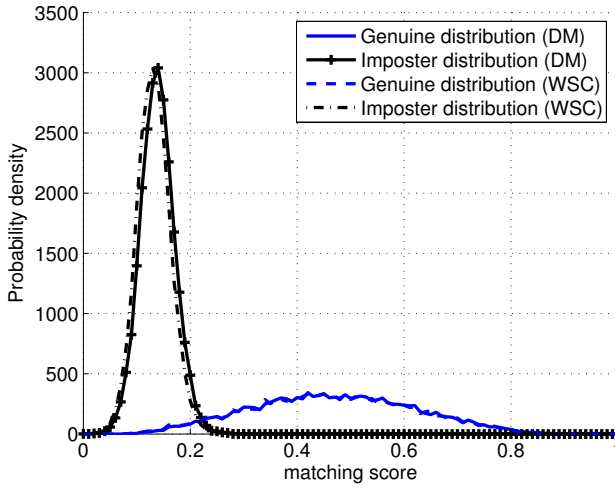


Fig. 3.5: Genuine and imposter distributions (the test dataset).
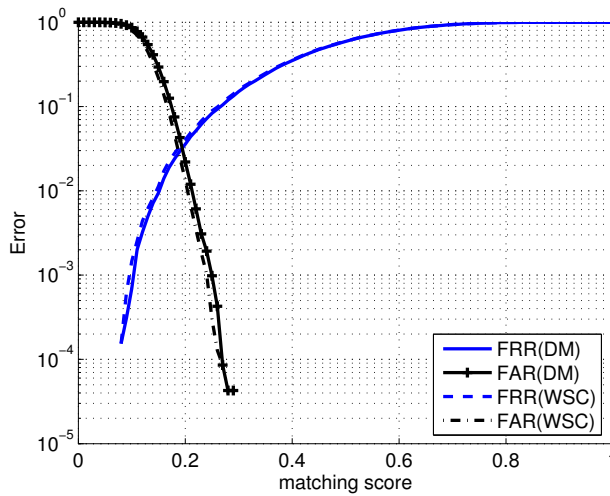


Fig. 3.6: FAR and FRR curves (the test dataset).
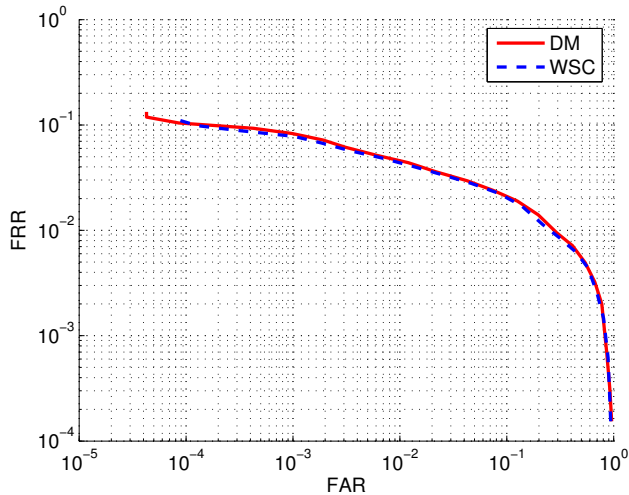
Fig. 3.7: DET curves (the test dataset).

To evaluate our algorithm, we compared our results with the ones from other finger-print recognition systems. From the academic domain, the MCYT organizer reports an EER with 5.5% using minutiae-based algorithm [46]. From the commercial domain, we tested the performance of VeriFinger from Neurotechnologija, whose algorithm achieved one of the best results in both FVC2006 and FpVTE 2003 from NIST [11]. VeriFinger received a much better result with an EER 0.34%. In our method, to combine with template protection schemes, we cannot perform an alignment between the reference and test minutiae sets, which is a crucial step for minutiae-based match-ing. This may cause the degradation of our algorithm. The comparison shows that although our result is acceptable for academic research, we still need to improve our algorithm to reach the security level of the current top fingerprint recognition systems.

### 3.2.5    Conclusion

The spectral minutiae representation is a new minutiae-based approach. Our method represents an unordered minutiae set as a fixed-length feature vector, which enables the combination of fingerprint recognition systems and template protection schemes. Moreover, this method avoids the minutiae registration difficulties by representing a minutiae set as a translation-invariant spectrum, in which the rotation and scaling become translations, so that they can be easily compensated for. In this paper, we also presented spectral minutiae matching algorithms and showed the experimental results. However, severe fingerprint non-linear distortions, noisy and missing minutiae can reduce the accuracy of our system. To make our method more robust to minutiae errors is our future work.

# 3.3 Spectral Minutiae Representations of Fingerprints Enhanced by Quality Data

**Abstract**

Many fingerprint recognition systems are based on minutiae matching. However, the recognition accuracy of minutiae-based matching algorithms is highly dependent on the fingerprint minutiae quality. Therefore, in this paper, we introduce a quality integrated spectral minutiae algorithm, in which the minutiae quality information is incorporated to enhance the performance of the spectral minutiae fingerprint recognition system. In our algorithm, two types of quality data are used. The first one is the minutiae reliability, expressing the probability that a given point is indeed a minutia; the second one is the minutiae location accuracy, quantifying the error on the minutiae location. We integrate these two types of quality information into the spectral minutiae representation algorithm and achieve a decrease in the equal error rate of over 20% in the experiment.

## 3.3.1 Introduction

Recognition of persons by means of biometric characteristics is gaining importance. Among various biometric techniques, such as face, signature and voice, the fingerprint has one of the highest levels of distinctiveness and performance [35] and it is the most commonly used biometric modality. Many fingerprint recognition systems are based on minutiae matching [7], [11]. Minutiae are the endpoints and bifurcations of fingerprint ridges. They are known to remain unchanged over an individual's lifetime and allow a very discriminative classification of fingerprints. The spectral minutiae representation [34] is a novel method to represent a minutiae set as a fixed-length feature vector, which is invariant to translation, and in which rotation and scaling become translations, so that they can be easily compensated for. These characteristics enable the combination of fingerprint recognition systems with template protection schemes[1] and allow for faster matching as well.

However, the recognition accuracy of minutiae-based matching algorithms is highly dependent on the fingerprint minutiae quality. Reference [64] shows that minutiae-based fingerprint recognition algorithms are less robust to the image quality degradation compared with image-based algorithms. Nowadays, investigating the influence of the fingerprint quality on recognition performances also gains more and more attention [65], [66].

The study presented in [34] shows that the spurious and missing minutiae or/and minutiae location errors can degrade the performance of the spectral minutiae recognition system. To cope with low quality fingerprints and to make the spectral minutiae

---

[1]Our method is designed to use in combination with template protection schemes that are based on fuzzy commitment and helper data schemes, such as [5] and [33], that require as an input a fixed-length feature vector representation of a biometric modality. Other template protection systems exist [32] [29] that do not pose this fixed-length feature vector requirement.

representation algorithm more robust against minutiae errors, we introduce *quality integrated spectral minutiae representations* of fingerprints, in which the quality information of minutiae is incorporated in the fingerprint representation to enhance the performance of the spectral minutiae fingerprint recognition system.

This paper is organized as follows. First, a review of the spectral minutiae representation is presented in Section 3.3.2. Next, in Section 3.3.3, the quality integrated spectral minutiae representations are introduced. Finally, Section 3.3.4 presents the experimental results and we draw conclusions in Section 3.3.5.

### 3.3.2 Background

The spectral minutiae representation is based on the shift, scale and rotation properties of the two-dimensional continuous Fourier transform. In [34], the concept of two representation methods are introduced: the *location-based spectral minutiae representation* (SML) and the *orientation-based spectral minutiae representation* (SMO).

#### 3.3.2.1 Spectral Minutiae Representations

Assume we have a fingerprint with $Z$ minutiae. In SML, with every minutia, a function $m_i(x, y) = \delta(x - x_i, y - y_i), i = 1, \ldots, Z$ is associated where $(x_i, y_i)$ represents the location of the $i$-th minutia in the fingerprint image. Thus, in the spatial domain, every minutia is represented by a Dirac pulse. The Fourier transform of $m_i(x, y)$ is given by:

$$\mathscr{F}\{m_i(x, y)\} = \exp(-\mathrm{j}(\omega_\mathrm{x} x_i + \omega_\mathrm{y} y_i)), \tag{3.18}$$

and the location-based spectral minutiae representation is defined as

$$\mathcal{M}_\mathrm{L}(\omega_\mathrm{x}, \omega_\mathrm{y}) = \sum_{i=1}^{Z} \exp(-\mathrm{j}(\omega_\mathrm{x} x_i + \omega_\mathrm{y} y_i)). \tag{3.19}$$

In order to reduce the sensitivity to small variations in minutiae locations in the spatial domain, we use a Gaussian low-pass filter to attenuate the higher frequencies. This multiplication in the frequency domain corresponds to a convolution in the spatial domain where every minutia is now represented by a Gaussian pulse.

Following the shift property of the Fourier transform, the magnitude of $\mathcal{M}$ is taken in order to make the spectrum invariant to translation of the input and we obtain

$$\left|\mathcal{M}_\mathrm{L}(\omega_\mathrm{x}, \omega_\mathrm{y}; \sigma_\mathrm{L}^2)\right| = \left|\exp\left(-\frac{\omega_\mathrm{x}^2 + \omega_\mathrm{y}^2}{2\sigma_\mathrm{L}^{-2}}\right) \sum_{i=1}^{Z} \exp(-\mathrm{j}(\omega_\mathrm{x} x_i + \omega_\mathrm{y} y_i))\right|. \tag{3.20}$$

The location-based spectral minutiae representation (SML) only uses the minutiae location information. However, including the minutiae orientation as well may give better discrimination. Therefore, it can be beneficial to also include the orientation information in our spectral representation. The orientation $\theta$ of a minutia can be incorporated by using the spatial derivative of $m(x, y)$ in the direction of the minutia orientation. Thus, to every minutia in a fingerprint, a function $m_i(x, y, \theta)$ is assigned being the derivative of $m_i(x, y)$ in the direction $\theta_i$, such that

$$\mathscr{F}\{m_i(x, y, \theta)\} = \mathrm{j}(\omega_\mathrm{x} \cos \theta_i + \omega_\mathrm{y} \sin \theta_i) \cdot \exp(-\mathrm{j}(\omega_\mathrm{x} x_i + \omega_\mathrm{y} y_i)). \tag{3.21}$$

As with the SML algorithm, using a Gaussian filter and taking the magnitude of the spectrum yields

$$\left| \mathcal{M}_\mathrm{O}(\omega_\mathrm{x}, \omega_\mathrm{y}; \sigma_\mathrm{O}^2) \right| = \left| \exp\left( -\frac{\omega_\mathrm{x}^2 + \omega_\mathrm{y}^2}{2\sigma_\mathrm{O}^{-2}} \right) \right.$$
$$\left. \sum_{i=1}^{Z} \mathrm{j}(\omega_\mathrm{x} \cos \theta_i + \omega_\mathrm{y} \sin \theta_i) \cdot \exp(-\mathrm{j}(\omega_\mathrm{x} x_i + \omega_\mathrm{y} y_i)) \right|. \tag{3.22}$$

In order to obtain the final spectral representations, the continuous spectra (3.20) and (3.22) are sampled on a polar-logarithmic grid. In the radial direction $\lambda$, we use $M = 128$ samples between $\lambda_\mathrm{l} = 0.1$ and $\lambda_\mathrm{h} = 0.6$. In the angular direction $\beta$, we use $N = 256$ samples uniformly distributed between $\beta = 0$ and $\beta = \pi$. Because of the symmetry of the Fourier transform for real-valued functions, using the interval between 0 and $\pi$ is sufficient. This polar-logarithmic sampling process is illustrated in Figures 3.8 and 3.9. For each spectrum, the horizontal axis represents the rotation angle of the spectral magnitude (from 0 to $\pi$); the vertical axis represents the frequency of the spectral magnitude (the frequency increases from top to bottom). The resulting representation in the polar-logarithmic domain is invariant to translation, while rotation and scaling of the input have become translations along the polar-logarithmic coordinates.

### 3.3.2.2  Spectral Minutiae Matching

Let $R(m, n)$ and $T(m, n)$ be the two sampled minutiae spectra respectively achieved from the *reference* fingerprint and *test* fingerprint. Both $R(m, n)$ and $T(m, n)$ are normalized to have zero mean and unit energy. We use the two-dimensional correlation coefficient between $R$ and $T$ as a measure of their similarity.

In practice, the input fingerprint images are rotated and might be scaled (for example, depending on the sensor that is used to acquire an image). Assume that the scaling has already been compensated for on the level of the minutiae sets [43]. Then we
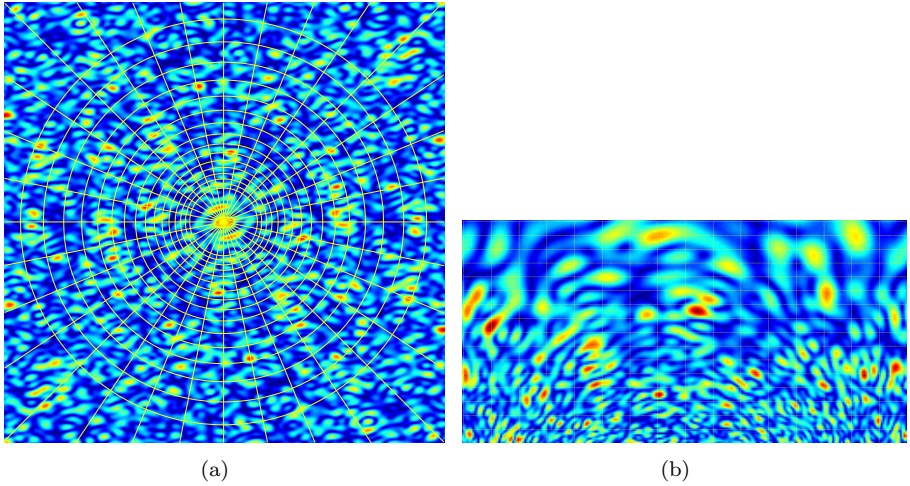
Fig. 3.8: Illustration of the polar-logarithmic sampling (SML spectra). (a) the Fourier spectrum in a Cartesian coordinate and a polar-logarithmic sampling grid; (b) the Fourier spectrum sampled on a polar-logarithmic grid.
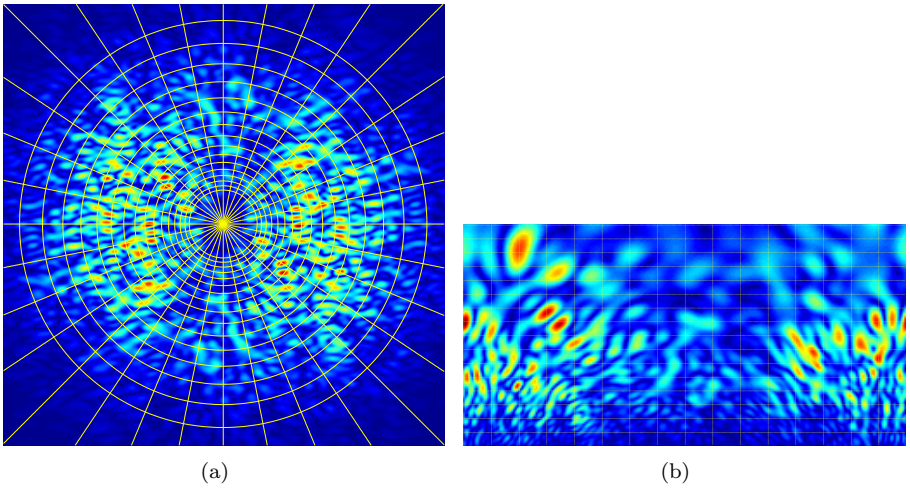


Fig. 3.9: Illustration of the polar-logarithmic sampling (SMO spectra). (a) the Fourier spectrum in a Cartesian coordinate and a polar-logarithmic sampling grid; (b) the Fourier spectrum sampled on a polar-logarithmic grid.

only need to test a few rotations, which become the circular shifts in the horizontal direction. We denote $T(m, n - n_{cs})$ as a circular shifted version of $T(m, n)$. We use the fast rotation shift searching algorithm that was presented in [56][2] and choose the maximum score of the different combinations as the final matching score between $R$ and $T$,

$$S^{(R,T)} = \max_{n_{cs}} \{ \frac{1}{MN} \sum_{m,n} R(m,n)T(m, n - n_{cs}) \},$$
$$-15 \leq n_{cs} \leq 15. \qquad (3.23)$$

### 3.3.3    Quality Integrated Spectral Minutiae Representations

In order to improve the performance of the spectral minutiae representation, we incorporate minutiae quality data in the calculation of the spectral minutiae. Minutiae quality is described by two numbers. The first one is the *minutiae reliability* (QM), expressing the probability that a given point is indeed a minutia. This measure is recorded following the specification of the minutiae template standard ISO/IEC 19794-2 [43]: the quality figure ranges from 100 as a maximum to 1 as a minimum. The other quality data we incorporated is the *minutiae location accuracy* (QL), quantifying the error on the minutiae location. This measure is defined as the radius, in pixels, of a circle from the found minutiae position, within which the minutiae position is located. It is provided by a proprietary algorithm.

#### 3.3.3.1    Using Quality of Minutiae Reliability (QM)

The quality of minutiae reliability (QM) gives the certainty that a given point is indeed a minutia. We use it in the spectral minutiae representation by weighing the Dirac pulse assigned to each minutia. For each minutia, the weight $w$ depends linearly on the minutiae reliability quality $q_M$. A higher $q_M$ (which means a minutia with higher reliability) corresponds to a higher weight $w$. Then, SML in (3.20) becomes

$$\left| \mathcal{M}_L(\omega_x, \omega_y; \sigma_L^2) \right| = \left| \exp\left( -\frac{\omega_x^2 + \omega_y^2}{2\sigma_L^{-2}} \right) \sum_{i=1}^{Z} w_i \exp(-j(\omega_x x_i + \omega_y y_i)) \right|, \qquad (3.24)$$

and SMO in (3.22) becomes

---

[2]In [56], totaly 9 rotations are tested in a range of $-10\,^{\circ}$ to $+10\,^{\circ}$ in case of $N = 256$ samples between 0 to $\pi$.

$$\left|\mathcal{M}_{\mathrm{O}}(\omega_{\mathrm{x}},\omega_{\mathrm{y}};\sigma_{\mathrm{O}}^2)\right| = \left|\exp\left(-\frac{\omega_{\mathrm{x}}^2+\omega_{\mathrm{y}}^2}{2\sigma_{\mathrm{O}}^{-2}}\right)\right.$$

$$\left.\sum_{i=1}^{Z}\mathrm{j}(\omega_{\mathrm{x}}\cos\theta_i+\omega_{\mathrm{y}}\sin\theta_i)\cdot w_i\exp(-\mathrm{j}(\omega_{\mathrm{x}}x_i+\omega_{\mathrm{y}}y_i))\right|. \tag{3.25}$$

Equations (3.24) and (3.25) are the expressions of the minutiae reliability incorporated SML and SMO.

### 3.3.3.2 Using Quality of Minutiae Location Accuracy (QL)

The quality of minutiae location accuracy (QL) quantifies the error on the minutiae location. As we mentioned in Section 3.3.2, we use a Gaussian low-pass filter to attenuate the higher frequencies in the minutiae spectrum in order to reduce the sensitivity to the minutiae location errors in the spatial domain. Therefore, we use this minutiae location quality measure to adjust the Gaussian parameters $\sigma_{\mathrm{L}}$ and $\sigma_{\mathrm{O}}$ in the spectral minutiae representations. For each minutia, the Gaussian parameter $\sigma$ depends linearly on the minutiae location accuracy $q_{\mathrm{L}}$. A higher $q_{\mathrm{L}}$ (which means a minutia with lower location accuracy) corresponds to a higher $\sigma$. Then, SML in (3.20) becomes

$$\left|\mathcal{M}_{\mathrm{L}}(\omega_{\mathrm{x}},\omega_{\mathrm{y}})\right| = \left|\sum_{i=1}^{Z}\exp\left(-\frac{\omega_{\mathrm{x}}^2+\omega_{\mathrm{y}}^2}{2\sigma_{\mathrm{L}i}^{-2}}\right)\cdot\exp(-\mathrm{j}(\omega_{\mathrm{x}}x_i+\omega_{\mathrm{y}}y_i))\right|, \tag{3.26}$$

and SMO in (3.22) becomes

$$\left|\mathcal{M}_{\mathrm{O}}(\omega_{\mathrm{x}},\omega_{\mathrm{y}})\right| = \left|\sum_{i=1}^{Z}\exp\left(-\frac{\omega_{\mathrm{x}}^2+\omega_{\mathrm{y}}^2}{2\sigma_{\mathrm{O}i}^{-2}}\right)\right.$$

$$\left.\mathrm{j}(\omega_{\mathrm{x}}\cos\theta_i+\omega_{\mathrm{y}}\sin\theta_i)\cdot\exp(-\mathrm{j}(\omega_{\mathrm{x}}x_i+\omega_{\mathrm{y}}y_i))\right|. \tag{3.27}$$

Equations (3.26) and (3.27) are the expressions of the minutiae location accuracy incorporated SML and SMO.

### 3.3.3.3 Using both QM and QL

If we incorporate both QM and QL following the algorithms presented in 3.3.3.1 and 3.3.3.2, we obtain SML in (3.20) as

$$|\mathcal{M}_{\mathrm{L}}(\omega_{\mathrm{x}}, \omega_{\mathrm{y}})| = \left| \sum_{i=1}^{Z} \exp\left( -\frac{\omega_{\mathrm{x}}^2 + \omega_{\mathrm{y}}^2}{2\sigma_{\mathrm{L}i}^{-2}} \right) \cdot w_i \exp(-\mathrm{j}(\omega_{\mathrm{x}} x_i + \omega_{\mathrm{y}} y_i)) \right|, \qquad (3.28)$$

and SMO in (3.22) as

$$|\mathcal{M}_{\mathrm{O}}(\omega_{\mathrm{x}}, \omega_{\mathrm{y}})| = \left| \sum_{i=1}^{Z} \exp\left( -\frac{\omega_{\mathrm{x}}^2 + \omega_{\mathrm{y}}^2}{2\sigma_{\mathrm{O}i}^{-2}} \right) \right.$$
$$\left. \mathrm{j}(\omega_{\mathrm{x}} \cos\theta_i + \omega_{\mathrm{y}} \sin\theta_i) \cdot w_i \exp(-\mathrm{j}(\omega_{\mathrm{x}} x_i + \omega_{\mathrm{y}} y_i)) \right|. \qquad (3.29)$$

Equations (3.28) and (3.29) are the expressions of the quality integrated SML and SMO.

### 3.3.4   Experiments

We test the quality integrated spectral minutiae representations (Equations (3.24) to (3.29)) in a verification setting. The matching performance of a fingerprint verification system can be evaluated by the *false acceptance rate* (FAR), the *false rejection rate* (FRR), and the *equal error rate* (EER). When the decision threshold of a biometric security system is set such that the FAR and FRR are equal, the common value of FAR and FRR is referred to as the EER. In this paper, we use FAR, EER and the *genuine acceptance rate* (GAR), GAR= 1−FRR, as performance indicators of our scheme.

The proposed algorithms are evaluated on the FVC2002-DB2 [48] fingerprint database. The minutiae sets including the minutiae quality data are extracted by a proprietary method. The experiment is implemented following the experimental setting and test protocol in [34][3]. A correlation based matching algorithm is used and a score level sum rule for SML and SMO is applied.

From our experiments, we noticed that for SML and SMO, we need to choose different Gaussian parameters ($\sigma_{\mathrm{L}}$ and $\sigma_{\mathrm{O}}$) to achieve the best performances. Figures 3.10 and 3.11 show the influence of the Gaussian parameter $\sigma$ to the performances of SML and SMO[4]. We noticed that the Gaussian parameter has larger effects on SML than on SMO. Moreover, a Gaussian kernel is needed for SMO for achieving a better performance, while for SML it is not. The reason is that because the minutiae orientation is

---

[3]In [34], for each fingerprint, maximum two cores or/and two deltas were used to improve the performance. In this paper, only the upper core is used as a reference point to enhance the recognition accuracy.

[4]Figures 3.10 and 3.11 are acquired by the experiments on the MCYT fingerprint database in [34]. The influence of the Gaussian parameter $\sigma$ to the SML and SMO performances is similar for different fingerprint databases.
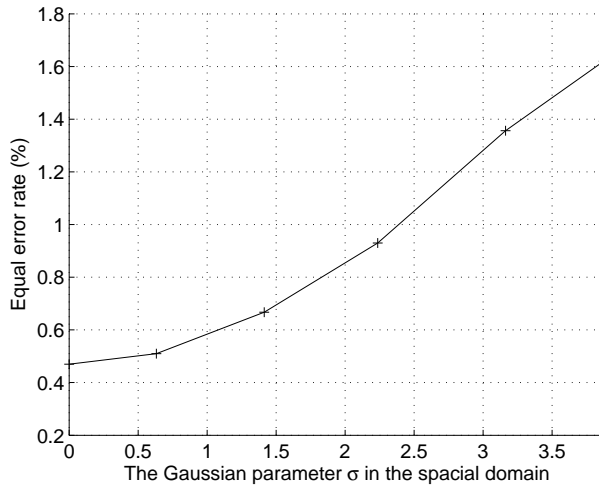
Fig. 3.10: Relationship of the Gaussian parameter $\sigma$ (in the spacial domain) and SML performances (MCYT VeriFinger minutiae set in [34]).
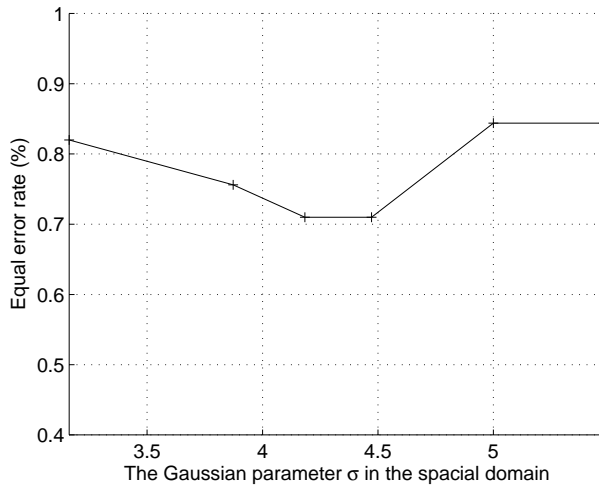


Fig. 3.11: Relationship of the Gaussian parameter $\sigma$ (in the spacial domain) and SMO performances (MCYT VeriFinger minutiae set in [34]).
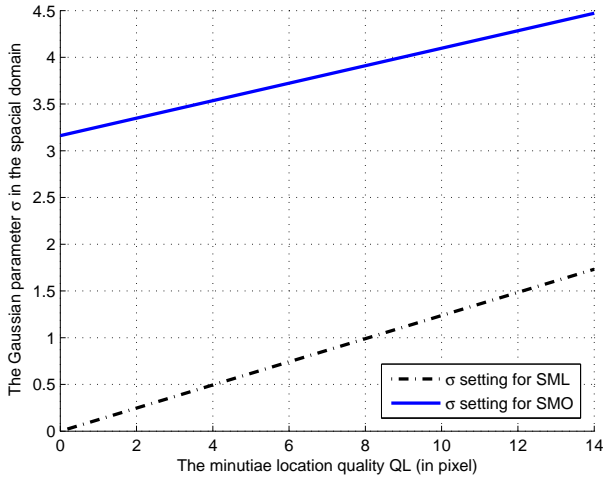
Fig. 3.12: Relationship of the Gaussian parameter $\sigma$ and the minutiae location quality QL.

incorporated as a derivative of the delta function (see Equation (3.21)), this will amplify the noise (both in minutiae location and orientation) in the high frequency part in SMO. Therefore, a Gaussian kernel is needed for SMO to attenuate the higher frequencies. In SML, the high frequency part contains discriminative information, while the noise is evenly distributed in all frequencies, therefore, a Gaussian kernel does not help for a better performance. In our experiments, when no minutiae location quality is incorporated, we chose $\sigma = 0$ for SML (in this case, no multiplication with Gaussian in the frequency domain) and $\sigma = 4.24$ for SMO. In case the fingerprint resolution is 569dpi (the FVC2002-DB2 database), the Gaussian parameter $\sigma = 4.24$(pixel) in the spacial domain is about 0.19(mm) in reality. When incorporating the minutiae location accuracy (QL), we use the linear relationships shown in Figure 3.12 to adjust the Gaussian parameter $\sigma$ according to the minutiae location quality.

The final recognition performances are shown in Table 3.2 and the ROC curves are shown in Figure 3.13. From the results, we can see that the recognition performance of the spectral minutiae representation improves after incorporating the minutiae reliability quality (QM). However, the improvement by using minutiae location accuracy (QL) is very limited. This may result from the low reliability of the minutiae location accuracy quality data. In Figure 3.14, we further illustrate the genuine and imposter matching score densities of different cases. From the matching score densities, we can notice that after incorporating the quality data, the imposter score densities are almost keep the same, while the genuine scores are increased. This also explains the enhancements in recognition accuracy after integrating the quality data into the spectral minutiae representations. By incorporating both quality data (QM and QL), we achieve a decrease of more than 20% in equal error rate in the experiment.

Table 3.2: Results on the FVC2002-DB2 database.

| Methods | EER | GAR | | |
|---------|-----|-----------|-------------|-----------|
|  |  | FAR = 1% | FAR = 0.1% | FAR = 0% |
| No quality | 4.5% | 94.2% | 91.7% | 88.8% |
| QM | 3.7% | 95.2% | 93.5% | 90.5% |
| QL | 4.0% | 94.3% | 92.0% | 89.0% |
| QM & QL | 3.5% | 95.2% | 93.2% | 91.0% |
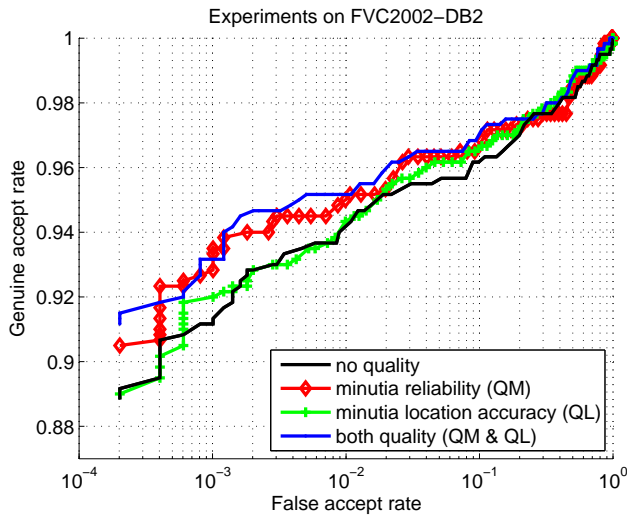


Fig. 3.13: ROC curves on FVC2002-DB2 for different cases.
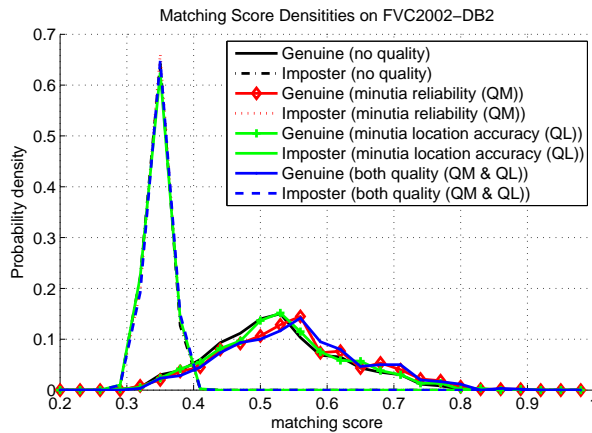


Fig. 3.14: Matching score densities on FVC2002-DB2 for different cases.

### 3.3.5 Conclusions

In fingerprint recognition systems, low quality fingerprints are unavoidable. To make the spectral minutiae representation system more robust against minutiae errors, we incorporate minutiae quality in the calculation of the spectral minutiae representation. In this paper, we introduce two methods to incorporate minutiae reliability (QM) and minutiae location accuracy (QL) respectively. The experiments show that the performance of the spectral minutiae representation can be improved by using the minutiae quality data. The QM incorporated spectral minutiae representation shows better results than the QL incorporated spectral minutiae representation. By using both quality data, we achieve overall the best result.

This paper presents the advantage of incorporating quality data in the spectral minutiae representation system. The proposed methods only vary the minutiae representations, while keeping the matching algorithm unchanged, so that they can be easily integrated in the spectral minutiae recognition system. Our future work will be the interoperability study of using quality data and algorithm optimization of incorporating the minutiae quality data to enhance the recognition performance.

## 3.4 Spectral Representations of Fingerprint Minutiae Subsets

**Abstract**

The investigation of the privacy protection of biometric templates gains more and more attention. The spectral minutiae representation is a novel method to represent a minutiae set as a fixed-length feature vector, which is invariant to translation, and in which rotation and scaling become translations, so that they can be easily compensated for. These characteristics enable the combination of fingerprint recognition systems with template protection schemes that require as an input a fixed-length feature vector. However, the limited overlap of a fingerprint pair can reduce the performance of the spectral minutiae representation algorithm. Therefore, in this paper, we introduce the spectral representations of fingerprint minutiae subsets to cope with the limited overlap problem. In the experiment, we improve the recognition performance from 0.32% to 0.12% in equal error rate after applying the spectral representations of minutiae subsets algorithm.

### 3.4.1 Introduction

Biometrics technologies are developing rapidly in order to meet high security requirements. Among various biometric characteristics, such as face, signature and voice, the fingerprint has higher levels of distinctiveness and performance [35] and it is the most commonly used biometric modality. Many fingerprint recognition systems are based on the use of a minutiae set [7], [11]. Minutiae are the endpoints and bifurcations of

fingerprint ridges. They are known to remain unchanged over an individual's lifetime and allow a very discriminative classification of fingerprints.

In the recent years, the privacy protection of biometric templates has drawn more and more attention of researchers [26], [27]. To enable the combination of fingerprint recognition systems with recently developed template protection schemes based on fuzzy commitment and helper data schemes, such as [5] and [33], a fixed-length feature vector representation of a biometric modality is required as an input[5]. The spectral minutiae [34] represents a minutiae set as a fixed-length feature vector, which is invariant to translation, and in which rotation and scaling become translations. These characteristics enable the combination of fingerprint recognition systems with template protection schemes and allow for faster matching as well.

However, in template protection systems where encrypted templates are stored, it is not possible to align the *reference* and *test* fingerprints using minutiae information in the spectral minutiae fingerprint recognition system. The study presented in [34] shows that the recognition errors occur when the percentage of corresponding minutiae is below 75 in an *ideal* situation (that is, no other errors present such as spurious and missing minutiae, minutiae location errors). Therefore, the limited overlap between a fingerprint pair can degrade the recognition performance of the spectral minutiae fingerprint recognition system. Some fingerprint recognition algorithms use reference points (such as core, delta) to pre-align fingerprints [5], [32]. However, these methods have problems to cope with. First, some fingerprints do not have such reference points. Second, the reference points may not appear in the fingerprint images during acquisition. Third, the reference points detector may fail to locate the points.

Therefore, in this paper, we present a *spectral representation of minutiae subset* algorithm to cope with the limited overlap problem, that does not rely on reference points. In this method, we generate several subsets from *one* minutiae set and then apply the spectral minutiae representation to the subsets. The corresponding minutiae percentage between the minutiae subsets can increase. In this way, by applying the spectral representations of minutiae subsets, our system is more robust against the limited overlap problem.

This paper is organized as follows. First, a review of the spectral minutiae representation is presented in Section 3.4.2. Next, in Section 3.4.3, the spectral representations of minutiae subsets algorithm is introduced. Finally, Section 3.4.4 presents the experimental results and we draw conclusions in Section 3.4.5.

## 3.4.2 Background

The spectral minutiae representation is based on the shift, scale and rotation properties of the two-dimensional continuous Fourier transform. In [34], the concept of and algorithms for two representation methods are introduced: the *location-based*

---

[5]Other template protection systems exist [32] that do not pose this fixed-length feature vector requirement.

(a)                                                        (b)
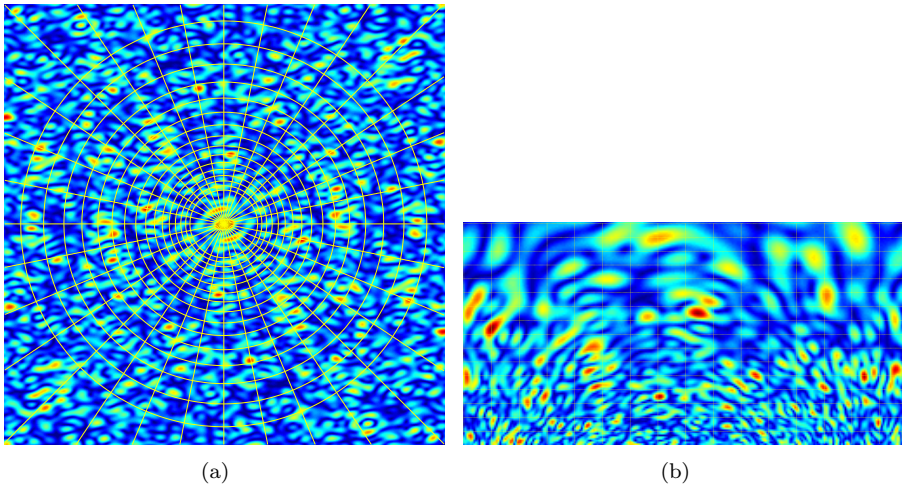
Fig. 3.15: Illustration of the polar-logarithmic sampling (SML spectra). (a) the Fourier spectrum in a Cartesian coordinate and a polar-logarithmic sampling grid; (b) the Fourier spectrum sampled on a polar-logarithmic grid.

*spectral minutiae representation* (SML) and the *orientation-based spectral minutiae representation* (SMO).

### 3.4.2.1   Spectral Minutiae Representations

Assume we have a fingerprint with $Z$ minutiae. In SML, with every minutia, a function $m_i(x, y) = \delta(x - x_i, y - y_i), i = 1, \ldots, Z$ is associated where $(x_i, y_i)$ represents the location of the $i$-th minutia in the fingerprint image. Thus, in the spatial domain, every minutia is represented by a Dirac pulse. The Fourier transform of $m_i(x, y)$ is given by:

$$\mathscr{F}\{m_i(x, y)\} = \exp(-\mathrm{j}(\omega_\mathrm{x} x_i + \omega_\mathrm{y} y_i)), \tag{3.30}$$

and the location-based spectral minutiae representation is defined as

$$\mathcal{M}_\mathrm{L}(\omega_\mathrm{x}, \omega_\mathrm{y}) = \sum_{i=1}^{Z} \exp(-\mathrm{j}(\omega_\mathrm{x} x_i + \omega_\mathrm{y} y_i)). \tag{3.31}$$

In order to reduce the sensitivity to small variations in minutiae locations in the spatial domain, we use a Gaussian low-pass filter to attenuate the higher frequencies. This multiplication in the frequency domain corresponds to a convolution in the spatial domain where every minutia is now represented by a Gaussian pulse.
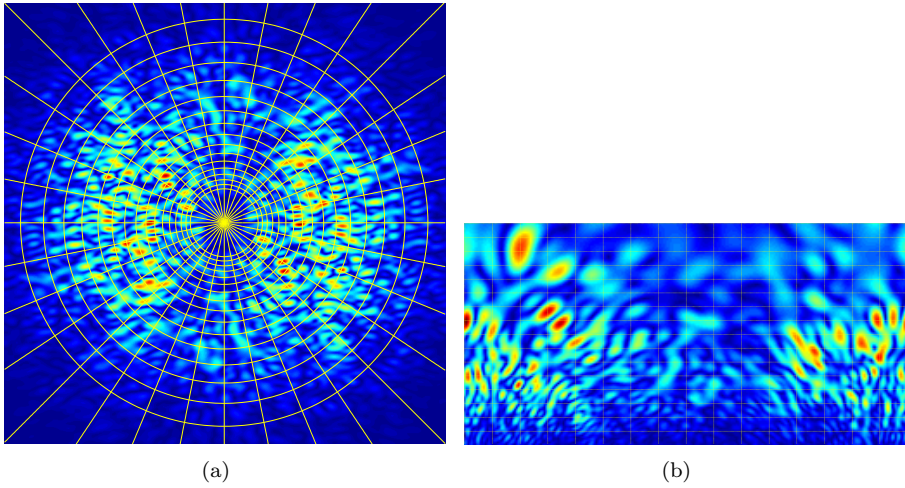
Fig. 3.16: Illustration of the polar-logarithmic sampling (SMO spectra). (a) the Fourier spectrum in a Cartesian coordinate and a polar-logarithmic sampling grid; (b) the Fourier spectrum sampled on a polar-logarithmic grid.

Following the shift property of the Fourier transform, the magnitude of $\mathcal{M}$ is taken in order to make the spectrum invariant to translation of the input and we obtain

$$\left| \mathcal{M}_{\mathrm{L}}(\omega_{\mathrm{x}}, \omega_{\mathrm{y}}; \sigma_{\mathrm{L}}^2) \right| = \left| \exp\left( -\frac{\omega_{\mathrm{x}}^2 + \omega_{\mathrm{y}}^2}{2\sigma_{\mathrm{L}}^{-2}} \right) \sum_{i=1}^{Z} \exp(-\mathrm{j}(\omega_{\mathrm{x}} x_i + \omega_{\mathrm{y}} y_i)) \right|. \qquad (3.32)$$

The location-based spectral minutiae representation (SML) only uses the minutiae location information. However, including the minutiae orientation as well may give better discrimination. Therefore, it can be beneficial to also include the orientation information in our spectral representation. The orientation $\theta$ of a minutia can be incorporated by using the spatial derivative of $m(x, y)$ in the direction of the minutia orientation. Thus, to every minutia in a fingerprint, a function $m_i(x, y, \theta)$ is assigned being the derivative of $m_i(x, y)$ in the direction $\theta_i$, such that

$$\mathscr{F}\{m_i(x, y, \theta)\} = \mathrm{j}(\omega_{\mathrm{x}} \cos\theta_i + \omega_{\mathrm{y}} \sin\theta_i) \cdot \exp(-\mathrm{j}(\omega_{\mathrm{x}} x_i + \omega_{\mathrm{y}} y_i)). \qquad (3.33)$$

As in the SML algorithm, using a Gaussian filter and taking the magnitude of the spectrum yields

$$\left| \mathcal{M}_{\mathrm{O}}(\omega_{\mathrm{x}}, \omega_{\mathrm{y}}; \sigma_{\mathrm{O}}^2) \right| = \left| \exp\left( -\frac{\omega_{\mathrm{x}}^2 + \omega_{\mathrm{y}}^2}{2\sigma_{\mathrm{O}}^{-2}} \right) \right.$$

$$\left. \sum_{i=1}^{Z} \mathrm{j}(\omega_{\mathrm{x}} \cos\theta_i + \omega_{\mathrm{y}} \sin\theta_i) \cdot \exp(-\mathrm{j}(\omega_{\mathrm{x}} x_i + \omega_{\mathrm{y}} y_i)) \right|. \qquad (3.34)$$

In order to obtain the final spectral representations, the continuous spectra (3.32) and (3.34) are sampled on a polar-logarithmic grid. In the radial direction $\lambda$, we use $M = 128$ samples between $\lambda_{\mathrm{l}} = 0.1$ and $\lambda_{\mathrm{h}} = 0.6$. In the angular direction $\beta$, we use $N = 256$ samples uniformly distributed between $\beta = 0$ and $\beta = \pi$. Because of the symmetry of the Fourier transform for real-valued functions, using the interval between 0 and $\pi$ is sufficient. This polar-logarithmic sampling process is illustrated in Figures 3.15 and 3.16. For each spectrum, the horizontal axis represents the rotation angle of the spectral magnitude (from 0 to $\pi$); the vertical axis represents the frequency of the spectral magnitude (the frequency increases from top to bottom). The resulting representation in the polar-logarithmic domain is invariant to translation, while rotation and scaling of the input have become translations along the polar-logarithmic coordinates.

### 3.4.2.2    Spectral Minutiae Matching

Let $R(m,n)$ and $T(m,n)$ be the two sampled minutiae spectra in the polar-logarithmic domain respectively achieved from the *reference* fingerprint and *test* fingerprint. Both $R(m,n)$ and $T(m,n)$ are normalized to have zero mean and unit energy. We use the two-dimensional correlation coefficient between $R$ and $T$ as a measure of their similarity.

In practice, the input fingerprint images are rotated and might be scaled (for example, depending on the sensor that is used to acquire an image). Since the minutiae spectra are translation invariant, but not rotation and scaling invariant, this method has to test a few different combinations of rotation and scaling, which are translations in the minutiae spectra. To be specific, the scaling becomes the shift (or translation) in the vertical direction, and the rotation becomes the circular shift in the horizontal direction. We denote $T(m - i, n - j)$ as a shifted version of $T(m,n)$, with a shift of $i$ in the vertical direction and a circular shift $j$ in the horizontal direction. Then, the correlation coefficient between $R$ and $T$ is defined as:

$$C^{(R,T)}(i,j) = \frac{1}{MN} \sum_{m,n} R(m,n) T(m - i, n - j). \qquad (3.35)$$

In most fingerprint databases, there is no scaling difference between the fingerprints, or the scaling can be compensated for on the level of the minutiae sets [43]. Therefore, in

practice only a few rotations need to be tested. We use the fast rotation shift searching algorithm that was presented in [56] (which tests 9 rotation possibilities in a range of $-10\,^\circ$ to $+10\,^\circ$) and finally the maximum score from the different combinations is the final matching score between $R$ and $T$,

$$S^{(R,T)} = \max_j \{C^{(R,T)}(0,j)\},\ -15 \le j \le 15. \tag{3.36}$$

### 3.4.3 Spectral Representations of Minutiae Subsets

#### 3.4.3.1 Fingerprint Minutiae Subsets Generation

In this method, we generate several minutiae subsets from one minutiae set by selecting minutiae in a number of rectangular areas of the same size.

Assume we have a minutiae set $M_{\mathrm{all}}$ with $Z$ minutiae, $\{(x_i, y_i)\}, i = 1, \ldots, Z$, with $(x_i, y_i)$ the location of the $i$-th minutia. Let $x_{\min}, x_{\max}, y_{\min}, y_{\max}$ denote the boundaries of the minutiae locations and $d_{\mathrm{x}}, d_{\mathrm{y}}$ the sides length of the fixed size rectangular area. Then, we can generate four minutiae subsets $M_{\mathrm{ul}}, M_{\mathrm{ur}}, M_{\mathrm{bl}}$ and $M_{\mathrm{br}}$ at the upper-left (ul), upper-right (ur), bottom-left (bl), bottom-right (br) part of the minutiae set, as

$$
\begin{aligned}
M_{\mathrm{ul}} &= \{(x,y)|x_{\min} \le x \le x_{\min} + d_{\mathrm{x}}, y_{\min} \le y \le y_{\min} + d_{\mathrm{y}}\}, \\
M_{\mathrm{ur}} &= \{(x,y)|x_{\max} - d_{\mathrm{x}} \le x \le x_{\max}, y_{\min} \le y \le y_{\min} + d_{\mathrm{y}}\}, \\
M_{\mathrm{bl}} &= \{(x,y)|x_{\min} \le x \le x_{\min} + d_{\mathrm{x}}, y_{\max} - d_{\mathrm{y}} \le y \le y_{\max}\}, \\
M_{\mathrm{br}} &= \{(x,y)|x_{\max} - d_{\mathrm{x}} \le x \le x_{\max}, y_{\max} - d_{\mathrm{y}} \le y \le y_{\max}\}.
\end{aligned}
$$

This procedure is illustrated in Figure 3.17.

#### 3.4.3.2 Matching Procedure

During the enrollment, the spectral minutiae representations of the *reference* minutiae set $M_{\mathrm{ref,all}}$ and its subsets $M_{\mathrm{ref,ul}}, M_{\mathrm{ref,ur}}, M_{\mathrm{ref,bl}}, M_{\mathrm{ref,br}}$ are stored as templates, denoted as $R_{\mathrm{all}}, R_{\mathrm{ul}}, R_{\mathrm{ur}}, R_{\mathrm{bl}}, R_{\mathrm{br}}$, respectively. During the verification, we use the following procedure to verify the *test* fingerprint.

1. The spectral minutiae representations of the test minutiae set $M_{\mathrm{test,all}}$ and its subsets $M_{\mathrm{test,ul}}, M_{\mathrm{test,ur}}, M_{\mathrm{test,bl}}, M_{\mathrm{test,br}}$ are taken respectively, denoted as $T_{\mathrm{all}}, T_{\mathrm{ul}}, T_{\mathrm{ur}}, T_{\mathrm{bl}}$ and $T_{\mathrm{br}}$.

2. Calculate the matching score $S_{\mathrm{all}}$ between $R_{\mathrm{all}}$ and $T_{\mathrm{all}}$ following Equation (3.36), $S_{\mathrm{all}} = S^{(R_{\mathrm{all}}, T_{\mathrm{all}})}$.
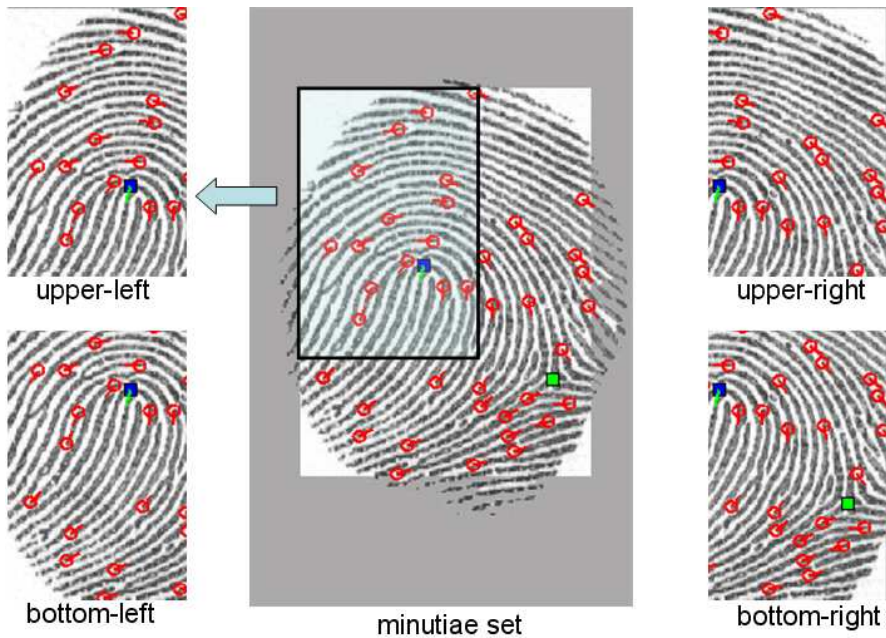
Fig. 3.17: Illustration of one minutiae set and its four subsets.

3. Calculate 16 matching scores between minutiae subsets and take the largest score as the spectral minutiae subsets score $S_{\mathrm{sub}}$, that is,

$$S_{\mathrm{sub}} = \max_{R,T}\{S^{(R,T)}|R \in \{R_{\mathrm{ul}}, R_{\mathrm{ur}}, R_{\mathrm{bl}}, R_{\mathrm{br}}\},$$

$$T \in \{T_{\mathrm{ul}}, T_{\mathrm{ur}}, T_{\mathrm{bl}}, T_{\mathrm{br}}\}\}. \tag{3.37}$$

4. Implement a score level sum-rule fusion of $S_{\mathrm{all}}$ and $S_{\mathrm{sub}}$.

5. The steps 1-4 are applied to SML and SMO respectively, and finally, a score level sum-rule fusion of the SML and SMO results is applied to achieve the final matching score.

### 3.4.4    Experiments

We test the spectral representations of fingerprint minutiae subsets in a verification setting. The matching performance of a fingerprint verification system can be evaluated by the *false acceptance rate* (FAR), the *false rejection rate* (FRR), and the *equal error rate* (EER). When the decision threshold of a biometric security system is set such that the FAR and FRR are equal, the common value of FAR and FRR is referred to as the EER. In this paper, we use FAR, EER and the *genuine acceptance*

Table 3.3: Experimental settings.

| | | |
|---|---|---|
| SML | $\sigma_{\mathrm{L}}$ | 0 |
| | $\lambda_{\mathrm{l}}$ | 0.1 |
| | $\lambda_{\mathrm{h}}$ | 0.6 |
| SMO | $\sigma_{\mathrm{O}}$ | 4.24 |
| | $\lambda_{\mathrm{l}}$ | 0.01 |
| | $\lambda_{\mathrm{h}}$ | 0.56 |
| $d_{\mathrm{x}}$ | | 120 (pixel) |
| $d_{\mathrm{y}}$ | | 180 (pixel) |

Table 3.4: Results on the MCYT database.

| Methods | EER | GAR | |
|---|---|---|---|
| | | FAR = 0.1% | FAR = 0% |
| No Minutiae Subsets | 0.32% | 99.5% | 99.1% |
| Minutiae Subsets | 0.12% | 99.9% | 99.7% |

*rate* (GAR), GAR= 1−FRR, as performance indicators of our scheme.

The proposed algorithms have been evaluated on the MCYT [46] fingerprint database. The fingerprint data that we used from MCYT are obtained from 100 individuals (person ID from 0000 to 0099 in MCYT, and finger ID for each individual is 0) and each individual contributed 12 samples. The minutiae sets were obtained by the VeriFinger minutiae extractor [11][6]. During the test, for each comparison, we chose two fingerprints from the data set: one as a *reference* fingerprint, another one as a *test* fingerprint. For matching genuine pairs, we used all the possible combinations. For matching imposter pairs, we chose the first sample from each identity. In total, we implement 6600 genuine comparisons and 4950 imposter comparisons. The experimental settings are shown in Table 3.3. The final results are shown in Table 3.4 and the ROC curves are shown in Figure 3.18. For comparison, the result of the spectral minutiae representation without using minutiae subsets is also shown.

From the results, we can see that the recognition performance of the spectral minutiae representation improves after applying the spectral representations of the minutiae subsets. This shows that by generating the minutiae subsets, the corresponding minutiae percentage between the minutiae subsets increase compared with the one between the total minutiae sets, and this results in an improved recognition accuracy. By applying the spectral representations of minutiae subsets, our system is more robust against the limited overlap problem.

---

[6]VeriFinger Extractor Version 5.0.2.0 is used.
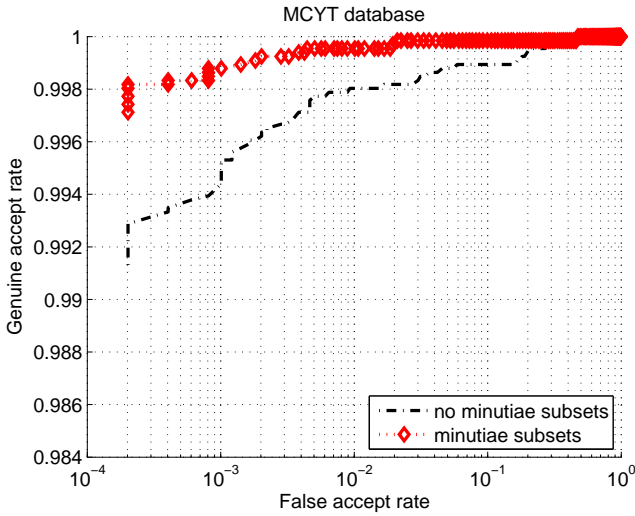
Fig. 3.18: ROC curves.

### 3.4.5 Conclusions

In fingerprint recognition systems, a limited overlap between the reference and test fingerprints is unavoidable. To make the spectral minutiae representation system more robust against the limited overlap problem, we introduce the algorithm of the spectral representations of fingerprint minutiae subsets. The experimental result shows a promising enhancement in recognition accuracy.

The algorithm we present in this paper does not rely on reference points. Therefore, this algorithm does not suffer from the problems that can be caused by reference points, such as the failure of reference points detection. Moreover, this method can be easily integrated to the large number of existing minutiae databases without requiring additional fingerprint image based information.

## 3.5 Chapter Conclusions

In this chapter, we proposed several enhancement methods to improve the performance of the spectral minutiae representations SML and SMO.

In Section 3.2, we first proposed the *weighted sum correlation matching* and *fast rotation shift searching* to improve the spectral minutiae matching algorithms. The fast rotation shift searching algorithm is especially effective in dealing with large rotations between the reference and test fingerprints. This method will be used in Chapters 4 and 5.

Next, in Section 3.3, we explored a method to enhance the recognition performance by incorporating *minutiae quality information* in both the SML and SMO features, denoted by *Enhancement by Quality*. This method makes the spectral minutiae representation system more robust against minutiae errors and low quality fingerprints. The experiments showed a promising improvement in recognition performance. Since minutiae quality is also defined in the *Finger Minutiae Data ISO/IEC 19794-2* Standard [43] and many minutiae extractors will provide this minutiae quality information, it is very easy to apply this enhancement method to the spectral minutiae representation. In Chapter 6, this method will be applied to another version of the spectral minutiae representations, called the *Complex Spectral Minutiae Representation* (SMC).

Finally, we use fingerprint minutiae subsets to cope with the limited overlap problem between the reference and test fingerprints in Section 3.4, denoted as *Minutiae Subsets*. This method is important for applications where only partial fingerprints are available, e.g., forensic applications.

Table 3.5: The contributions of Chapter 3 and their achieved targets.

| Contribution(s) | Target(s) |
|---|---|
| Enhancement by Quality Minutiae Subsets | Target IV: High recognition performance |

With regard to the research question and the targets of this thesis that are formulated in Section 1.3, this chapter addressed Target IV, high recognition performance. Considering the effectiveness and feasibility of all the proposed methods in this chapter, we will recommend to apply the enhancement by incorporating minutiae quality information. The contributions of this chapter together with their achieved targets are summarized in Table 3.5.

# Chapter 4

# Feature Set Reduction for Spectral Minutiae Representations

## 4.1 Chapter Introduction

PURPOSE. The spectral minutiae algorithm introduced in Chapter 2 received promising results. The spectral minutiae feature is a 32,768-dimensional real-valued feature vector. Due to this large dimensionality, the template storage requirement is high and the matching speed is limited. Furthermore, the high dimensionality can also lead to a small sample size problem, which is the result of overfitting on a limited amount of training data. Therefore, in this chapter, we will explore methods that reduce the spectral minutiae feature dimensionality.

CONTENTS. We explore two feature reduction methods. First, the *Column Principle Component Analysis* (CPCA) reduces the spectral minutiae feature in the vertical direction. Second, the *Line Discrete Fourier Transform* (LDFT) reduces the feature in the horizontal direction. The CPCA and LDFT feature reduction algorithms can be applied independently or in conjunction. Finally, both methods are applied to the SML and SMO features and are evaluated on the FVC2002-DB2 and MCYT databases. In the context of the system diagram, the content of this chapter and its referred blocks are highlighted in Figure 4.1. The CPCA and LDFT feature reduction methods will also be applied to the complex spectral minutiae feature that will be presented in Chapter 5. Based on the features after the CPCA and LDFT feature reductions, we will introduce two binary representation schemes in Chapter 6.

PUBLICATION(S). The content of Section 4.2 of this chapter has been published in [67]. Note: several small errors in equations in Section 4.2.4.2 are corrected in this book.
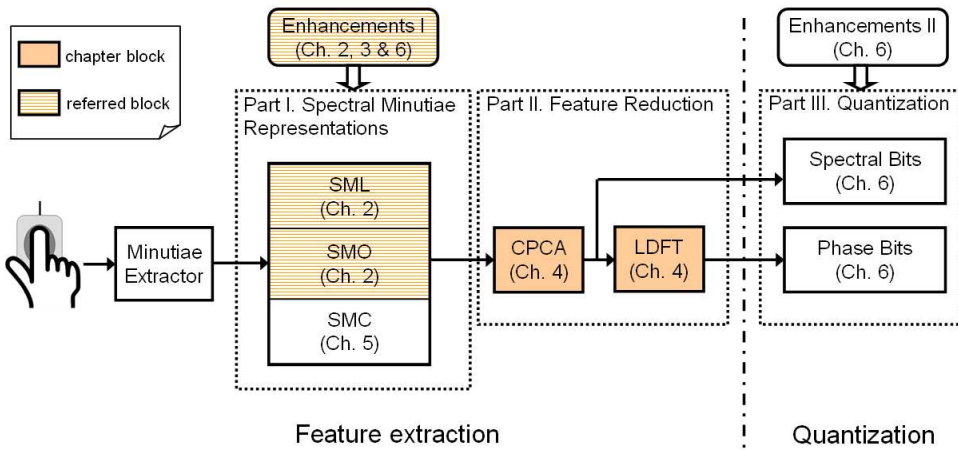
Fig. 4.1: *Block diagram of our designed system, highlighting the content of Chapter 4 and its referred blocks.*

A NOTE TO READERS. The readers can focus on the following subsections:  the CPCA and LDFT algorithms are introduced in 4.2.3 and  4.2.4 respectively and their performances are shown in 4.2.5.  Subsection 4.2.2 gives the background that have already been introduced in Chapter 2. The readers can skip this part.

## 4.2    A Fast Minutiae-based Fingerprint Recognition System

### Abstract

Based on the spectral minutiae features, this chapter introduces two feature reduction algorithms: the Column-PCA and the Line-DFT feature reductions, which can efficiently compress the template size with a reduction rate of 94%.  With reduced features, we can also achieve a fast minutiae-based matching algorithm. This chapter presents the performance of the spectral minutiae fingerprint recognition system and shows a matching speed with 125,000 comparisons per second on a PC with Intel Pentium D processor 2.80 GHz and 1 GB of RAM. This fast operation renders our system suitable as a pre-selector for a large-scale fingerprint identification system, thus significantly reducing the time to perform matching, especially in systems operating at geographical level (e.g., police patrolling) or in complex critical environments (e.g., airports).

### 4.2.1  Introduction

Fingerprint recognition systems have the advantages of both ease of use and low cost. The Unisys Security Index released in December 2008 reveals that fingerprint is the most acceptable biometric technology [3]. Most fingerprint recognition systems are based on the use of a minutiae set. Minutiae are the endpoints and bifurcations of fingerprint ridges. They are known to remain unchanged over an individual's lifetime and allow a very discriminative classification of fingerprints [35].

The spectral minutiae representation presented in [34] is a method to represent a minutiae set as a fixed-length feature vector, which is invariant to translation, and in which rotation and scaling become translations, so that they can be easily compensated for. These characteristics enable the combination of fingerprint recognition systems with recently developed template protection schemes based on fuzzy commitment and helper data schemes, such as [5] and [33], that require as an input a fixed-length feature vector representation of a biometric modality[1].

The spectral minutiae algorithm in [34] received promising results. The spectral minutiae feature is a 32,768-dimensional real-valued feature vector. The large dimensionality of the spectral minutiae feature can cause three problems. First, the storage requirement for a spectral minutiae fingerprint system is very high. Second, the high dimensionality leads to a computational burden and the matching speed will be limited, which is not desired for fingerprint identification systems with very large databases. Third, the high dimensionality can lead to a small sample size problem [68].

In this chapter, we will introduce two feature reduction methods in order to solve the above problems of the original spectral minutiae algorithm: the *Column Principal Component Analysis* (Column-PCA) and the *Line Discrete Fourier Transform* (Line-DFT) feature reduction algorithms. By applying Column-PCA and Line-DFT methods to the original spectral minutiae features, we can effectively compress the spectral minutiae templates and increase the matching speed as well.

For a large Automated Fingerprint Identification System (AFIS), the recognition accuracy, matching speed and its robustness to poor image quality are normally regarded as the most critical elements of system performance. Due to the fact that minutiae sets are unordered, the correspondence between individual minutia in two minutiae sets is unknown before matching. This makes it difficult to find the geometric transformation that optimally registers (or aligns) two minutiae sets. For fingerprint identification systems with very large databases [21], in which a fast comparison algorithm is necessary, most minutiae-based matching algorithms will fail to meet the high speed requirements. Compared with other AFIS vendors, our spectral minutiae fingerprint recognition system has the speed advantage: the experiment shows that our matching speed is more than 15 times faster than that of another commercial minutiae-based fingerprint matching algorithm (we will present the details later). To satisfy the high speed requirement, some AFIS vendors first use the global fingerprint

---

[1]Other template protection systems exist [32] that do not pose this fixed-length feature vector requirement.

characteristics (image-based features) as the first stage matching, and then use the minutiae matcher as the second stage matching [35]. However, this requires the original fingerprint images and such solutions cannot be integrated into the large amount of existing minutiae-based fingerprint recognition systems, in which only minutiae sets are stored as templates. The spectral minutiae representation we present in this paper only needs the minutiae templates as input, so that it can be easily integrated into any arbitrary minutiae-based fingerprint recognition system. This motivates us to consider our spectral minutiae algorithm as a pre-selector (or pre-filter) for a large-scale AFIS to improve the overall matching speed performance, especially in systems operating at geographical level (e.g., police patrolling) or in complex critical environments (e.g., airports). Besides the speed advantage, our algorithm can also be combined with template protection schemes, which gains more and more attention due to the substantial privacy concerns.

This paper is organized as follows. First, the background of the spectral minutiae representation is presented in Section 4.2.2. Next, in Section 4.2.3 and Section 4.2.4, we introduce the Column-PCA and Line-DFT feature reduction algorithms. Then, Section 4.2.5 presents the experimental results. Finally, we draw conclusions in Section 4.2.6.

## 4.2.2  Spectral Minutiae Representation

The spectral minutiae representation is based on the shift, scale and rotation properties of the two-dimensional continuous Fourier transform. In [34], the concept of two representation methods are introduced: the *location-based spectral minutiae representation* (SML) and the *orientation-based spectral minutiae representation* (SMO).

### 4.2.2.1  Location-based spectral minutiae representation (SML)

When implementing the Fourier transform there are two important issues that should be considered. First, when a discrete Fourier transform is taken of an image, this results in a representation of a periodic repetition of the original image. This is undesirable because it introduces errors due to discontinuities at the image boundaries. Second, the re-mapping onto a polar-logarithmic coordinate system after using a discrete Fourier transform introduces interpolation artifacts. Therefore, we introduce an *analytical* representation of the input minutiae, and then use *analytical* expressions of a continuous Fourier transform that are evaluated on a grid in the polar-logarithmic plane. These analytical expressions are obtained as follows. Assume we have a fingerprint with $Z$ minutiae. With every minutia, a function $m_i(x, y) = \delta(x - x_i, y - y_i), i = 1, \ldots, Z$ is associated where $(x_i, y_i)$ represents the location of the $i$-th minutia in the fingerprint image. Thus, in the spatial domain, every minutia is represented by a Dirac pulse. The Fourier transform of $m_i(x, y)$ is given by:

$$\mathcal{F}\{m_i(x,y)\} = \exp(-\mathrm{j}(\omega_\mathrm{x} x_i + \omega_\mathrm{y} y_i)), \tag{4.1}$$

and the location-based spectral minutiae representation is defined as

$$\mathcal{M}_\mathrm{L}(\omega_\mathrm{x}, \omega_\mathrm{y}) = \sum_{i=1}^{Z} \exp(-\mathrm{j}(\omega_\mathrm{x} x_i + \omega_\mathrm{y} y_i)). \tag{4.2}$$

In order to reduce the sensitivity to small variations in minutiae locations in the spatial domain, we use a Gaussian low-pass filter to attenuate the higher frequencies. This multiplication in the frequency domain corresponds to a convolution in the spatial domain where every minutia is now represented by a Gaussian pulse.

Following the shift property of the Fourier transform, the magnitude of $\mathcal{M}$ is taken in order to make the spectrum invariant to translation of the input and we obtain

$$\left|\mathcal{M}_\mathrm{L}(\omega_\mathrm{x}, \omega_\mathrm{y}; \sigma_\mathrm{L}^2)\right| = \left|\exp\left(-\frac{\omega_\mathrm{x}^2 + \omega_\mathrm{y}^2}{2\sigma_\mathrm{L}^{-2}}\right) \sum_{i=1}^{Z} \exp(-\mathrm{j}(\omega_\mathrm{x} x_i + \omega_\mathrm{y} y_i))\right|. \tag{4.3}$$

Equation (4.3) is the analytical expression for the spectrum which can directly be evaluated on a polar-logarithmic grid. The resulting representation in the polar-logarithmic domain is invariant to translation, while rotation and scaling of the input have become translations along the polar-logarithmic coordinates.

### 4.2.2.2  Orientation-based spectral minutiae representation (SMO)

The location-based spectral minutiae representation (SML) only uses the minutiae location information. However, including the minutiae orientation as well may give better discrimination. Therefore, it can be beneficial to also include the orientation information in our spectral representation. The orientation $\theta$ of a minutia can be incorporated by using the spatial derivative of $m(x,y)$ in the direction of the minutia orientation. Thus, to every minutia in a fingerprint, a function $m_i(x,y,\theta)$ is assigned being the derivative of $m_i(x,y)$ in the direction $\theta_i$, such that

$$\mathcal{F}\{m_i(x,y,\theta)\} = \mathrm{j}(\omega_\mathrm{x} \cos\theta_i + \omega_\mathrm{y} \sin\theta_i) \cdot \exp(-\mathrm{j}(\omega_\mathrm{x} x_i + \omega_\mathrm{y} y_i)). \tag{4.4}$$

As with the SML algorithm, using a Gaussian filter and taking the magnitude of the spectrum yields

$$\left|\mathcal{M}_O(\omega_x, \omega_y; \sigma_O^2)\right| = \left|\exp\left(-\frac{\omega_x^2 + \omega_y^2}{2\sigma_O^{-2}}\right)\right.$$

$$\left.\sum_{i=1}^{Z} j(\omega_x \cos\theta_i + \omega_y \sin\theta_i) \cdot \exp(-j(\omega_x x_i + \omega_y y_i))\right|. \tag{4.5}$$

### 4.2.2.3  Implementation

In the previous sections we introduced analytical expressions for the spectral minutiae representations of a fingerprint. In order to obtain our final spectral representations, the continuous spectra (4.3) and (4.5) are sampled on a polar-logarithmic grid. In the radial direction $\lambda$, we use $M = 128$ samples between $\lambda_l = 0.1$ and $\lambda_h = 0.6$. In the angular direction $\beta$, we use $N = 256$ samples uniformly distributed between $\beta = 0$ and $\beta = \pi$. Because of the symmetry of the Fourier transform for real-valued functions, using the interval between 0 and $\pi$ is sufficient. This polar-logarithmic sampling process is illustrated in Figures 4.2 and 4.3.

The sampled spectra (4.3) and (4.5) will be denoted by $S_L(m, n; \sigma_L)$ and $S_O(m, n; \sigma_O)$, respectively, with $m = 1, \ldots, M, n = 1, \ldots, N$. When no confusion can arise, the parameter $\sigma$ and the subscripts L and O will be omitted. For each spectrum, the horizontal axis represents the rotation angle of the spectral magnitude (from 0 to $\pi$); the vertical axis represents the frequency of the spectral magnitude (the frequency increases from top to bottom). It should be noted that the minutiae spectrum is periodic on the horizontal axis.

### 4.2.2.4  Spectral Minutiae Matching

Let $R(m, n)$ and $T(m, n)$ be the two sampled minutiae spectra respectively achieved from the *reference* fingerprint and the *test* fingerprint. Both $R(m, n)$ and $T(m, n)$ are normalized to have zero mean and unit energy. We use the two-dimensional correlation coefficient between $R$ and $T$ as a measure of their similarity.

In practice, the input fingerprint images are rotated and might be scaled (for example, depending on the sensor that is used to acquire an image). Assume that the scaling has already been compensated for on the level of the minutiae sets [43]. Then we only need to test a few rotations, which become the circular shifts in the horizontal direction. We denote $T(m, n - n_{cs})$ as a circular shifted version of $T(m, n)$. We use the fast rotation searching algorithm, based on variable stepsizes that was presented in [56][2] and choose the maximum score of the different combinations as the final matching score between $R$ and $T$,

---

[2]In [56], totaly 9 rotations are tested in a range of $-10°$ to $+10°$ in case of $N = 256$ samples between 0 to $\pi$.

Fig. 4.2: Illustration of the polar-logarithmic sampling (SML spectra). (a) the Fourier spectrum in a Cartesian coordinate and a polar-logarithmic sampling grid; (b) the Fourier spectrum sampled on a polar-logarithmic grid.
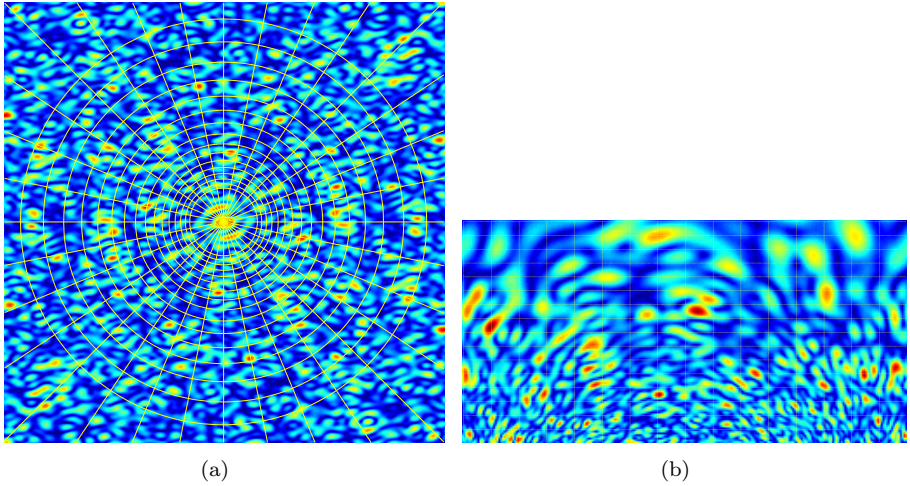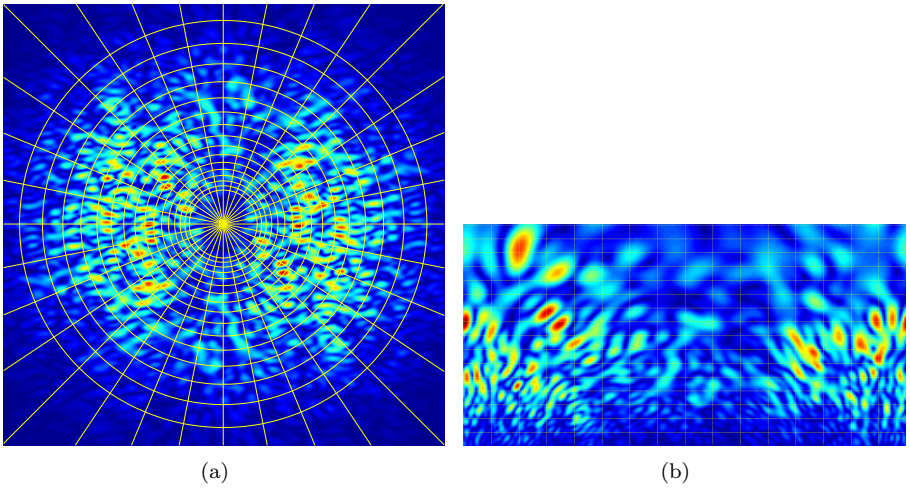


Fig. 4.3: Illustration of the polar-logarithmic sampling (SMO spectra). (a) the Fourier spectrum in a Cartesian coordinate and a polar-logarithmic sampling grid; (b) the Fourier spectrum sampled on a polar-logarithmic grid.

$$S^{(R,T)} = \max_{n_{cs}}\{\frac{1}{MN}\sum_{m,n}R(m,n)T(m,n-n_{cs})\},$$

$$-15 \le n_{cs} \le 15. \tag{4.6}$$

### 4.2.3   Column-PCA feature reduction (CPCA)

The spectral minutiae feature is a $d = M \times N = 32,768$ real-valued feature vector. This high dimensionality can lead to the small sample size problem [68]. Small sample size effects are normally encountered in applications with high dimensional features and a complex classification rule, while the number of available training samples is inadequate. A sophisticated classifier relies on assumptions about the statistics of the feature vectors that are obtained from training data. A mismatch between the actual statistics and the assumptions will lead to a loss of recognition performance. We can increase robustness against this type of mismatch by reducing the feature space dimensionality. PCA is a commonly used tool to achieve this, which at the same time decorrelates the features [69].

#### 4.2.3.1   PCA feature reduction and its problem on spectral minutiae representation

In order to illustrate the problem of directly applying PCA on the features $S_{\mathrm{L}}(m,n)$ and $S_{\mathrm{O}}(m,n)$, let $\vec{x} = (x_1, ..., x_D)^{\mathrm{T}}$ denote the unreduced spectral minutiae feature vector, that is, a one-dimensional form of the two-dimensional spectral minutiae $S(m,n)$, with $m = 1, \ldots, M, n = 1, \ldots, N$ ($M = 128$ and $N = 256$). Thus, the dimensionality of $\vec{x}$ is $D = M \times N = 32,768$.

If we have $L$ samples $\vec{x}_1, ..., \vec{x}_L$ in the training set, we can create a $D \times L$ data matrix $\mathbf{X}$ consisting of all the samples, as $\mathbf{X} = [\vec{x}_1, ..., \vec{x}_L]$. PCA can be implemented by doing a singular value decomposition (SVD) on the matrix $\mathbf{X}$,

$$\mathbf{X} = \mathbf{U}_{\mathrm{X}}\mathbf{S}_{\mathrm{X}}\mathbf{V}_{\mathrm{X}}^{\mathrm{T}}, \tag{4.7}$$

with $\mathbf{U}_{\mathrm{X}}$ a $D \times L$ ($D > L$) orthonormal matrix spanning the column space of $\mathbf{X}$, $\mathbf{S}_{\mathrm{X}}$ a $L \times L$ diagonal matrix of which the (non-negative) diagonal elements are the singular values of $\mathbf{X}$ in descending order, and $\mathbf{V}_{\mathrm{X}}$ a $L \times L$ orthonormal matrix spanning the row space of $\mathbf{X}$. Let $\widetilde{\mathbf{U}}_{\mathrm{X}}$ be the submatrix of $\mathbf{U}_{\mathrm{X}}$ consisting of the first $D_{\mathrm{PCA}}(D_{\mathrm{PCA}} < L)$ columns, then we can implement PCA by

$$\mathbf{Y} = \widetilde{\mathbf{U}}_{\mathrm{X}}^{\mathrm{T}}\mathbf{X}, \tag{4.8}$$

with $\mathbf{Y}$ the $D_{\mathrm{PCA}} \times L$ data matrix with reduced dimensionality.

However, there are two problems in performing PCA to implement feature reduction on the minutiae spectra. The first is the small sample size problem [68]. In case the feature vector is an unreduced spectral minutiae representation, the dimensionality of the feature vector is $D = 32,768$. A reliable PCA feature reduction requires a large number of fingerprint samples to implement the PCA training, which is difficult to acquire. The second problem is that the minutiae spectra are not rotation-invariant. As we mentioned in the previous section, the rotation of fingerprints becomes a circular shift of the minutiae spectra in the horizontal direction. For the PCA training, all the minutiae spectra must be aligned in order to get meaningful results. Then both the training and matching processes become complicated. To cope with the small sample size problem and to avoid the rotation alignment of minutiae spectra, we introduce the Column-PCA method to perform feature reduction.

### 4.2.3.2  Column-PCA: feature reduction without small sample size problems

We first look at the spectral minutiae feature $S$ in the 2D case as we presented in Section 4.2.2.3. From Figures 4.2 and 4.3, we can see that the minutiae spectrum is periodic on the horizontal axis. Moreover, on the vertical axis, the spectra with different frequencies are correlated. Therefore, we consider to use PCA to decorrelate the spectra with different frequencies in the vertical direction. To achieve this, we regard each column of $S$ as a new feature vector $\vec{z} = (z_1, ..., z_M)^{\mathrm{T}}$ (we will call $\vec{z}$ a column feature vector later in this paper), then each (sampled) minutiae spectrum $S(m, n)$ consists of $N$ feature vectors $\vec{z}$, $S = (\vec{z}_1, ..., \vec{z}_N)$.

If we have $L$ samples $S_1, ..., S_L$ in the training set, we can create a $M \times L_{\mathrm{N}}$ ($L_{\mathrm{N}} = N \times L$, $N = 256$) data matrix $\mathbf{Z}$ consists of all the samples, as $\mathbf{Z} = [\vec{z}_1, ..., \vec{z}_{L_{\mathrm{N}}}]$. In this case, the dimensionality of the column feature vector $\vec{z}$, $M = 128$, is N times smaller than the dimensionality of the spectral minutiae $D = M \times N = 32,768$. At the same time, the sample size $L_{\mathrm{N}}$ is N times bigger than the previous sample size $L$. If we denote $r_{\mathrm{s}}$ as the rate of the sample size $l$ to the feature dimensionality $d$, $r_{\mathrm{s}} = \frac{l}{d}$, we can see that in case the sample number $L$ keeps the same, the $r_{\mathrm{s}}$ of using the column feature vector is $N^2 = 65,536$ times bigger than the one of using the original feature vector. Therefore, by using column feature vectors of spectral minutiae to implement PCA feature reduction, we can avoid the small sample size problem.

As we indicated in the previous section, another problem of directly using minutiae spectra to implement PCA feature reduction is that a rotation alignment of the minutiae spectra is needed, which is difficult to implement. In the spectral minutiae representation, the rotation operator commutes with column transformation. By using column feature vectors, the rotation variation becomes the samples sequence difference in the training procedure. This will not have any influence on the PCA feature reduction results. Therefore, by using column feature vectors to implement PCA feature reduction, we can cope with both the small sample size problem and avoid the rotation alignment of minutiae spectra as well. We call this method as the Column-PCA feature reduction (CPCA).

To implement CPCA, we first subtract the sample mean (column mean) from the data matrix $\mathbf{Z}$. The next step is to apply SVD on $\mathbf{Z}$,

$$\mathbf{Z} = \mathbf{U}_\mathrm{Z}\mathbf{S}_\mathrm{Z}\mathbf{V}_\mathrm{Z}^\mathrm{T}, \tag{4.9}$$

with $\mathbf{U}_\mathrm{Z}$ a $M \times M$ orthonormal matrix spanning the column space of $\mathbf{Z}$, $\mathbf{S}_\mathrm{Z}$ a $M \times M$ diagonal matrix of which the (non-negative) diagonal elements are the singular values of $\mathbf{Z}$ in descending order, and $\mathbf{V}_\mathrm{Z}$ a $L_\mathrm{N} \times M$ orthonormal matrix spanning the row space of $\mathbf{Z}$. Finally we can obtain the CPCA transform matrix $\widetilde{\mathbf{U}}_\mathrm{Z}$ by retaining the first $M_\mathrm{CPCA}(M_\mathrm{CPCA} \leq M)$ columns of $\mathbf{U}_\mathrm{Z}$. The CPCA transform on the minutiae spectra $S(m,n)$ is written as

$$\mathbf{S}_\mathrm{CPCA} = \widetilde{\mathbf{U}}_\mathrm{Z}^\mathrm{T}\mathbf{S}, \tag{4.10}$$

with $\mathbf{S}_\mathrm{CPCA}$ the $M_\mathrm{CPCA} \times N$ data matrix with reduced dimensionality. After the CPCA feature reduction, the relation of the energy retainment rate $E_\mathrm{CPCA}$ and $M_\mathrm{CPCA}$ is

$$E_\mathrm{CPCA}(M_\mathrm{CPCA}) = \frac{\displaystyle\sum_{n=1}^{M_\mathrm{CPCA}} \mathbf{S}_\mathrm{Z}(n,n)}{\displaystyle\sum_{n=1}^{M} \mathbf{S}_\mathrm{Z}(n,n)}, \; 1 \leq M_\mathrm{CPCA} \leq M, \tag{4.11}$$

and

$$M_\mathrm{CPCA}(E_\mathrm{CPCA}) = \arg\min_{1 \leq \widetilde{M} \leq M} \left| \frac{\displaystyle\sum_{n=1}^{\widetilde{M}} \mathbf{S}_\mathrm{Z}(n,n)}{\displaystyle\sum_{n=1}^{M} \mathbf{S}_\mathrm{Z}(n,n)} - E_\mathrm{CPCA} \right|. \tag{4.12}$$

The CPCA transform is illustrated in Figures 4.4(a) and 4.4(b) (here we choose $\widetilde{\mathbf{U}}_\mathrm{Z} = \mathbf{U}_\mathrm{Z}$, that is, $M_\mathrm{CPCA} = M$ for a clear illustration). We can see that after the CPCA transform, the main energy of the original minutiae spectrum $S$ is concentrated in the top lines of $S_\mathrm{CPCA}$. By only retaining the top $M_\mathrm{CPCA}$ lines, we perform the CPCA feature reduction, with a reduction rate $R_\mathrm{CPCA} = (M - M_\mathrm{CPCA})/M$. Because the rotation operator commutes with column transformation, the minutiae spectrum $S_\mathrm{CPCA}$ remains periodic on the horizontal axis after the CPCA transform.
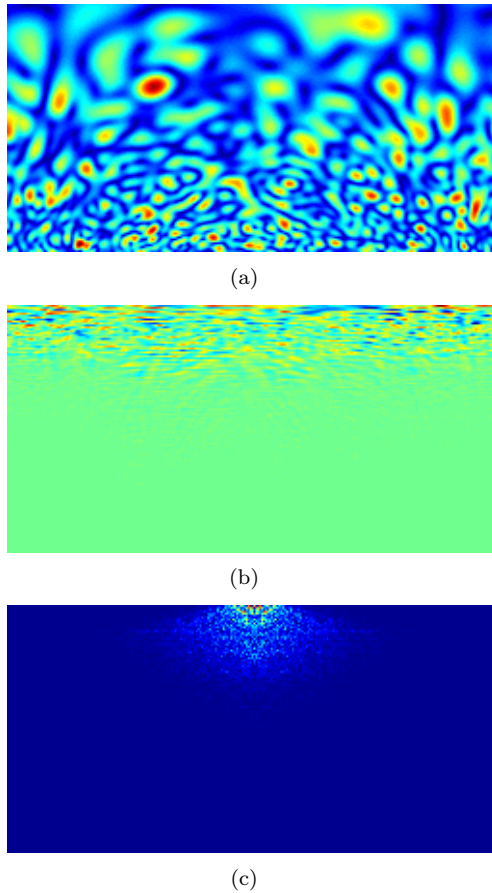
(a)



(b)



(c)

Fig. 4.4: Illustration of the CPCA transform and the LDFT representation. (a) the location-based spectral minutiae; (b) the minutiae spectrum after the CPCA transform; (c) the magnitude of the LDFT representation of (b).

### 4.2.4   Line-DFT feature reduction (LDFT)

The CPCA feature reduction method reduces the minutiae spectrum feature $S$ in the vertical direction. In this section, we will introduce the Line-DFT feature reduction (LDFT) method, which will reduce the feature in the horizontal direction. This method is based on the fact that the minutiae spectrum $S$ is periodic on the horizontal axis. Therefore, it can be applied both independently and in combination with the CPCA feature reduction.

#### 4.2.4.1   Line-DFT representation of the minutiae spectrum

We denote each line of the minutiae spectrum $S$ (here $S$ can be the original minutiae spectrum or the minutiae spectrum after the CPCA feature reduction) as a line feature vector $\vec{y} = (y_1, ..., y_N)$, thus $S = (\vec{y}_1, ..., \vec{y}_M)^{\mathrm{T}}$. Then we can regard each line feature vector as a periodic discrete-time signal (or sequence) with period $N$, and we denote this signal as $y_m(n)$, $(m = 1, ..., M)$ ($M = 128$ for the original minutiae spectrum or $M = M_{\mathrm{CPCA}}$ for the spectrum after the CPCA feature reduction). The discrete Fourier transform [70] of $y_m(n)$ is given by

$$Y_m(k) = \sum_{n=0}^{N-1} y_m(n)\exp(-\mathrm{j}\frac{2\pi}{N}kn),\ k = 0, 1, ..., N-1,\ m = 1, ..., M. \qquad (4.13)$$

Because $y_m(n)$ is periodic, by performing a DFT (implemented as FFT) on each line $y_m(n)$ of the minutiae spectrum $S$, we obtain $S_{\mathrm{LDFT}} = (Y_1(k), ..., Y_M(k))^{\mathrm{T}}, S_{\mathrm{LDFT}} \in \mathbb{C}^M$, which is an exact representation of $S$.

The LDFT representation is illustrated in Figures 4.4(b) and 4.4(c) (here the LDFT representation after the CPCA feature reduction is presented). We can see that after the LDFT representation, the main energy is concentrated in the low frequency part (the middle columns). Therefore, for each line of the LDFT representation $S_{\mathrm{LDFT}}$, we only retain the Fourier components with a certain percentage of energy (for example, 80%) in the lower frequency part. By reducing the number of Fourier components, we implement the LDFT feature reduction. For each line $m$, the relation of the energy retainment rate $E_{\mathrm{LDFT}}$ after the LDFT feature reduction and $N_{\mathrm{LDFT}}$ (which indicates that only the $N_{\mathrm{LDFT}}$ Fourier components from the low frequency part are retained) is

$$E_{\mathrm{LDFT}}(N_{\mathrm{LDFT}}; m) = \frac{\displaystyle\sum_{k=0}^{N_{\mathrm{LDFT}}-1} |Y_m(k)|^2}{\displaystyle\sum_{k=0}^{N/2} |Y_m(k)|^2}, \ 1 \leq N_{\mathrm{LDFT}} \leq \frac{N}{2} + 1, \qquad (4.14)$$

and

$$N_{\text{LDFT}}(E_{\text{LDFT}}; m) = \arg \min_{1 \leq \widetilde{N} \leq N/2+1} \left| \frac{\displaystyle\sum_{k=0}^{\widetilde{N}-1} |Y_m(k)|^2}{\displaystyle\sum_{k=0}^{N/2} |Y_m(k)|^2} - E_{\text{LDFT}} \right|. \qquad (4.15)$$

As we mentioned in Section 4.2.2.4, the rotation of the fingerprint becomes the circular shift of the minutiae spectrum along the horizontal axis in the space domain. To test different fingerprint rotations (see Section 4.2.2.4) after applying the LDFT representation, we will implement the shift operation in the frequency domain according to the shift property of the discrete Fourier transform. Thus, the Line-DFT transformation of $T(m, n - n_{cs})$ in Equation (4.6) becomes

$$T(m, n - n_{cs}) = (y_1(n - n_{cs}), ..., y_M(n - n_{cs}))^{\text{T}}$$
$$\xrightarrow{\text{LDFT}} \exp(-\text{j}\frac{2\pi}{N} k n_{cs})(Y_1(k), ..., Y_M(k))^{\text{T}} \qquad (4.16)$$

### 4.2.4.2  Transform of Fourier components to a real-valued feature vector

Consider two discrete-time, periodic signals $f_1[n]$ and $f_2[n]$, $f_1[n], f_2[n] \in \mathbb{R}^N$, with period $N$ ($N$ is an even number), and their discrete Fourier transform are $F_1[k]$ and $F_2[k]$ respectively. The DFT is orthnormal, thus it preserves inner products. Therefore, because of the symmetry properties of the DFT for real-valued signals, the correlation of $f_1[n]$ and $f_2[n]$ becomes

$$\sum_{n=0}^{N-1} f_1[n]f_2^*[n] = \frac{1}{N} \sum_{k=0}^{N-1} F_1[k]F_2^*[k] \qquad (4.17)$$

$$= \frac{1}{N}\left( F_1[0]F_2[0] + 2\Re \sum_{k=1}^{\frac{N}{2}-1} F_1[k]F_2^*[k] + F_1[\frac{N}{2}]F_2[\frac{N}{2}] \right), (4.18)$$

where * denotes the complex conjugate and $\Re$ denotes the real part.

Because $F_1[k]$ and $F_2[k]$ are complex numbers, we can write them as

$$F_i[k] = A_i[k] + \text{j}B_i[k], \, i = 1, 2, \qquad (4.19)$$

with $A_i[k]$ the real part, and $B_i[k]$ the imaginary part. Then, Equation (4.17) becomes

$$
\begin{aligned}
\sum_{n=0}^{N-1} f_1[n] f_2^*[n] = \frac{1}{N} \Big( & A_1[0] A_2[0] \\
& + 2 \sum_{k=1}^{\frac{N}{2}-1} (A_1[k] A_2[k] + B_1[k] B_2[k]) + A_1[\frac{N}{2}] A_2[\frac{N}{2}] \Big).
\end{aligned}
\tag{4.20}
$$

Therefore, we can generate two one dimensional real-valued feature vectors $\vec{v_1}$ and $\vec{v_2}$ from the Fourier components, as

$$
\begin{aligned}
\vec{v_i} = \Big( & \frac{1}{\sqrt{N}} A_i[0], \sqrt{\frac{2}{N}} A_i[1], ..., \sqrt{\frac{2}{N}} A_i[\frac{N}{2} - 1], \frac{1}{\sqrt{N}} A_i[\frac{N}{2}], \\
& \sqrt{\frac{2}{N}} B_i[1], ..., \sqrt{\frac{2}{N}} B_i[\frac{N}{2} - 1] \Big), i = 1, 2.
\end{aligned}
\tag{4.21}
$$

The correlation of $\vec{v_1}$ and $\vec{v_2}$ is exactly the same as the correlation of the real-valued signals $f_1[n]$ and $f_2[n]$. Therefore, by generating the new feature vectors as $\vec{v_1}$ and $\vec{v_2}$, we can continue using the correlation-based spectral minutiae matching algorithm. Moreover, by performing the correlation of $\vec{v_1}$ and $\vec{v_2}$, instead of implementing the complex number multiplications as in Equation (4.17), we can save about half of the real multiplications.

In case the LDFT feature reduction, with $1 < N_{\text{LDFT}} \leq \frac{N}{2}$, the reduced feature vectors $\vec{v_1}$ and $\vec{v_2}$ become

$$
\begin{aligned}
\vec{v_i} = \Big( & \frac{1}{\sqrt{N}} A_i[0], \sqrt{\frac{2}{N}} A_i[1], ..., \sqrt{\frac{2}{N}} A_i[N_{\text{LDFT}} - 1], \\
& \sqrt{\frac{2}{N}} B_i[1], ..., \sqrt{\frac{2}{N}} B_i[N_{\text{LDFT}} - 1] \Big), i = 1, 2.
\end{aligned}
\tag{4.22}
$$

For the matching algorithm presented in Section 4.2.2.4, we denote $v_r$ and $v_{t,n_{cs}}$ as the reduced features of $R(m,n)$ and $T(m, n - n_{cs})$ respectively, then Equation (4.6) becomes

$$
S^{(R,T)} = \max_{n_{cs}} \{ \frac{1}{MN} \sum v_r v_{t,n_{cs}} \}, \ -15 \leq n_{cs} \leq 15.
\tag{4.23}
$$

### 4.2.5 Experiments

#### 4.2.5.1 Measurements

We test the spectral minutiae representation in a verification setting. The matching performance of a fingerprint verification system can be evaluated by means of several measures. Commonly used are the *false acceptance rate* (FAR), the *false rejection rate* (FRR), and the *equal error rate* (EER). In this paper, we use FAR, EER and the *genuine acceptance rate* (GAR), GAR= $1-$FRR, as performance indicators of our scheme.

#### 4.2.5.2 Experimental settings

The proposed algorithms have been evaluated on MCYT [46] and FVC2002-DB2 [48] fingerprint databases. The fingerprint data that we used from MCYT are obtained from 145 individuals (person ID from 0000 to 0144 and finger ID 0) and each individual contributes 12 samples. We use samples from person ID 0100 to 0144 for the CPCA and LDFT training (totally 540 fingerprints) and samples from person ID 0000 to 0099 for test (totally 1200 fingerprints). We also tested our algorithms on the FVC2002-DB2 because it is a public-domain fingerprint database. Compared with MCYT, the fingerprints in FVC2002 have lower quality and bigger displacements. For the FVC database, we apply the same experimental protocol as in the FVC competition: the samples from finger ID 101 to 110 for the CPCA and LDFT training (totally 40 fingerprints) and samples from person ID 1 to 100 for test (totally 400 fingerprints)[3]. The minutiae sets were obtained by the VeriFinger minutiae extractor [11][4].

We test our algorithm in a verification setting. For matching genuine pairs, we used all the possible combinations. For matching imposter pairs, we chose the first sample from each identity. We will further follow the same parameter setting in [34][5].

#### 4.2.5.3 Results without CPCA and LDFT feature reductions

For a comparison with the results after the CPCA and the LDFT feature reductions, we first tested our algorithm without feature reductions. The results are shown in Table 4.1 and the ROC curves are shown in Figures 4.5(a) and 4.6(a). From the results, we can see that the MCYT database received much better results than the

---

[3]We propose to use our algorithm in a high security scenario. In FVC2002 databases, samples 3, 4, 5 and 6 were obtained by requesting the biometric data subjects to provide fingerprints with exaggerated displacement and rotation. In a high security scenario where the biometric data subject is aware that cooperation is crucial for security reasons, he will be cooperative. Therefore, only samples 1, 2, 7 and 8 are chosen. To deal with the large rotations, an absolute pre-alignment based on core and its direction can be applied.

[4]VeriFinger Extractor Version 5.0.2.0 is used.

[5]We will only present the sum-rule fusion results of SML and SMO in this paper. We also use the singular points to assist the verification, following the procedure in [34].

Table 4.1: Results without CPCA and LDFT feature reductions.

| Databases | EER | GAR | | |
|---|---|---|---|---|
| | | FAR = 1% | FAR = 0.1% | FAR = 0% |
| MCYT | 0.30% | 99.8% | 99.7% | 99.1% |
| FVC2002-DB2 | 3.86% | 95.5% | 92.7% | 89.7% |

FVC database. This shows that our algorithms are sensitive to the minutiae quality and fingerprint quality.

### 4.2.5.4   Results after CPCA and LDFT feature reductions

In case of using SML and SMO fusion, the spectral minutiae representation results in a 65,536 real-valued feature vector. For fingerprint identification systems with very large databases, using the spectral minutiae representation requires a big template storage space and its matching speed is also limited. Therefore, applying the proposed CPCA and LDFT feature reduction algorithms is needed. To evaluate the two feature reduction methods, we tested them in three cases: (1) only applying the CPCA feature reduction; (2) only applying the LDFT feature reduction; (3) applying both the CPCA and the LDFT feature reductions.

From our experiments, we noticed that the selection of the energy retainment rates $E_{\text{CPCA}}$ and $E_{\text{LDFT}}$ are essential for a high performance. When $E_{\text{CPCA}}$ and $E_{\text{LDFT}}$ are chosen, we can calculate $M_{\text{CPCA}}$ and $N_{\text{LDFT}m}$ using the fingerprints in the training sets, according to Equations (4.12) and (4.15).

### 4.2.5.5   Only applying the CPCA feature reduction

When only applying the CPCA feature reduction, the energy retainment rates $E_{\text{CPCA}}$ and the feature reduction rates for the two databases are shown in Table 4.2. The results we achieved are shown in Table 4.3 and the ROC curves are shown in Figures 4.5(b) and 4.6(b). From Figures 4.5(b) and 4.6(b), we can see that the CPCA feature reduction does not degrade the recognition performance of the system. At the same time, we reach a feature reduction rate of more than 70% (the feature length is about 4 times smaller). In the FVC2002-DB2 case, we only used 40 fingerprints for the training and we still performed an effective feature reduction. This illustrates that the CPCA feature reduction does not suffer from the small sample size problem.

### 4.2.5.6   Only applying the LDFT feature reduction

When only applying the LDFT feature reduction, the energy retainment rates $E_{\text{LDFT}}$ and the feature reduction rates for the two databases are shown in Table 4.4. From
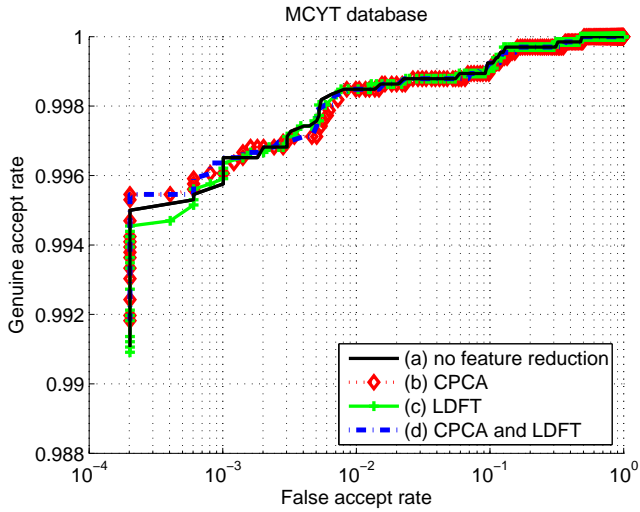
Fig. 4.5: ROC curves (MCYT database).
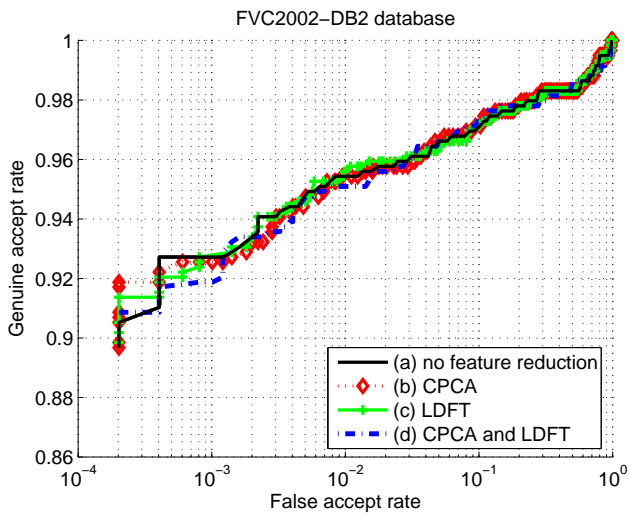


Fig. 4.6: ROC curves (FVC2002-DB2 database).

Table 4.2: Parameters of the CPCA feature reduction.

| | MCYT | | | FVC2002-DB2 | | |
|---|---|---|---|---|---|---|
| | SML | SMO | Fusion | SML | SMO | Fusion |
| $E_{\text{CPCA}}$ | 85% | 90% | 87.5% | 85% | 90% | 87.5% |
| Reduction | 76.6% | 78.1% | 77.3% | 67.2% | 76.6% | 71.9% |

Table 4.3: Results after the CPCA feature reduction.

| Databases | EER | GAR | | |
|---|---|---|---|---|
| | | FAR = 1% | FAR = 0.1% | FAR = 0% |
| MCYT | 0.30% | 99.8% | 99.6% | 99.2% |
| FVC2002-DB2 | 3.72% | 95.4% | 92.6% | 89.7% |

Table 4.4: Parameters of the LDFT feature reduction.

| | MCYT | | | FVC2002-DB2 | | |
|---|---|---|---|---|---|---|
| | SML | SMO | Fusion | SML | SMO | Fusion |
| $E_{\text{LDFT}}$ | 97% | 99.5% | 98.3% | 97% | 99.8% | 98.4% |
| Reduction | 81.4% | 88.5% | 84.9% | 77.5% | 89.0% | 83.3% |

Table 4.5: Results after the LDFT feature reduction.

| Databases | EER | GAR | | |
|---|---|---|---|---|
| | | FAR = 1% | FAR = 0.1% | FAR = 0% |
| MCYT | 0.29% | 99.8% | 99.7% | 99.1% |
| FVC2002-DB2 | 3.72% | 95.6% | 92.7% | 89.7% |

Table 4.4 we can see that we achieved a higher reduction rate for SMO, at the same time the energy retainment is also higher. The reason is that for SMO, we used a Gaussian kernel to attenuate the higher frequencies. The LDFT feature reduction can achieve a higher reduction rate in case the minutiae spectra are with lower frequencies.

The results we achieved after the LDFT feature reduction are shown in Table 4.5 and the ROC curves are shown in Figures 4.5(c) and 4.6(c). From Figures 4.5(c) and 4.6(c), we can see that the LDFT feature reduction does not degrade the recognition performance of the system. At the same time, we reach a feature reduction rate of about 84% (the feature length is more than 6 times smaller). The same as the CPCA feature reduction, the LDFT feature reduction also does not suffer from the small sample size problem.

### 4.2.5.7 Applying both the CPCA and the LDFT feature reductions

After testing the CPCA and the LDFT feature reductions separately, we tested the combination of the two methods. We applied the LDFT feature reduction after the CPCA feature reduction. The final energy retainment rates $E_{\text{CPCA}}$ and $E_{\text{LDFT}}$, and the feature reduction rates for the two databases are shown in Table 4.6. The results we achieved are shown in Table 4.7 and the ROC curves are shown in Figures 4.5(d) and 4.6(d). From Figures 4.5(d) and 4.6(d), we can see that after applying the CPCA and the LDFT feature reductions, the recognition performance is not degraded. We finally reach a feature reduction rate of about 92-94% (the feature length is more than 13-15 times smaller).

Comparing the three different feature reduction cases (the ROC curves in Figures 4.5(b)-(d) and 4.6(b)-(d)), we can see that all these three cases show similar recognition performances, while the combination of CPCA and LDFT received the biggest feature reduction rates.

For fingerprint identification systems with very large databases, the matching speed is crucial. In case the feature length is $d$ and $n_{\text{r}}$ rotation possibilities are tested (in our experiments $n_{\text{r}} = 9$), we need to implement $n_{\text{r}}d$ real multiplications. Therefore, applying the feature reductions to decrease $d$ will improve the speed performance of our scheme. We tested the matching speed for the fusion case of SML and SMO before and after the CPCA and the LDFT feature reductions (using the MCYT database). Without feature reductions, we can implement 8,000 comparisons per second using optimized C language programming on a PC with Intel Pentium D processor 2.80 GHz and 1 GB of RAM. After applying CPCA and LDFT, we can implement 125,000 comparisons (the speed is more than 15 times faster) under the same setting.

### 4.2.5.8 Comparison

We compared our results with other well-known minutiae matchers on the FVC2002-DB2 database: VeriFinger[6] and Fuzzy Vault according to the protocol in [32]. The results are shown in Table 4.8. We notice that the commercial minutiae matcher VeriFinger obtained much better results than ours. One reason is that the VeriFinger matcher uses some fingerprint features that are not defined in the ISO minutiae template [43]. Another reason is that, with our global representation, we cannot perform minutiae pair searching, which is a crucial step for the minutiae-based matching. These two reasons may cause the degradation of our algorithm compared with VeriFinger.

We also compared the performance of our method with a minutiae-based fingerprint recognition system combined with a template protection scheme based on fuzzy vault, which is presented in [32]. The reason of this comparison is that in [32] an alignment between a fingerprint pair using minutiae information is also not possible. It should be noted that [32] includes a template protection scheme, whereas our system does

---

[6]VeriFinger Extractor Version 5.0.2.0 and VeriFinger Matcher version 5.0.2.1 are used.

Table 4.6: Parameters of the CPCA and the LDFT feature reductions.

| Methods | MCYT | | | FVC2002-DB2 | | |
|---|---|---|---|---|---|---|
| | SML | SMO | Fusion | SML | SMO | Fusion |
| $E_{\text{CPCA}}$ | 83% | 90% | 86.5% | 75% | 92% | 83.5% |
| Reduction | 78.1% | 78.1% | 78.1% | 75% | 75% | 75% |
| $E_{\text{LDFT}}$ | 99% | 99% | 99% | 97% | 98% | 97.5% |
| Reduction | 69.5% | 74.2% | 72.0% | 68.1% | 72.5% | 70.4% |
| $E_{\text{Total}}$ | 82.2% | 89.1% | 85.6% | 72.8% | 90.2% | 81.5% |
| Reduction | 92.9% | 94.0% | 93.5% | 92.0% | 93.1% | 92.6% |

Table 4.7: Results after the CPCA and the LDFT feature reductions.

| Databases | EER | GAR | | |
|---|---|---|---|---|
| | | FAR = 1% | FAR = 0.1% | FAR = 0% |
| MCYT | 0.30% | 99.8% | 99.7% | 99.2% |
| FVC2002-DB2 | 3.52% | 95.1% | 92.0% | 90.7% |

Table 4.8: Results comparison on FVC2002-DB2.

| Methods | EER | GAR | | |
|---|---|---|---|---|
| | | FAR = 1% | FAR = 0.1% | FAR = 0% |
| Our method | 3.52% | 95.1% | 92.0% | 90.7% |
| VeriFinger | 1.0% | 99% | 98.8% | 98.6% |
| Fuzzy Vault | – | – | 91% | 86% |

Table 4.9: Performances after CPCA and LDFT for high GAR.

| Databases | FAR | | |
|---|---|---|---|
| | GAR = 100% | GAR = 99.9% | GAR = 99% |
| MCYT | 49.4% | 6.7% | 0% |
| FVC2002-DB2 | 90.0% | 88.5% | 45.5% |

not. Moreover, because [32] implemented an alignment using high curvature points, this caused a 2% *failure to capture rate* (FTCR), while our method does not suffer from this.

Regarding the speed performance[7], using the spectral minutiae representation after the CPCA and the LDFT feature reductions, we can implement 125,000 comparisons per second. We also tested the VeriFinger matcher using the same PC setting and the matching speed is 8,000 comparisons per second. Our matching speed advantage is due to the fact that our algorithm uses a fixed-length feature vector and avoids fingerprint alignment. After applying CPCA and LDFT, the feature length is greatly reduced, which leads to a promising matching speed.

In case of fingerprint identification systems with very large databases, we might combine good identification performance and speed by using the spectral minutiae as a pre-selector, that finds a number of best matches and then use a standard minutiae comparison for a good accuracy. As a pre-selector, the recognition performance in the area of high GAR is important. We show the performance of the spectral minutiae in this area in Table 4.9. From Table 4.9, we can see that in case of good quality fingerprints (MCYT), we can use the spectral minutiae algorithm as a pre-selector to speed up the minutiae-based matching algorithm. However, the spectral minutiae algorithm is not robust to the low quality fingerprints. The fingerprint outliers will degrade the recognition accuracy, which limits the application of the spectral minutiae algorithm.

## 4.2.6   Conclusions

The spectral minutiae representation is a novel method to represent a minutiae set as a fixed-length feature vector, which is invariant to translation, and in which rotation and scaling become translations, so that they can be easily compensated for. Based on the spectral minutiae feature, this paper introduces two feature reduction methods: the Column-PCA and the Line-DFT feature reduction algorithms. The experiments show that these methods effectively decrease the spectral minutiae feature dimensionality with a reduction rate of 94%, while at the same time, the recognition performance of the fingerprint system is not degraded. The proposed spectral minutiae fingerprint recognition system also shows a promising matching speed with 125,000 comparisons per second. This algorithm overcomes the speed disadvantage of most minutiae-based algorithms and enables the application of a minutiae-based fingerprint identification system with a large database.

The spectral minutiae representation also enables the combination of fingerprint recognition systems and template protection schemes. In order to be able to apply the spectral minutiae representation with a template protection scheme, for example based on a fuzzy extractor [53], the next step would be to extract bits that are stable for

---

[7]For fingerprint identification systems with large databases, only matching time is crucial. For the enrollment speed, because our algorithm only uses one-sample enrollment, our enrollment time is comparable to the one from VeriFinger.

the genuine user and completely random for an arbitrary user. For example, we can apply 2D Gabor filters for bit extraction, which has been used in iris codes [54]. Another possibility is to first apply additional dimensionality reduction by a combination of PCA and LDA and then apply single bit extraction according to the reliable component scheme or multi bit extraction [55].

In this paper, we presents the experimental results using two fingerprint databases: the MCYT and the FVC2002-DB2 databases. The MCYT database gives much better results than the FVC database. This shows that our algorithms are sensitive to the minutiae quality as well as the fingerprint quality. To cope with the low quality fingerprints and minutiae errors are topics of our further research.

## 4.3    Chapter Conclusions

In this chapter, we introduced two feature reduction methods to reduce the spectral minutiae feature set: the *Column Principle Component Analysis* (CPCA) feature reduction algorithm, which reduces the spectral minutiae feature in the vertical direction, and the *Line Discrete Fourier Transform* (LDFT) feature reduction algorithm, which reduces the feature in the horizontal direction.

The CPCA and LDFT feature reduction algorithms can effectively reduce the feature dimensionality, while maintaining the recognition performance. These two methods can be applied independently or in conjunction. In Chapters 5 and 6, these two methods will also be applied to the Complex Spectral Minutiae Representation (SMC).

Table 4.10: The contributions of Chapter 4 and their achieved targets.

| Contribution(s) | Target(s) |
|---|---|
| CPCA | Target V: High comparison speed |
| LDFT | |

With regard to the research question and the targets of this thesis that are brought forward in Section 1.3, this chapter addressed Target V, high comparison speed. With CPCA and LDFT, we can reduce the template size significantly and increase the comparison speed up to 15 times. The contributions of this chapter together with their achieved targets are summarized in Table 4.10.

# Chapter 5

# Complex Spectral Minutiae Representation

## 5.1  Chapter Introduction

PURPOSE. Up to now, we have introduced two spectral minutiae representation methods: SML and SMO. Although SMO incorporates the minutiae orientations, it did not show better results than SML in the experiments shown in the previous chapters. This motivated us to design another spectral minutiae representation that incorporates minutiae orientations. In this chapter, we will introduce this new version: the *complex spectral minutiae representation* (SMC).

CONTENTS. We first illustrate a general procedure of the spectral minutiae representations. Then we present the complex spectral minutiae representation (SMC) together with the previous SML and SMO representations. Finally, we evaluate the performances of SML, SMO and SMC on the FVC2002-DB2 and MCYT databases. In the experiments, the CPCA and LDFT feature reduction methods are also evaluated on all the SML, SMO and SMC features. The results show that SMC improves the recognition accuracy, expressed in terms of the equal error rate, about 2-4 times compared with SML and SMO. In the context of the system diagram, the content of this chapter and its referred blocks are highlighted in Figure 5.1. Since SMC outperformed SML and SMO, in Chapter 6, the binary representations will be mainly investigated for the SMC features.

PUBLICATION(S). The content of Section 5.2 of this chapter has been published in [71].

A NOTE TO READERS. The readers can focus on Section 5.2.2 that introduces the SMC algorithm. The SML (Section 5.2.2.1) and SMO (Section 5.2.2.2) parts are
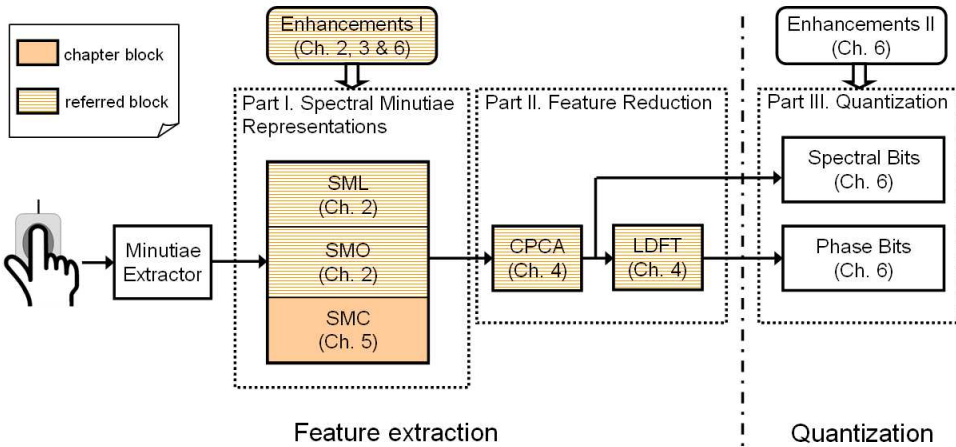
Fig. 5.1: *Block diagram of our designed system, highlighting the content of Chapter 5 and its referred blocks.*

repetitive from Chapter 2, and the CPCA and LDFT feature reduction algorithms (Section 5.2.3) have already been introduced in Chapter 4. The readers can skip these parts.

## 5.2  Complex Spectral Minutiae Representation For Fingerprint Recognition

**Abstract**

The spectral minutiae representation is designed for combining fingerprint recognition with template protection. This puts several constraints to the fingerprint recognition system: first, no relative alignment of two fingerprints is allowed due to the encrypted storage; second, a fixed-length feature vector is required as input of template protection schemes. The spectral minutiae representation represents a minutiae set as a fixed-length feature vector, which is invariant to translation, rotation and scaling. These characteristics enable the combination of fingerprint recognition systems with template protection schemes and allow for fast minutiae-based matching as well. In this paper, we introduce the complex spectral minutiae representation (SMC): a spectral representation of a minitiae set, as the location-based and the orientation-based spectral minutiae representations (SML and SMO), but it encodes minutiae orientations differently. SMC improves the recognition accuracy, expressed in terms of the equal error rate, about 2-4 times compared with SML and SMO. In addition, the paper presents two feature reduction algorithms: the Column-PCA and the Line-DFT feature reductions, which achieve a template size reduction around 90% and results in a 10-15 times higher matching speed (with 125,000 comparisons per second).

### 5.2.1  Introduction

Fingerprint recognition systems have the advantages of both ease of use and low cost. Nowadays, most fingerprint recognition systems are based on minutiae matching [35]. However, minutiae-based fingerprint matching algorithms have some drawbacks that limit their application.

First, due to the fact that minutiae sets are unordered, the correspondence between individual minutia in two minutiae sets is unknown before matching and this makes it difficult to find the geometric transformation that optimally registers (or aligns) two sets. This registration challenge causes minutiae-based matching algorithms to become rather slow. For fingerprint identification systems with very large databases [21], in which a fast comparison algorithm is necessary, minutiae-based matching algorithms will fail to meet the high performance speed requirement.

Second, the increasing widespread use of biometrics has raised substantial privacy concerns [27]. Researchers have shown the possibility of reconstructing fingerprints from minutiae templates [72]. Therefore, protecting minutiae templates becomes necessary. To combine fingerprint recognition with template protection, there are new constraints to the fingerprint recognition system: (1) no relative alignment of two fingerprints is allowed due to the encrypted storage; (2) the recently developed template protection schemes based on fuzzy commitment and helper data schemes, such as [5] and [33], require as an input a fixed-length feature vector representation of a biometric modality[1].

There are several algorithms to extract a fixed-length feature vector from fingerprints. The FingerCode as presented in [4] is based on ridge features. The author concluded that FingerCodes are not as distinctive as minutiae and they can be used as complementary information for fingerprint matching. Willis and Myers brought forward a fixed-length minutiae wedge-ring feature [60], which recorded the minutiae numbers on a pattern of wedges and rings. However, this method can only perform a coarse fingerprint authentication, and cannot handle big translations and rotations. Park et al. proposed a feature vector based on the distribution of the pairwise distances between minutiae [61]. However, this algorithm is only evaluated on the manually labeled minutiae and the performance is not satisfying.

The spectral minutiae representation is a method that overcomes the drawbacks of the minutiae algorithms, thus broadening the application of minutiae-based algorithms [34]. This method represents a minutiae set as a fixed-length feature vector, which is invariant to translation, and in which rotation and scaling become translations, so that they can be easily compensated for. These characteristics enable the combination of fingerprint recognition systems with template protection schemes and allow for faster matching as well. Moreover, the spectral minutiae representation method can be easily integrated into a minutiae-based fingerprint recognition system. Minutiae sets can be directly transformed to this new representation, which makes

---

[1]Other template protection systems exist [32] that do not pose this fixed-length feature vector requirement.
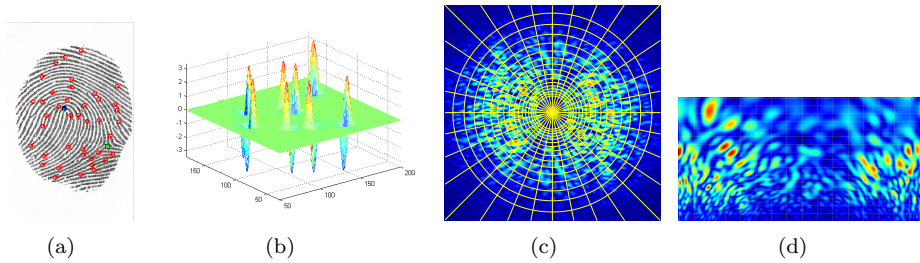
(a)            (b)            (c)            (d)

Fig. 5.2: Illustration of the general spectral minutiae representation procedure (images from the SMO case). (a) a fingerprint and its minutiae; (b) representation of minutiae points as real (or complex) valued continuous functions; (c) the 2D Fourier spectrum of 'b' in a Cartesian coordinate and a polar-logarithmic sampling grid; (d) the Fourier spectrum sampled on a polar-logarithmic grid.

this method compatible with the large amount of existing minutiae databases.

In [34], the concept of the two representation methods are introduced: the *location-based spectral minutiae representation* (SML) that codes the minutiae locations, and the *orientation-based spectral minutiae representation* (SMO) that codes both minutiae locations and orientations. Although SMO incorporates the minutiae orientations, it did not show better results than SML in the experiments performed in [34]. This motivated us to design another spectral minutiae representation that incorporates minutiae orientations: the *complex spectral minutiae representation* (SMC). We denote it as *complex* in the sense that minutiae are represented as complex valued continuous functions in the spatial domain. We will also present two feature reduction algorithms designed for the spectral minutiae representations: the *Column Principal Component Analysis* (CPCA) and the *Line Discrete Fourier Transform* (LDFT) feature reduction algorithms. By applying feature reductions, we can reduce the template storage and at the same time increase the matching speed, which is a critical factor for many large-scale biometric identification systems.

This paper is organized as follows. First, we give the background of the spectral minutiae representation and introduce the complex spectral minutiae representation in Section 5.2.2. Next, in Section 5.2.3, we present the Column-PCA and the Line-DFT feature reduction algorithms. Then, Section 5.2.4 shows the experimental results. Finally, we draw conclusions in Section 5.2.5.

### 5.2.2  Spectral Minutiae Representations

The objective of the spectral minutiae representation is to represent a minutiae set as a fixed-length feature vector, which is invariant to translation, rotation and scaling. In Figure 5.2, a general procedure of the spectral minutiae representation is illustrated. Step 1: we represent minutiae points as real (or complex) valued continuous functions, illustrated in Figure 5.2(b). In this representation, translation, rotation
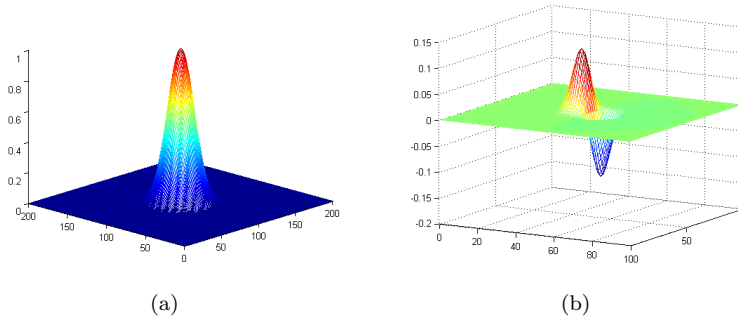
Fig. 5.3: Representations of one minutiae point as a real valued continuous function. (a) SML; (b) SMO.

and scaling may exist, depending on the fingerprint sensors that have been used and how the user has put his finger on the sensor. Step 2: a two-dimensional continuous Fourier transform is performed and only the Fourier magnitude is kept, illustrated in Figure 5.2(c). This representation is now translation invariant according to the shift property of the continuous Fourier transform. Step 3: the Fourier spectrum is re-mapped onto a polar-logarithmic coordinate system, illustrated in Figure 5.2(d). According to the scale and rotation properties of the two-dimensional continuous Fourier transform, now the rotation and scaling become translations along the new coordinate axes. It should be noted that this representation can be computed *analytically.* We will present the details later. In this paper, we will review SML and SMO, and then introduce SMC. These three representations are different in the "Step 1": SML and SMO represent minutiae points as real-valued continuous functions, while SMC represents minutiae as complex-valued continuous functions.

### 5.2.2.1   Location-based spectral minutiae representation (SML)

Assume we have a fingerprint with $Z$ minutiae. In SML, we code the minutiae locations by indicator functions,

$$m(x, y; \sigma_{\mathrm{L}}^2) = \sum_{i=1}^{Z} \frac{1}{2\pi\sigma_{\mathrm{L}}^2} \exp(-\frac{(x - x_i)^2 + (y - y_i)^2}{2\sigma_{\mathrm{L}}^2}), \qquad (5.1)$$

with $(x_i, y_i)$ the location of the $i$-th minutia in the fingerprint image. Thus, in the spatial domain, each minutia is represented by an isotropic two-dimensional Gaussian function, illustrated in Figure 5.3(a).

Taking the Fourier transform of $m(x, y; \sigma_{\mathrm{L}}^2)$ and keeping only the magnitude of the Fourier spectrum (in order to make the spectrum invariant to translation of the input), we obtain the location-based spectral minutiae representation

$$\mathcal{M}_{\mathrm{L}}(\omega_{\mathrm{x}}, \omega_{\mathrm{y}}; \sigma_{\mathrm{L}}^2) = \left| \exp\left( -\frac{\omega_{\mathrm{x}}^2 + \omega_{\mathrm{y}}^2}{2\sigma_{\mathrm{L}}^{-2}} \right) \sum_{i=1}^{Z} \exp(-\mathrm{j}(\omega_{\mathrm{x}} x_i + \omega_{\mathrm{y}} y_i)) \right|. \tag{5.2}$$

#### 5.2.2.2 Orientation-based spectral minutiae representation (SMO)

The SML only uses the minutiae location information. However, including the minutiae orientation as well may give better discrimination. Therefore, it can be beneficial to also include the orientation information in our spectral representation. In SMO, the orientation $\theta$ of a minutia is incorporated by using the spatial derivative of $m(x, y)$ in the direction of the minutia orientation, illustrated in Figure 5.3(b). As with the SML algorithm, taking the magnitude of the Fourier spectrum yields

$$\mathcal{M}_{\mathrm{O}}(\omega_{\mathrm{x}}, \omega_{\mathrm{y}}; \sigma_{\mathrm{O}}^2) = \left| \exp\left( -\frac{\omega_{\mathrm{x}}^2 + \omega_{\mathrm{y}}^2}{2\sigma_{\mathrm{O}}^{-2}} \right) \right.$$
$$\left. \times \sum_{i=1}^{Z} \mathrm{j}(\omega_{\mathrm{x}} \cos\theta_i + \omega_{\mathrm{y}} \sin\theta_i) \cdot \exp(-\mathrm{j}(\omega_{\mathrm{x}} x_i + \omega_{\mathrm{y}} y_i)) \right|. \tag{5.3}$$

#### 5.2.2.3 Complex spectral minutiae representation (SMC)

Although SMO incorporates the minutia orientation $\theta$, it did not show better results than SML in the experiments performed in [34]. The main reason is: in SMO, the minutiae orientation is incorporated as a derivative of the delta function, and this amplifies the minutiae noise (both in location and orientation) in the high frequency part of SMO. Therefore, a Gaussian kernel with higher $\sigma$ is needed for SMO to attenuate the noise in higher frequencies. However, the high frequency part also contains discriminative information, especially in case the minutiae have good quality. This limitation of SMO motivated us to design another spectral minutiae representation that incorporates minutiae orientation: SMC.

In SMC, each minutia is first represented by an isotropic two-dimensional Gaussian function in the spatial domain (here it is the same as SML). Then we incorporate the minutiae orientation by assigning each Gaussian a complex amplitude $\mathrm{e}^{\mathrm{j}\theta_i}$, illustrated in Figure 5.4. This results in a phase shift in the frequency domain. Taking the magnitude of the Fourier spectrum yields

$$\mathcal{M}_{\mathrm{C}}(\omega_{\mathrm{x}}, \omega_{\mathrm{y}}; \sigma_{\mathrm{C}}^2) = \left| \exp\left( -\frac{\omega_{\mathrm{x}}^2 + \omega_{\mathrm{y}}^2}{2\sigma_{\mathrm{C}}^{-2}} \right) \sum_{i=1}^{Z} \exp(-\mathrm{j}(\omega_{\mathrm{x}} x_i + \omega_{\mathrm{y}} y_i) + \mathrm{j}\theta_i) \right|. \tag{5.4}$$
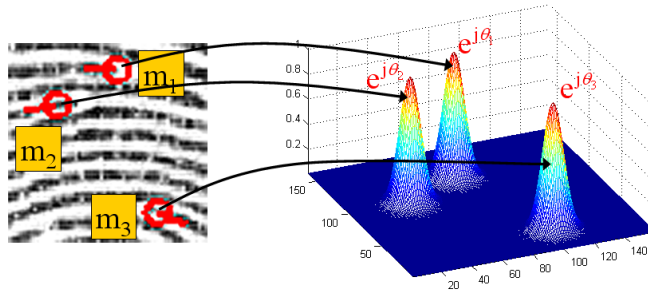
Fig. 5.4: An illustration of three minutiae points represented as complex valued continuous functions.

#### 5.2.2.4   Polar-logarithmic (or polar) sampling

In order to obtain the final spectral representations, the continuous spectra SML (5.2), SMO (5.3) and SMC (5.4) need to be sampled on a polar-logarithmic (or polar-linear) grid. A polar mapping transforms rotation to translation in the horizontal direction, while a logarithmic mapping transforms scaling to translation in the vertical direction[2]. In the radial direction $\lambda$, we use $M = 128$ samples between $\lambda_l$ and $\lambda_h$. In the angular direction $\beta$, we use $N = 256$ samples uniformly distributed between $\beta = 0$ and $\beta = \pi$ or $2\pi$ (because of the symmetry of the Fourier transform for real-valued functions, using the interval between 0 and $\pi$ for SML and SMO is sufficient). A polar-logarithmic sampling process is illustrated in Figures 5.2(c) and 5.2(d). The sampled spectra (5.2), (5.3) and (5.4) will be denoted by $S_L(m, n; \sigma_L)$, $S_O(m, n; \sigma_O)$ and $S_C(m, n; \sigma_C)$, respectively. When no confusion can arise, the parameter $\sigma$ and the subscripts L, O and C will be omitted.

Examples of the minutiae spectra achieved with SMC are shown in Figure 5.5. For each spectrum, the horizontal axis represents the rotation angle of the spectral magnitude (from 0 to $2\pi$); the vertical axis represents the frequency of the spectral magnitude (the frequency increases from top to bottom). It should be noted that the minutiae spectrum is periodic on the horizontal axis.

#### 5.2.2.5   Spectral Minutiae Matching

Let $R(m, n)$ and $T(m, n)$ be the two sampled minutiae spectra, respectively, achieved from the *reference* fingerprint and *test* fingerprint. Both $R(m, n)$ and $T(m, n)$ are normalized to have zero mean and unit energy. We use the two-dimensional correlation coefficient between $R$ and $T$ as a measure of their similarity.

---

[2]In most fingerprint databases, there is no scaling difference between the fingerprints, or the scaling can be compensated for on the level of the minutiae sets [43]. Therefore, we sample SML and SMO in a polar-logarithmic grid in order to be consistent with [34], while we sample SMC in a polar-linear grid, which can provide more samples in the higher frequency part.

(a)                                          (b)

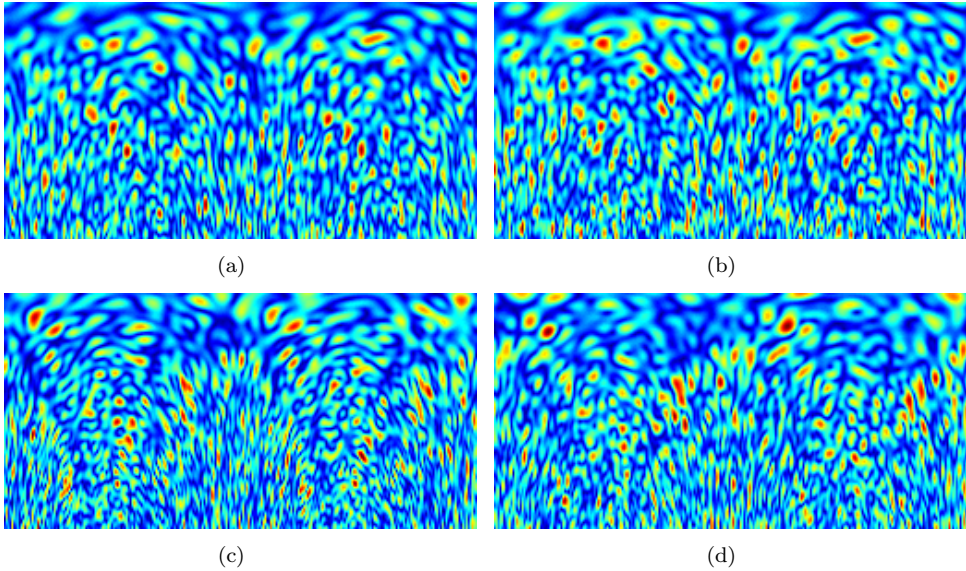(c)                                          (d)

Fig. 5.5: Examples of minutiae spectra using SMC. (a) and (b) are the SMC spectra from the same finger; (c) and (d) are the SMC spectra from the same finger.

In practice, the input fingerprint images are rotated and might be scaled (for example, depending on the sensor that is used to acquire an image). Assume that the scaling has already been compensated for on the level of the minutiae sets [43]. Then we only need to test a few rotations, which become the circular shifts in the horizontal direction. We denote $T(m, n - j)$ as a circularly shifted version of $T(m, n)$. We use the fast rotation shift searching algorithm, based on variable stepsizes that was presented in [56][3] and finally the maximum score from different combinations is the final matching score between $R$ and $T$,

$$S^{(R,T)} = \max_j \{ \frac{1}{MN} \sum_{m,n} R(m, n) T(m, n - j) \},$$

$$-15 \leq j \leq 15. \tag{5.5}$$

### 5.2.3   Spectral Minutiae Feature Reduction

The spectral minutiae feature is a 32,768-dimensional real-valued feature vector. The large dimensionality of the spectral minutiae feature can cause three problems. First, the template storage requirement is very high. Second, the high dimensionality leads

---

[3]In [56], totaly 9 rotations are tested in a range of $-20\,^\circ$ to $+20\,^\circ$ in case of $N = 256$ samples between 0 to $2\pi$.

to a computational burden and the matching speed will be limited. Third, the high dimensionality can lead to a small sample size problem [68]. In order to cope with these problems, we introduce two feature reduction methods: the *Column Principal Component Analysis* (CPCA) and the *Line Discrete Fourier Transform* (LDFT) feature reduction algorithms, which can be applied in conjunction.

### 5.2.3.1   Column-PCA feature reduction (CPCA)

Principal component analysis (PCA) if often used in dimensionality reduction. However, there are two problems in implement PCA on the spectral minutiae representations. The first is the small sample size problem. An unreduced spectral minutiae representation has a dimensionality of $D = 32,768$. A reliable PCA feature reduction requires a large number of fingerprint samples to implement the PCA training, which is difficult to acquire. The second problem is that the minutiae spectra are not rotation-invariant. As we mentioned in the previous section, the rotation of fingerprints becomes a circular shift in the horizontal direction. For the PCA training, all the minutiae spectra must be aligned beforehand in order to get meaningful results. Then both the training and matching processes become complicated. To cope with these problems, we introduce the Column-PCA method to perform a feature reduction.

We first look at the spectral minutiae feature $S$ in the 2D case as we presented in Section 5.2.2.4. From Figure 5.5, we can see that the minutiae spectrum is periodic on the horizontal axis. Moreover, on the vertical axis, the spectra with different frequencies are correlated. Therefore, we consider to use PCA to decorrelate the spectra with different frequencies in the *vertical* direction. To achieve this, we regard each column of $S$ as a new feature vector, thus $S = (\vec{z}_1, ..., \vec{z}_N)$, with $\vec{z}$ column feature vectors.

If we have $L$ samples $S_1, ..., S_L$ in the training set, we can create a $M \times L_N$ ($L_N = N \times L, N = 256$) data matrix $\mathbf{Z}$ consists of all the samples, as $\mathbf{Z} = [\vec{z}_1, ..., \vec{z}_{L_N}]$. To implement CPCA, we first subtract the sample mean (column mean) from the data matrix $\mathbf{Z}$. The next step is to apply SVD on $\mathbf{Z}$,

$$\mathbf{Z} = \mathbf{U}_Z \mathbf{S}_Z \mathbf{V}_Z^T. \tag{5.6}$$

Finally we can obtain the CPCA transform matrix $\widetilde{\mathbf{U}}_Z$ by retaining the first $M_{\text{CPCA}}$ ($M_{\text{CPCA}} \leq M$) columns of $\mathbf{U}_Z$. The CPCA transform on the minutiae spectra $S(m,n)$ is written as

$$\mathbf{S}_{\text{CPCA}} = \widetilde{\mathbf{U}}_Z^T \mathbf{S}, \tag{5.7}$$

with $\mathbf{S}_{\text{CPCA}}$ the $M_{\text{CPCA}} \times N$ data matrix with reduced dimensions. After the CPCA feature reduction, the relation of the energy retainment rate $E_{\text{CPCA}}$ and $M_{\text{CPCA}}$ is

$$E_{\text{CPCA}}(M_{\text{CPCA}}) = \frac{\sum_{n=1}^{M_{\text{CPCA}}} \mathbf{S}_{\text{Z}}(n,n)}{\sum_{n=1}^{M} \mathbf{S}_{\text{Z}}(n,n)}, \ 1 \le M_{\text{CPCA}} \le M, \tag{5.8}$$

and the retained dimensionality at a target energy retainment rate $\tilde{E}_{\text{CPCA}}$

$$M_{\text{CPCA}}(\tilde{E}_{\text{CPCA}}) = \arg \min_{1 \le \widetilde{M} \le M} \left| \frac{\sum_{n=1}^{\widetilde{M}} \mathbf{S}_{\text{Z}}(n,n)}{\sum_{n=1}^{M} \mathbf{S}_{\text{Z}}(n,n)} - \tilde{E}_{\text{CPCA}} \right|. \tag{5.9}$$

The CPCA transform is illustrated in Figures 5.6(a) and 5.6(b). We can see that after the CPCA transform, the main energy of the original minutiae spectrum $S$ is concentrated in the top lines of $S_{\text{CPCA}}$. By only retaining the top $M_{\text{CPCA}}$ lines, we perform the CPCA feature reduction, with a reduction rate $R_{\text{CPCA}} = (M - M_{\text{CPCA}})/M$. Because the rotation operator commutes with column transformation, the minutiae spectrum $S_{\text{CPCA}}$ remains periodic on the horizontal axis after the CPCA transform.

### 5.2.3.2   Line-DFT feature reduction (LDFT)

The CPCA feature reduction method reduces the minutiae spectrum feature $S$ in the *vertical* direction. In this section, we will introduce the Line-DFT feature reduction (LDFT) method, which will reduce the feature in the *horizontal* direction. This method is based on the fact that the minutiae spectrum $S$ is periodic on the horizontal axis. Therefore, LDFT can be applied both independently and in combination with the CPCA.

We denote each line of the minutiae spectrum $S$ as a line feature vector $\vec{y}$, thus $S = (\vec{y}_1, ..., \vec{y}_M)^{\text{T}}$. Because each line $y_m[n], (m = 1, ..., M)$ is a periodic discrete-time signal, by performing DFT (implemented as a FFT) on each $y_m[n]$, we can obtain $S_{\text{LDFT}} = (Y_1[k], ..., Y_M[k])^{\text{T}}, S_{\text{LDFT}} \in \mathbb{C}^M$, which is an exact representation of $S$.

The LDFT representation is illustrated in Figures 5.6(b) and 5.6(c). We can see that after the LDFT representation, the main energy is concentrated in the low frequency part (the middle columns). Therefore, for each line of the LDFT representation $S_{\text{LDFT}}$, we only retain the Fourier components with a certain percentage of energy (for example, 80%) in the lower frequency part. By reducing the number of Fourier components, we implement the LDFT feature reduction. For each line $m$, the relation of the energy retainment rate $E_{\text{LDFT}}$ after the LDFT feature reduction and $N_{\text{LDFT}}$
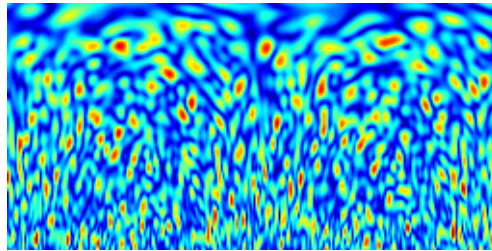
(a)
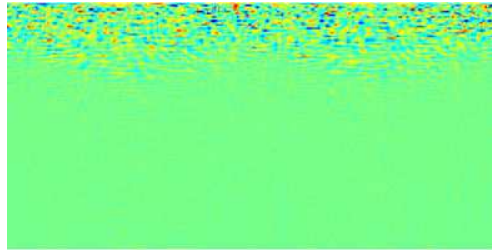


(b)
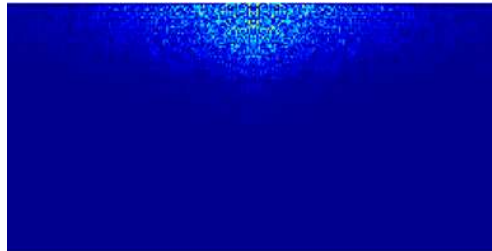


(c)

Fig. 5.6: Illustration of the CPCA transform and the LDFT representation. (a) the complex spectral minutiae; (b) the minutiae spectrum after the CPCA transform; (c) the magnitude of the LDFT representation of (b).

(which indicates that only the $N_{\text{LDFT}}$ Fourier components from the low frequency part are retained) is

$$
E_{\text{LDFT}}(N_{\text{LDFT}}; m) = \frac{\sum_{k=0}^{N_{\text{LDFT}}-1} |Y_m(k)|^2}{\sum_{k=0}^{N/2} |Y_m(k)|^2}, \ 1 \leq N_{\text{LDFT}} \leq \frac{N}{2} + 1, \tag{5.10}
$$

and the retained dimensionality at a target energy retainment rate $\tilde{E}_{\text{LDFT}}$

$$
N_{\text{LDFT}}(\tilde{E}_{\text{LDFT}}; m) = \arg \min_{1 \leq \tilde{N} \leq N/2+1} \left| \frac{\sum_{k=0}^{\tilde{N}-1} |Y_m(k)|^2}{\sum_{k=0}^{N/2} |Y_m(k)|^2} - \tilde{E}_{\text{LDFT}} \right|. \tag{5.11}
$$

As we mentioned in Section 5.2.2.5, the rotation of the fingerprint becomes the circular shift of the minutiae spectrum along the horizontal axis in the space domain. To test different fingerprint rotations (see Section 5.2.2.5) after applying the LDFT representation, we will implement the shift operation in the frequency domain according to the shift property of the discrete Fourier transform. Thus, the Line-DFT transformation of $T(m, n - n_{cs})$ in Equation (5.5) becomes

$$
T(m, n - n_{cs}) = (y_1(n - n_{cs}), ..., y_M(n - n_{cs}))^{\text{T}}
$$
$$
\xrightarrow{\text{LDFT}} \exp(-\text{j}\frac{2\pi}{N}kn_{cs})(Y_1(k), ..., Y_M(k))^{\text{T}} \tag{5.12}
$$

The DFT is orthnormal, thus it preserves inner products. Consider two discrete-time, periodic signals $f_1[n]$ and $f_2[n]$, $f_1[n], f_2[n] \in \mathbb{R}^N$, with period $N$ ($N$ is an even number), because of the symmetry properties of the DFT for real-valued signals, the correlation of $f_1[n]$ and $f_2[n]$ becomes

$$
\sum_{n=0}^{N-1} f_1[n]f_2^*[n] = \frac{1}{N}\Big( A_1[0]A_2[0]
$$
$$
+ 2 \sum_{k=1}^{\frac{N}{2}-1} (A_1[k]A_2[k] + B_1[k]B_2[k]) + A_1[\frac{N}{2}]A_2[\frac{N}{2}] \Big). \tag{5.13}
$$

where * denotes the complex conjugate, $\Re$ denotes the real part, $A_i[k]$ and $B_i[k]$ are

the real and the imaginary part of the Fourier coefficients.

Equation (5.13) shows that we can generate two one dimensional real-valued feature vectors $\vec{v_1}$ and $\vec{v_2}$ from the Fourier components, that are,

$$\vec{v_i} = \frac{1}{\sqrt{N}} \left( A_i[0], \sqrt{2}A_i[1], ..., \sqrt{2}A_i[\frac{N}{2}-1], A_i[\frac{N}{2}], \right.$$
$$\left. \sqrt{2}B_i[1], ..., \sqrt{2}B_i[\frac{N}{2}-1] \right), \, i = 1, 2. \qquad (5.14)$$

The correlation of $\vec{v_1}$ and $\vec{v_2}$ is exactly the same as the correlation of the real-valued signals $f_1[n]$ and $f_2[n]$. Thus, we can continue using the correlation-based spectral minutiae matching algorithm. In the LDFT feature reduction, only the $N_{\text{LDFT}} \, (N_{\text{LDFT}} \leq \frac{N}{2}+1)$ Fourier components from the low frequency part are retained. For the matching algorithm presented in Section 5.2.2.5, we denote $v_r$ and $v_{t,n_{cs}}$ as the reduced features of $R(m,n)$ and $T(m, n-n_{cs})$ respectively, then Equation (5.5) becomes

$$S^{(R,T)} = \max_{n_{cs}}\{\frac{1}{MN} \sum v_r v_{t,n_{cs}}\}, \, -15 \leq n_{cs} \leq 15. \qquad (5.15)$$

### 5.2.4   Experiments

#### 5.2.4.1   Experimental settings

The proposed algorithms have been evaluated on MCYT [46] and FVC2002-DB2 [48] fingerprint databases. The fingerprint data that we used from MCYT are obtained from 145 individuals (person ID from 0000 to 0144 and finger ID 0) and each individual contributes 12 samples. We use samples from person ID 0100 to 0144 for the CPCA and LDFT training (totally 540 fingerprints) and samples from person ID 0000 to 0099 for test (totally 1200 fingerprints). We also tested our algorithms on the FVC2002-DB2 because it is a public-domain fingerprint database. Compared with MCYT, the fingerprints in FVC2002 have lower quality and bigger displacements. For the FVC databases, we apply the same experimental protocol as in the FVC competition: the samples from finger ID 101 to 110 for the CPCA and LDFT training (totally 40 fingerprints) and samples from person ID 1 to 100 for test (totally 400 fingerprints)[4]. The minutiae sets were obtained by the VeriFinger minutiae extractor [11][5].

---

[4]We propose to use our algorithm in a high security scenario. In FVC2002 databases, samples 3, 4, 5 and 6 were obtained by requesting the biometric data subject to provide fingerprints with exaggerated displacement and rotation. In a high security scenario where the biometric data subject is aware that cooperation is crucial for security reasons, he will be cooperative. Therefore, only samples 1, 2, 7 and 8 are chosen. To deal with the large rotations, an absolute pre-alignment based on core and its direction can be applied.

[5]VeriFinger Extractor Version 5.0.2.0 is used.

Table 5.1: Parameters of CPCA and LDFT (MCYT database).

| Methods | SML | SMO | SMC |
|---|---|---|---|
| $E_{\text{CPCA}}$ | 83% | 90% | 84.7% |
| Reduction | 78.1% | 78.1% | 75% |
| $E_{\text{LDFT}}$ | 99% | 99% | 75% |
| Reduction | 67.8% | 72.8% | 58.3% |
| $E_{\text{Total}}$ | 82.2% | 89.1% | 63.5% |
| Reduction | 92.9% | 94.0% | 89.6% |

Table 5.2: Parameters of CPCA and LDFT (FVC2002-DB2 database).

| Methods | SML | SMO | SMC |
|---|---|---|---|
| $E_{\text{CPCA}}$ | 75% | 92% | 66.2% |
| Reduction | 75% | 75% | 75% |
| $E_{\text{LDFT}}$ | 97% | 98% | 70% |
| Reduction | 68.1% | 72.5% | 51.1% |
| $E_{\text{Total}}$ | 72.8% | 90.2% | 46.3% |
| Reduction | 92.0% | 93.1% | 81.5% |

We test our algorithm in a verification setting. For matching genuine pairs, we used all the possible combinations. For matching imposter pairs, we chose the first sample from each identity. For the parameters $\sigma_{\text{L}}, \sigma_{\text{O}}$ and $\sigma_{\text{C}}$ in Equations (5.2), (5.3) and (5.4), we chose $\sigma = 0$ for SML and SMC (in this case, no multiplication with Gaussian in the frequency domain) and $\sigma = 4.24$ for SMO (the explanation of parameter settings can be found in [34]). In our experiment, we also use the core as a reference point to assist the verification, following the procedure in [34][6].

### 5.2.4.2    Results

We test the SML, SMO and SMC representations in the two databases. We present the results in both with and without CPCA and LDFT cases to evaluate the performances of the feature reduction algorithms. During feature reduction, the selection of the energy retainment rates $E_{\text{CPCA}}$ and $E_{\text{LDFT}}$ are important for the performance. When $E_{\text{CPCA}}$ and $E_{\text{LDFT}}$ are chosen, we can calculate $M_{\text{CPCA}}$ and $N_{\text{LDFT}m}$ using the fingerprints in the training sets, according to Equations (5.9) and (5.11).

The feature reduction parameters are shown in Tables 5.1 and 5.2. We can see that regarding LDFT, SMC has lower reduction rates and energy retainment compared with SML and SMO. The reason is that SMC samples a $2\pi$ range in the horizontal direction, while SML and SMO a range of $\pi$. Therefore, the horizontal feature

---

[6]In [34], for each fingerprint, maximum two cores or/and two deltas were used to improve the performance. In this paper, only the upper core is used.
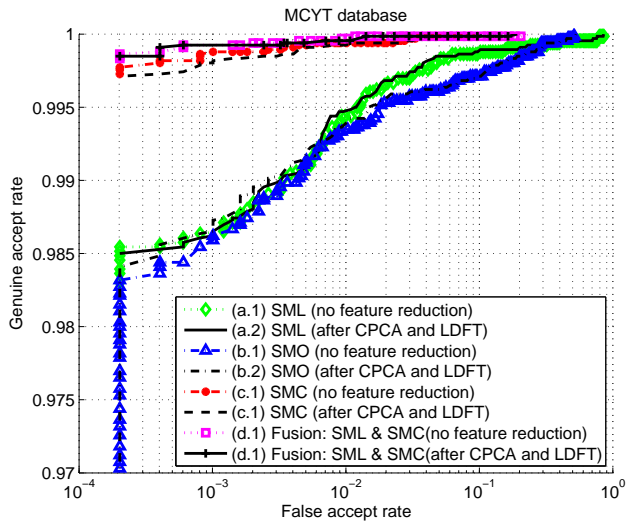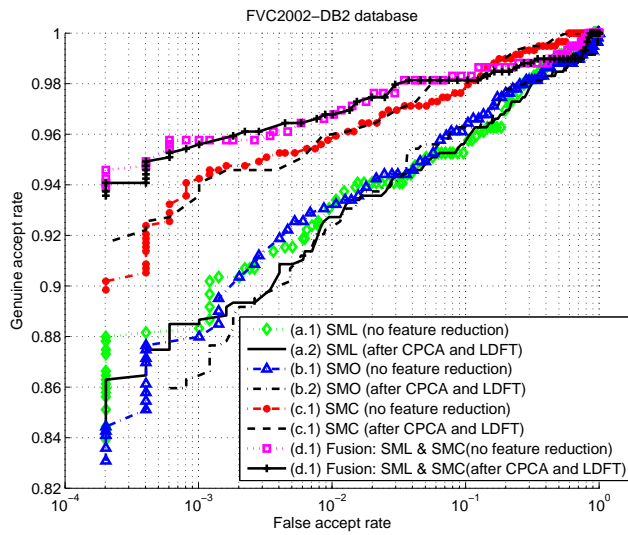
Fig. 5.7: ROC curves (MCYT database).



Fig. 5.8: ROC curves (FVC2002-DB2 database).

Table 5.3: Results after CPCA and LDFT (MCYT database).

| Methods | EER | GAR @ FAR=0.1% |
|---|---|---|
| SML | 0.67% | 98.8% |
| SMO | 0.71% | 98.6% |
| SMC | 0.16% | 99.8% |
| Fusion SML and SMC | 0.06% | 99.9% |

Table 5.4: Results after CPCA and LDFT (FVC2002-DB2 database).

| Methods | EER | GAR @ FAR=0.1% |
|---|---|---|
| SML | 5.1% | 88.7% |
| SMO | 4.51% | 86.6% |
| SMC | 3.05% | 94.1% |
| Fusion SML and SMC | 2.48% | 95.6% |

reduction rates for SMC are lower.

The performances of SML, SMO, SMC and the feature reduction results are shown in Tables 5.3 and 5.4 and the ROC curves are in Figures 5.7 and 5.8. From the ROC curves, we can see that there is no noticeable performance degradation after the CPCA and LDFT feature reductions. By using both methods, we can achieve a template size reduction around 90%.

From Tables 5.3 and 5.4, we can see that the recognition rates of SMC have substantial improvements compared with SML and SMO (the improvement factors range from 1.5 to 4.4 in the EERs). It is understandable that SMC outperformed SML because SMC incorporates the minutiae orientation information. As for SMO, we explained perviously that in the SMO representation, the critical information of minutiae orientations is in the high frequency region, where also contains more noise. While with SMC, this critical information is spread over the entire spectrum. This explains how the SMC overcomes the drawback of the SMO technique. A preliminary attempt of SML and SMC fusion (considering the recognition performances of SML and SMC, a score level sum-rule fusion with weights 1:2 has been applied) is also applied and results in some clear improvements in accuracy.

Without feature reductions, we can implement 8,000 comparisons per second using optimized C language programming on a PC with Intel Pentium D processor 2.80 GHz and 1 GB of RAM. After applying CPCA and LDFT, we can implement 125,000 comparisons (the speed is more than 15 times faster) under the same setting. We also tested the VeriFinger matcher, a fast commercial minutiae-based matcher, using the same PC setting and the matching speed is 8,000 comparisons per second. Our matching speed will be slowed down by incorporating core information (reduces 2 times) and fusion of SML and SMC (reduces 2 times). After including these factors, our spectral minutiae matching still has speed advantages compared with most existing minutiae-based algorithms.

### 5.2.5 Conclusions and future work

Minutiae-based matching is the most widely used technique in fingerprint recognition systems. However, the low matching speed is limiting their application. At the same time, the increasing security and privacy concerns make minutiae template protection one of the most crucial tasks. The spectral minutiae representation has coped with the above issues.

In this paper, we present the complex spectral minutiae representation and the CPCA and LDFT feature reduction algorithms. These new techniques enhance the recognition accuracy and increase the matching speed as well, thus broaden the application of the spectral minutiae representation algorithm. In addition, our other preliminary research showed that we can further improve accuracy about 20% to 70% by applying minutiae quality data and minutiae subsets [57], [58]. We will continue exploring the potential of increasing recognition accuracy.

Furthermore, in order to be able to apply the spectral minutiae representation with a template protection scheme, for example based on a fuzzy extractor [53], the next step would be to extract bits that are stable for the genuine user and completely random for an arbitrary user. A fixed-length binary representation also has other advantages such as the small template storage and high matching speed. This will also be our future work.

## 5.3 Chapter Conclusions

In this chapter, we proposed the *Complex Spectral Minutiae Representation* (SMC), a new version of the spectral minutiae representations. Compared with SMO, SMC improves the recognition performance significantly by incorporating the minutiae orientation in a different way. In this chapter, the CPCA and LDFT feature reduction algorithms that introduced in Chapter 4 are also applied to SMC.

Up to now, we have already presented three spectral minutiae representation methods: SML, SMO and SMC. They share the same basic principle. SMC showed the best recognition performance and it is recommended for the application of the spectral minutiae representations. In Chapter 6, the binary representations will also be mainly investigated for the SMC features.

Table 5.5: The contributions of Chapter 5 and their achieved targets.

| Contribution(s) | Target(s) |
|---|---|
| SMC | Target I: Fixed-length feature vector |
| | Target II: Translation and rotation invariance |
| | Target IV: High recognition performance |

With regard to the research question and the targets of this thesis that are formulated
in Section 1.3, this chapter addressed Target I, fixed-length feature vector, Target II,
translation and rotation invariance, and Target IV, high recognition performance.
Targets I and II are achieved by the basic principle of the spectral minutiae represen-
tation. Target IV is achieved by the SMC feature, which incorporating the minutiae
orientation in a more effective way that leads to a higher recognition performance.
The contributions of this chapter together with their achieved targets are summarized
in Table 5.5.

# Chapter 6

# Binary Representations of Spectral Minutiae Features

## 6.1 Chapter Introduction

PURPOSE. The template protection schemes based on the helper data schemes require a fixed-length *binary* feature vector as input. In the previous chapters, we introduced the spectral minutiae representation, which represents a fingerprint minutiae set as a fixed-length *real-valued* feature vector. In this chapter, we will investigate methods that quantize the real-valued spectral minutiae features into binary strings. Furthermore, we will explore several biometric fusion algorithms to improve the recognition performance of the spectral minutiae representation algorithm.

CONTENTS. Based on the complex spectral minutiae representation (SMC) introduced in Chapter 5, we first propose two methods to quantize the real-valued spectral minutiae features into binary strings: the *Spectral Bits* and the *Phase Bits* in Section 6.2. The algorithms are evaluated on the FVC2002-DB2 database. Next, in Section 6.3, we investigate the multi-sample fusion algorithms to improve the recognition performance. Furthermore, in the same section, we also propose different schemes to mask out unreliable bits. The algorithms are evaluated on the FVC2000-DB2 database. In the context of the system diagram, the content of this chapter and its referred blocks are highlighted in Figure 6.1.

PUBLICATION(S). Section 6.2 has been published in [73] and Section 6.3 has been published in [74].

A NOTE TO READERS. The readers can focus on the following subsections: (1) 6.2.4 introduces two spectral minutiae quantization methods, the *Spectral Bits* and the *Phase Bits*; (2)based on the *Spectral Bits* algorithm, 6.3.3.3 explores different schemes
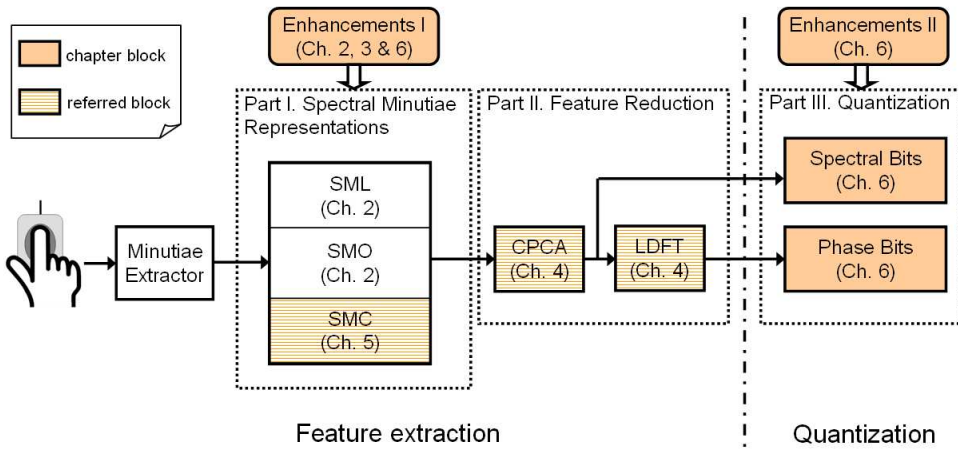
Fig. 6.1: *Block diagram of our designed system, highlighting the content of Chapter 6 and its referred blocks.*

to mask out unreliable bits; (3) 6.3.4 investigate the multi-sample fusion algorithms to improve the recognition performance of the spectral minutiae representation. Subsections 6.2.2, 6.3.2.2 and 6.3.2.3 give the background that have already been introduced in Chapter 5. The readers can skip these parts.

## 6.2   Binary Representations of Fingerprint Spectral Minutiae Features

**Abstract**

A fixed-length binary representation of a fingerprint has the advantages of a fast operation and a small template storage. For many biometric template protection schemes, a binary string is also required as input. The spectral minutiae representation is a method to represent a minutiae set as a fixed-length real-valued feature vector. In order to be able to apply the spectral minutiae representation with a template protection scheme, we introduce two novel methods to quantize the spectral minutiae features into binary strings: Spectral Bits and Phase Bits. The experiments on the FVC2002 database show that the binary representations can even outperformed the spectral minutiae real-valued features.

### 6.2.1   Introduction

Minutiae-based matching is the most widely used technique in fingerprint recognition systems. However, the low matching speed is limiting its application. At the same
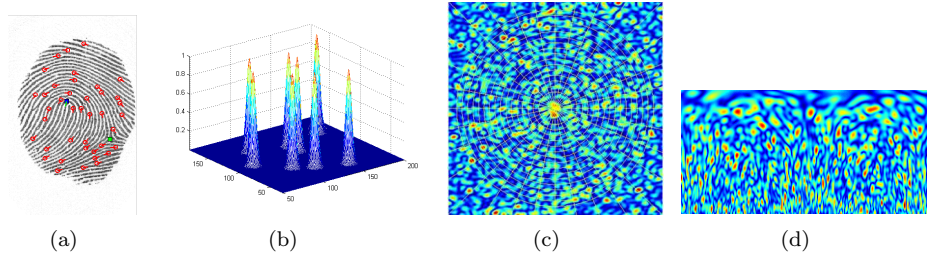
Fig. 6.2: Illustration of the complex spectral minutiae representation procedure. (a) a fingerprint and its minutiae; (b) representation of minutiae points as complex valued continuous functions; (c) the 2D Fourier spectrum of 'b' in a Cartesian coordinate and a polar sampling grid; (d) the Fourier spectrum sampled on a polar grid.

time, increasing security and privacy concerns make minutiae template protection a crucial task. The spectral minutiae representation is a method to represent a minutiae set as a fixed-length feature vector, which is invariant to translation, and in which rotation and scaling become translations, so that they can be easily compensated for. These characteristics enable the combination of fingerprint recognition systems with template protection schemes and allow for a fast minutiae-based matching as well.

In order to apply the spectral minutiae representation with a template protection scheme, for example, based on a fuzzy extractor [53] or fuzzy commitment [33], we need to quantize the spectral minutiae real-valued features into binary strings. A fixed-length binary representation also has additional advantages such as small template storage and high matching speed.

The main contributions of this paper are: we propose two novel quantization schemes to convert the real-valued spectral minutiae features into binary strings: *Spectral Bits* and *Phase Bits*. We also evaluate our algorithms on the FVC2002-DB2 database and show that the two binary representations achieved very promising results.

In this paper, we will first present the complex spectral minutiae representation (SMC), a new spectral minutiae representation method in Section 6.2.2. Next, in Section 6.2.3, we will briefly review the Column-PCA and Line-DFT feature reduction algorithms, which can greatly compact the spectral minutiae features. Then, in Section 6.2.4, we will introduce two novel methods to quantize the spectral minutiae features into binary strings: Spectral Bits and Phase Bits. Finally, we will show the experimental results in Section 6.2.5 and draw conclusions in Section 6.2.6.

## 6.2.2  Complex Spectral Minutiae Representation

The objective of the spectral minutiae representation is to represent a minutiae set as a fixed-length feature vector, which is invariant to translation and rotation [34, 71]. We assume that the scaling has already been compensated for on the level of the minutiae sets. This is for instance possible if minutiae are presented in a standard

like [43], which includes sensor resolution. In Figure 6.2, the procedure of the complex spectral minutiae representation (SMC) is illustrated.

Assume a fingerprint with $Z$ minutiae. First, we code the minutiae locations by indicator functions, which are isotropic two-dimensional Gaussian functions in the spatial domain. Then we incorporate the minutiae orientation by assigning each Gaussian a complex amplitude $e^{j\theta_i}, i = 1...Z$. In this way, we represent minutiae points as complex valued continuous functions, the magnitude of which is shown in Figure 6.2(b). In this representation, translation and rotation may exist, depending on how the user has put his finger on the sensor.

Next, a two-dimensional continuous Fourier transform is performed and only the Fourier magnitude is kept, illustrated in Figure 6.2(c). This representation is now translation invariant according to the shift property of the continuous Fourier transform. This representation can be computed *analytically*,

$$\mathcal{M}_{\mathrm{C}}(\omega_{\mathrm{x}}, \omega_{\mathrm{y}}; \sigma_{\mathrm{C}}^2) = \left| \exp\left( -\frac{\omega_{\mathrm{x}}^2 + \omega_{\mathrm{y}}^2}{2\sigma_{\mathrm{C}}^{-2}} \right) \sum_{i=1}^{Z} \exp(-j(\omega_{\mathrm{x}} x_i + \omega_{\mathrm{y}} y_i) + j\theta_i) \right|. \qquad (6.1)$$

with $(x_i, y_i, \theta_i)$ the location and orientation of the $i$-th minutia in the fingerprint image, and $(\omega_{\mathrm{x}}, \omega_{\mathrm{y}}; \sigma_{\mathrm{C}}^2)$ are the spatial frequencies and the Gaussian parameter respectively.

Finally, the Fourier spectrum is re-mapped onto a polar coordinate system, illustrated in Figure 6.2(d). In the radial direction $\lambda$, we use $M = 128$ samples between $\lambda_{\mathrm{l}} = 0.05$ and $\lambda_{\mathrm{h}} = 0.58$. In the angular direction $\beta$, we use $N = 256$ samples uniformly distributed between $\beta = 0$ and $\beta = 2\pi$. Since our target application is in a high security scenario with reasonable good quality fingerprints, we choose $\sigma_{\mathrm{C}} = 0$ for the best performance. In this case, there is no multiplication with Gaussian in the frequency domain. An analysis of the selection of the Gaussian parameter $\sigma$ can be found in [34]. According to the rotation properties of the two-dimensional continuous Fourier transform, now the rotation becomes translation along the new coordinate axis.

Let $R(m, n)$ and $T(m, n)$ be the two sampled minutiae spectra that are achieved from the *reference* fingerprint and *test* fingerprint respectively. Both $R(m, n)$ and $T(m, n)$ are normalized to have zero mean and unit energy. We use the two-dimensional correlation coefficient between $R$ and $T$ as a measure of their similarity.

In practice, the input fingerprint images are rotated. Therefore, we need to test a few rotations, which become the circular shifts in the horizontal direction. We denote $T(m, n - j)$ as a circularly shifted version of $T(m, n)$ and the final matching score between $R$ and $T$ is,

$$S^{(R,T)} = \max_j \{ \frac{1}{MN} \sum_{m,n} R(m,n)T(m,n-j) \},$$

$$-15 \leq j \leq 15. \tag{6.2}$$

### 6.2.3  Feature Reduction

The spectral minutiae feature is a 32,768-dimensional real-valued feature vector. The large dimensionality of the spectral minutiae feature can cause three problems. First, the template storage requirement is very high. Second, the high dimensionality leads to a computational burden and the matching speed will be limited. Third, the high dimensionality can lead to a small sample size problem [68]. In order to cope with these problems, we will apply two feature reduction methods that are introduced in [67]: the *Column Principal Component Analysis* (CPCA) and the *Line Discrete Fourier Transform* (LDFT) feature reduction algorithms, which can be applied in conjunction.

The idea of Column PCA (CPCA) is applying the well known Principal Component Analysis technique to the SMC columns. PCA has two functions: it decorrelates features and concentrates power. The CPCA representation is shown in Figure 6.3(b). We can see that after CPCA, the power is concentrated in the upper lines. The features in the lower parts are close to zero, so we can remove them from the representation.

After the CPCA feature reduction, the minutiae spectrum remains periodic on the horizontal axis. Therefore, applying Discrete Fourier Transform to each line generates an exact representation. From Figure 6.3(c), we can see that the Fourier coefficients concentrate power in the low frequency part. Therefore, we can achieve feature reduction by removing the Fourier coefficients in the higher frequency part. In this paper, we improved the LDFT feature reduction algorithm represented in [67]. In our previous work [67], we kept the energy in each line of the spectral minutiae feature constant when reducing the Fourier coefficients. However, since the energy of each line is probably unevenly distributed, see Figure 6.3(c), this may not be the most efficient way to perform feature reduction. In this paper, we keep a fixed-length Fourier coefficients with a maximum overall energy retainment. We gain this information in the training procedure. In this way, we can increase the feature reduction rate from 51% to 78% while keeping a similar performance (we will show the details in Section 2.2.4).

### 6.2.4  Quantization

In this section, we will introduce two quantization methods: *Spectral Bits*, which is applied in conjunction with the CPCA feature reduction, and *Phase Bits*, which is applied in conjunction with the LDFT feature reduction.
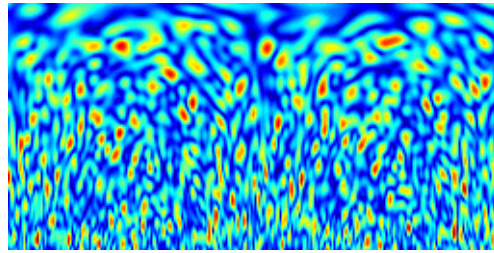
(a)
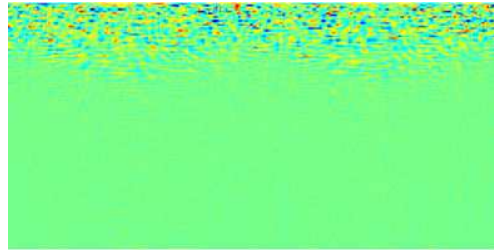


(b)
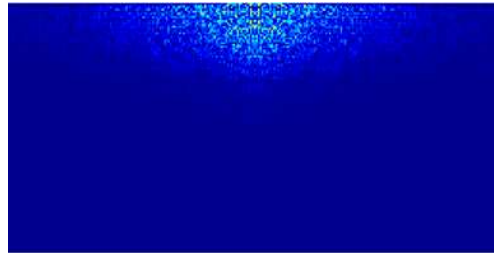


(c)

Fig. 6.3: Illustration of the CPCA transform and the LDFT representation. (a) the SMC feature; (b) the minutiae spectrum after the CPCA transform; (c) the magnitude of the LDFT representation of (b).

(a)



(b)

Fig. 6.4: Example of Spectral Bits (SMC spectra after CPCA). (a) the Sign Bit; (b) the Mask Bit.

### 6.2.4.1   Spectral Bits

The Spectral Bits quantization is applied to the real-valued features after the CPCA feature reduction. First, each real-valued feature is quantized as one bit (1 if the feature is greater than zero and 0 otherwise, we call it sign bit), shown in Figure 6.4(a). Second, since the quantization boundary is zero, and the features close to zero are unstable and likely to flip, they may cause errors. Therefore,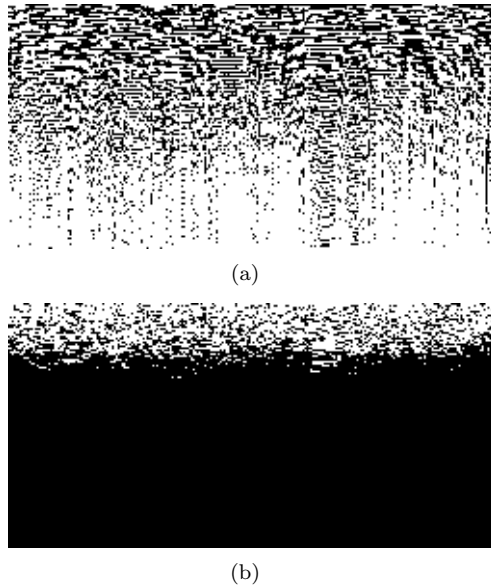 we will mask out the features of which the absolute values are below a certain threshold. For the best recognition performance, we set the threshold to 0.8 after normalizing the spectra to have unit energy. We found this parameter empirically by testing thresholds on different fingerprint databases. The resulting mask bit is shown in Figure 6.4(b).

### 6.2.4.2   Phase Bits

The Phase Bits quantization is applied to the complex-valued features after the LDFT feature reduction. Each complex component is quantized as 2 bits and the quantization scheme is shown in Figure 6.5. The sign bit and the mask bit generation is similar as the procedure in the Spectral Bits quantization, shown in Figure 6.6. We set the mask threshold to 1.2 empirically after normalizing the spectra to have unit energy.
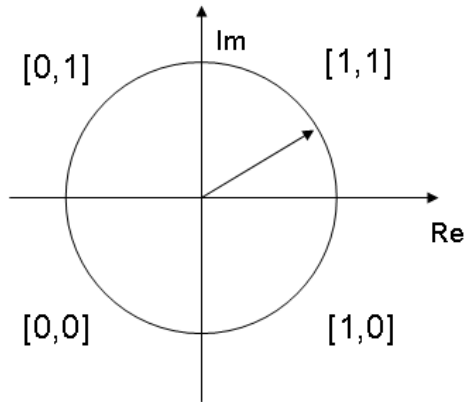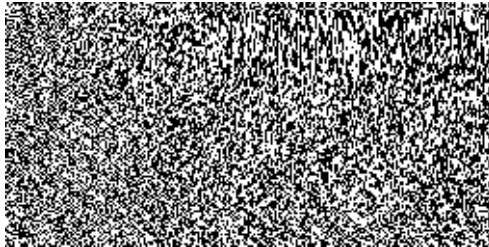
Fig. 6.5: Quantization scheme.



(a)



(b)

Fig. 6.6: Example of Phase Bits (SMC spectra after LDFT). (a) the Sign Bit; (b) the Mask Bit.

Table 6.1: Results.

| Methods | EER | FRR@FAR0.1% |
|---|---|---|
| 1. Real features | 3.2% | 6.1% |
| 2. Spectral Bits | 3.2% | 5.9% |
| 3. Phase Bits | 3.8% | 6.3% |
| 4. Fusion of (2) and (3) | 3.0% | 5.4% |

### 6.2.4.3   Fractional Hamming Distance

After generating sign bit and mask bit vectors, we can compute a Fractional Hamming distance (FHD) as a measure of the dissimilarity between two fingerprints spectra $R(m, n)$ and $T(m, n)$, whose sign bit vectors are denoted as {codeR, codeT} and mask bit vectors as {maskR, maskT},

$$HD = \frac{||(\text{codeR} \otimes \text{codeT}) \cap \text{maskR} \cap \text{maskT}||}{||\text{maskR} \cap \text{maskT}||}. \qquad (6.3)$$

## 6.2.5   Results

The proposed algorithms have been evaluated on the FVC2002-DB2 [48] fingerprint database. We apply the same experimental protocol as in the FVC competition: the samples from finger ID 101 to 110 for the CPCA and LDFT training and samples from person ID 1 to 100 for test. We propose to use our algorithm in a high security scenario. In the FVC2002-DB2 databases, samples 3, 4, 5 and 6 were obtained by requesting the biometric data subject to provide fingerprints with exaggerated displacement and rotation. In a high security scenario where the biometric data subject is aware that cooperation is crucial for security reasons, he will be cooperative. Therefore, we chose samples 1, 2, 7 and 8 for a more realistic evaluation. To deal with the large rotations, an absolute pre-alignment based on core and its direction can be applied. We obtain the minutiae sets using the VeriFinger minutiae extractor [11](VeriFinger Extractor Version 5.0.2.0 is used).

We test our algorithm in a verification setting. For matching genuine pairs, we used all the possible combinations. For matching imposter pairs, we chose the first sample from each identity. Therefore, we have totally 600 genuine scores and 4950 imposter scores.

In our experiment, we also use the core as a reference point to assist the verification, following the procedure in [34] (for each fingerprint, maximum two cores or/and two deltas were used to improve the performance in [34], while in this paper, only the upper core is used).
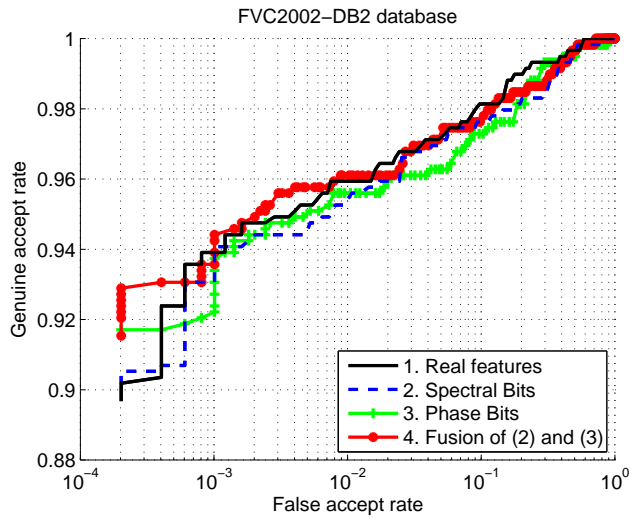
Fig. 6.7: ROC curves.

We test both the Spectral Bits and the Phase Bits results. For the CPCA feature reduction, we keep the top 35 lines, with a feature reduction rate of 73%. Therefore, we generate 8960 bits for the Spectral Bits string, among which we mask out about 40%. For the LDFT feature reduction, we keep the first 1000 components with largest magnitudes, with a feature reduction rate of 78%. Thus, we generate 2000 bits for the Phase Bits string, among which we mask out about 45%. For the LDFT feature reduction, it should be noted that if we apply the LDFT feature reduction on SMC features using the method in [67], we can only achieve a feature reduction rate of 51% for the similar performance.

For comparison, we also present the results of real-valued features (before quantization). To improve the binary results, we also tried the fusion of the Spectral Bits and the Phase Bits (a score level sum-rule fusion is applied). The results are shown in Tables 6.1 and the ROC curves are shown in Figures 6.7. From the results, we can see that both the Spectral Bits and the Phase Bits hardly degrade the performance compared with the real-valued features. The Spectral Bits performs better than the Phase Bits. The fusion of these two quantization schemes gives the best performance, which is also outperformed the spectral minutiae real-valued features.

## 6.2.6   Discussion and Conclusion

In this paper, we introduce two methods to extract bits from the spectral minutiae features: the Spectral Bits and the Phase Bits. Both quantization schemes show promising results. These two methods are based on the spectral minutiae features after the CPCA and LDFT feature reduction, which has already decreased the com-

putational complexity for more than 10 times [67]. The fixed-length binary representations proposed in this paper further compact the template and increase the matching speed.

To apply the spectral minutiae representation with a template protection scheme, for example, based on fuzzy commitment [33], an error correcting step is needed. Erasure decoding can handle the masking of bits. Furthermore, to enhance the recognition accuracy, we can use multi-sample enrolment to improve the biometric template quality. Investigating the possible error correcting codes and multi-sample enrolment schemes will be our future work.

## 6.3 Binary Spectral Minutiae Representation with Multi-Sample Fusion For Fingerprint Recognition

**Abstract**

Biometric fusion is the approach to improve the biometric system performance by combining multiple sources of biometric information. The binary spectral minutiae representation is a method to represent a fingerprint minutiae set as a fixed-length binary string. This binary representation has the advantages of a fast operation and a small template storage. It also enables the combination of a biometric system with template protection schemes that require a fixed-length feature vector as input. In this paper, based on the spectral minutiae representation algorithm, we investigate the multi-sample fusion algorithms at the feature-, score-, and decision-level respectively. Furthermore, we propose different schemes to mask out unreliable bits. The algorithms are evaluated on the FVC2000-DB2 database and showed promising results.

### 6.3.1   Introduction

Recognition of individuals by means of biometric characteristics is gaining importance due to the high security and user convenience. Among various biometric characteristics, such as face, signature and voice, fingerprint has one of the highest levels of distinctiveness and performance [1] and it is the most commonly used biometric modality. Most fingerprint recognition systems are based on the use of a minutiae set. However, the low comparison (or matching) speed is limiting its application to search large databases. At the same time, the increasing *privacy concerns* make minutiae template protection a crucial task. The spectral minutiae representation is a method to represent a minutiae set as a fixed-length feature vector, which is invariant to translation, and in which rotation and scaling become translations, so that they can be easily compensated for [34, 71, 73]. These characteristics enable the combination

of fingerprint recognition systems with template protection schemes and allow for a fast minutiae-based matching as well.

In order to apply the spectral minutiae representation with a template protection scheme based on fuzzy commitment and helper data schemes, such as [33] and [5], we need to quantize the real-valued spectral minutiae features into binary strings. A fixed-length binary representation also has additional advantages such as small template storage and high matching speed. Based on the *complex spectral minutiae representation* (SMC) [71], the *Spectral Bits* binary spectral minutiae representation was proposed in [73] and showed promising results. Since the recognition performance is the most important factor for a biometric system, in this paper, we will investigate methods to improve the recognition performance by fusing multiple spectral minutiae representations.

Biometric fusion, also known as multibiometrics, is the approach to improve the biometric system performance by combining multiple sources of biometric information. Ross et al. [50] describe five scenarios that are possible to obtain multiple sources of information: (1) Multi-sensor systems, where the information from a single biometric characteristic is obtained from different sensors; (2) Multi-algorithm systems, where the same biometric data is processed using different algorithms; (3) Multi-instance systems, where multiple units of the same biometric characteristic (for example, the left and right index fingers) are combined; (4) Multi-sample systems, where a single sensor is used to acquire multiple impressions of the same biometric characteristic; (5) Multi-modal system, where different biometric characteristics (such as iris and fingerprint) from the same person are combined. Considering the cost effectiveness and user convenience, scenarios (1)(3)(5) may not be preferred. Scenario (2) is a popular cost-effective way to improve the biometric recognition performance. Prabhakar and Jain tried several attempts of combining multiple classifiers, and concluded that the improvement in recognition performance is closely related to the independence among various classifiers [75]. In this paper, we focus on the spectral minutiae algorithm and we will not involve other classifiers in this paper (for instance, a non-minutiae based classifier). Therefore, we will investigate scenario (4), fusing multiple enrollment samples, to improve the recognition performance.

Based on the difference in the level of available information, fusion strategies can be applied at image-level, feature-level, score-level and decision-level [1,50]. In this paper, we focus on the procedures after the fingerprint minutiae extraction. Therefore, we will discuss the fusion strategies at feature-, score- and decision-level, respectively.

The main contributions of this paper are: (1) based on the method presented in [57], the minutiae quality data are incorporated to enhance the Complex Spectral Minutiae Representation (SMC) performance; (2) we investigate the multiple enrollment samples fusion at the feature-, score-, and decision-level respectively; (3) we investigate and evaluate several masking schemes, and discuss their application in context with template protection and error correction schemes.

In this paper, we will first present the *minutiae quality incorporated complex spectral minutiae representation* together with the *Column-PCA* feature reduction algorithm
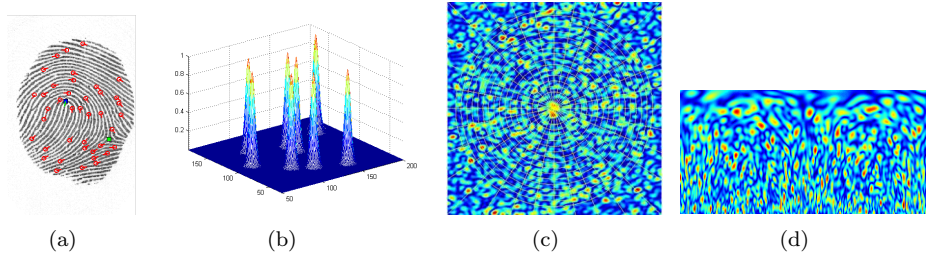
(a)                    (b)                    (c)                    (d)

Fig. 6.8: Illustration of the complex spectral minutiae representation procedure. (a) a finger-
print and its minutiae; (b) representation of minutiae points as complex valued continuous
functions; (c) the 2D Fourier spectrum of 'b' in a Cartesian coordinate and a polar sampling
grid; (d) the Fourier spectrum sampled on a polar grid.

in Section 6.3.2. Next, in Section 6.3.3, we will briefly review the *Spectral Bits* quan-
tization method, and propose several masks schemes. Then, in Section 6.3.4, we will
discuss several methods to implement multi-sample fusions. Finally, we will show the
experimental results in Section 6.3.5 and draw conclusions in Section 6.3.7.

## 6.3.2   Complex Spectral Minutiae Representation

### 6.3.2.1   Minutiae Quality Incorporated Complex Spectral Minutiae Rep-
resentation

The objective of the spectral minutiae representation is to represent a minutiae set as
a fixed-length feature vector, which is invariant to translation and rotation [34]. We
assume that the scaling has already been compensated for on the level of the minutiae
sets. This is for instance possible if minutiae are presented in a standard like [43],
which includes sensor resolution. In Figure 6.8, the procedure of the complex spectral
minutiae representation (SMC) is illustrated.

Assume a fingerprint with $Z$ minutiae. First, we code the minutiae locations by indi-
cator functions, which are isotropic two-dimensional Gaussian kernels in the spatial
domain. Then we incorporate the minutiae orientation by assigning each Gaussian
a complex amplitude $e^{j\theta_i}, i = 1, \ldots, Z$. In this way, we represent minutiae points
as complex valued continuous functions, the magnitude of which is shown in Fig-
ure 6.8(b). In this representation, translation and rotation may exist, depending on
how the user has put his finger on the sensor.

Next, a two-dimensional continuous Fourier transform is performed and only the
Fourier magnitude is kept, illustrated in Figure 6.8(c). This representation is now
translation invariant according to the shift property of the continuous Fourier trans-
form. In addition, we incorporate the minutiae quality data as presented in [57] into
SMC. This representation can be computed *analytically*,

$$\mathcal{M}_{\mathrm{C}}(\omega_{\mathrm{x}},\omega_{\mathrm{y}};\sigma_{\mathrm{C}}^2) = \left| \exp\left( -\frac{\omega_{\mathrm{x}}^2 + \omega_{\mathrm{y}}^2}{2\sigma_{\mathrm{C}}^{-2}} \right) \sum_{i=1}^{Z} \exp(-\mathrm{j}(\omega_{\mathrm{x}}x_i + \omega_{\mathrm{y}}y_i) + \mathrm{j}\theta_i) \right|. \qquad (6.4)$$

with $(x_i, y_i, \theta_i, w_i)$ the location, orientation and quality of the $i$-th minutia in the fingerprint, and $(\omega_{\mathrm{x}}, \omega_{\mathrm{y}}; \sigma_{\mathrm{C}}^2)$ are the frequencies and the parameters of the Gaussian kernel function respectively.

Finally, the Fourier spectrum is re-mapped onto a polar coordinate system, illustrated in Figure 6.8(d). In the radial direction $\lambda$, we use $M = 128$ samples between $\lambda_{\mathrm{l}} = 0.05$ and $\lambda_{\mathrm{h}} = 0.58$. In the angular direction $\beta$, we use $N = 256$ samples uniformly distributed between $\beta = 0$ and $\beta = 2\pi$. Since our target application is in a high security scenario with reasonable good quality fingerprints, we choose $\sigma_{\mathrm{C}} = 0$ for the best good performance. In this case, there is no multiplication with a Gaussian in the frequency domain (an analysis of the selection of the Gaussian parameter $\sigma$ can be found in [34]). According to the rotation properties of the two-dimensional continuous Fourier transform, now the rotation becomes translation along the new coordinate axis.

### 6.3.2.2   Spectral Minutiae Matching

Let $R(m, n)$ and $T(m, n)$ be the two sampled minutiae spectra, respectively, achieved from the *reference* fingerprint and *test* fingerprint. Both $R(m, n)$ and $T(m, n)$ are normalized to have zero mean and unit energy. We use the two-dimensional correlation coefficient between $R$ and $T$ as a measure of their similarity.

In practice, the input fingerprint images are rotated. Therefore, we need to test a few rotations, which become the circular shifts in the horizontal direction. We denote $T(m, n-j)$ as a circularly shifted version of $T(m, n)$, the final matching score between $R$ and $T$ is,

$$S^{(R,T)} = \max_j \{ \frac{1}{MN} \sum_{m,n} R(m,n)T(m,n-j) \},$$
$$-15 \le j \le 15. \qquad (6.5)$$

### 6.3.2.3   Feature Reduction

The spectral minutiae feature is a 32,768-dimensional real-valued feature vector. This large dimensionality of the spectral minutiae feature can cause three problems. First, the template storage requirement is very high. Second, the high dimensionality leads to a computational burden and the matching speed will be limited. Third, the high dimensionality can lead to a small sample size problem [68]. In order to cope with
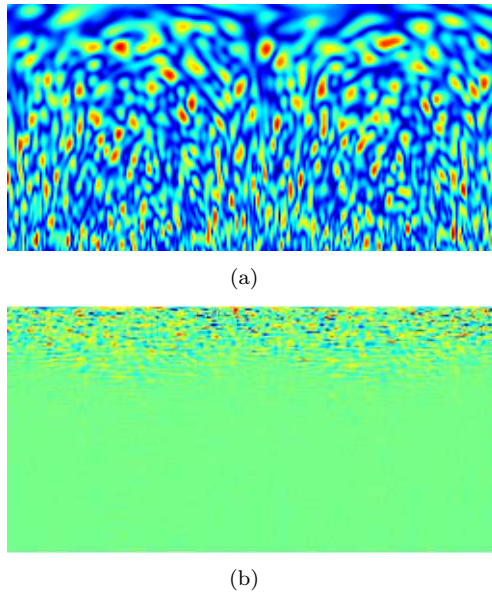
(a)



(b)

Fig. 6.9: Illustration of the CPCA transform. (a) the SMC feature; (b) the minutiae spectrum
after the CPCA transform.

these problems, we will apply the *Column Principal Component Analysis* (CPCA)
feature reduction method introduced in [67].

The idea of CPCA is to apply the well known Principal Component Analysis (PCA)
technique to the SMC columns. PCA has two functions: it decorrelates features and
concentrates power. The CPCA representation is shown in Figure 6.9(b). We can see
that after CPCA, the power is concentrated in the upper lines. The features in the
lower parts are close to zero, so we can remove them from the representation. For the
CPCA feature reduction, we keep the top 40 lines, with a feature reduction rate of
69%.

## 6.3.3   Quantization and Masking

### 6.3.3.1   Spectral Bits

In this section, we will first review the quantization method *Spectral Bits* introduced
in [73]. The Spectral Bits quantization is applied to the real-valued features after
the CPCA feature reduction. First, each real-valued feature is quantized as one bit
(1 if the feature is greater than zero and 0 otherwise, we call it sign bit), shown in
Figure 6.10(a). Second, since the quantization boundary is zero, and the features
close to zero are unstable and likely to flip, they may cause errors. Therefore, we will
mask out the features of which the absolute values are below a certain threshold. For

(a)



(b)
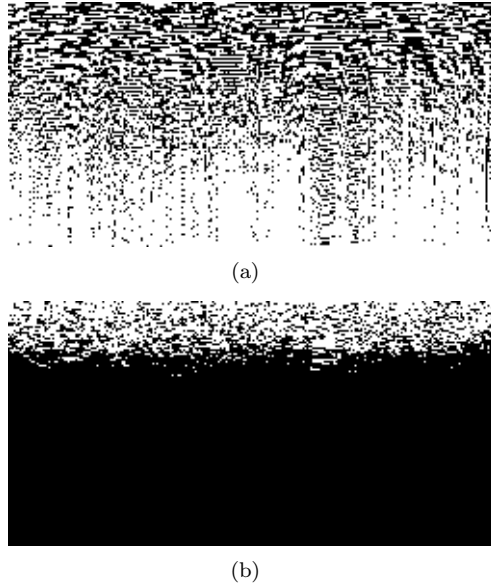
Fig. 6.10: Example of Spectral Bits (SMC spectra after CPCA). (a) the Sign Bit; (b) the Mask Bit.

the best recognition performance, we set the threshold to 0.6 after normalizing the spectra to have a standard deviation (STD) equal to 1. By testing different thresholds on different fingerprint databases, we found out that this parameter can be chosen empirically and it will not cause critical degradation of recognition performance. An example of the resulting mask bit is shown in Figure 6.10(b).

### 6.3.3.2   Fractional Hamming Distance (FHD)

After generating sign bit and mask bit vectors, we can compute a Fractional Hamming distance (FHD) [76] as a measure of the dissimilarity between two fingerprints spectra $R(m, n)$ and $T(m, n)$, whose sign bit vectors are denoted {codeR, codeT} and whose mask bit vectors are decoded {maskR, maskT},

$$FHD = \frac{||(\text{codeR} \otimes \text{codeT}) \cap \text{maskR} \cap \text{maskT}||}{||\text{maskR} \cap \text{maskT}||}. \tag{6.6}$$

### 6.3.3.3   FHD with Different Masks Schemes

As shown in Equation (6.6), we use the fractional Hamming Distance (FHD) as the similarity measure between two binary strings. This is the same measure applied for

iris recognition by Daugman [76]. For a biometric verification system, we call maskR
and maskT in Equation (6.6) the *enrollment mask* and *verification mask* respectively.

To combine a biometric system with template protection schemes based on fuzzy com-
mitment and helper data schemes, such as [33] and [5], an *error correction scheme* [77]
is needed to correct the bit errors. However, incorporating masks will introduce com-
plexity to the error correction scheme, since at the time of encoding, only the en-
rollment mask is known, not the verification mask. For this reason, Hao et al. did
not incorporate masks when applying template protection to iris recognition [78].
Bringer et al. proposed a method to enable masks by enhancing the fuzzy commit-
ment scheme [79]. In this method, the error correction decoding also need to correct
the masks errors.

Including masks in the similarity measurement can improve the recognition perfor-
mance. To include masks, and at the same time, not to complicate the error correc-
tion and template protection scheme, we would like to investigate different masking
schemes that can be easily incorporated to the error correction schemes.

In order to reach this target, we first impose several constraints on our masking
schemes: (1) in case that an enrollment mask is used, the verification mask will be
the same as the enrollment mask, and the number of masked components should be
fixed to avoid the error correction coding difficulties. (2) In case that a verification
mask will be used, we will not include enrollment mask. In this case, the verification
mask can be incorporated by using erasure decoding.

Before presenting the masking schemes, we would like to introduce two components
selection algorithms: *Largest Components Selection* (LCS) and *Reliable Components
Selection* (RCS).

**Largest Components Selection (LCS).** LCS is a straightforward method that has
been applied to the Spectral Bits mask selection. LCS will select the features with
the largest absolute values. The features that are not chosen will be masked out.

**Reliable Components Selection (RCS).** To implement RCS, we need to estimate
the within-class variance based on the multiple enrollment samples from the same
subject [5]. Assume we have $N_E$ enrollment spectral minutiae representation samples,
$R_1(m, n), \ldots, R_{N_E}(m, n)$, $\mu_{m,n}$ and $\sigma^2_{m,n}$ are the mean and variance of each component
at location $(m, n)$. Since the spectral minutiae features in the same row is uniformly
sampled (see Section 6.3.2), we assume that they have equal within-class variance.
In this way, we can make a more reliable estimation of the within-class variance per
line $\sigma^2_m$ by average $\sigma^2_{m,n}$. Finally, the reliability factor $q_{m,n}$ of each component is
calculated as

$$q_{m,n} = \frac{|\mu_{m,n}|}{\sigma_m}, \tag{6.7}$$

and the components with largest $q_{m,n}$ will be selected in the RCS scheme.

Based on the constraints imposed on our masking schemes and the two components selection methods LCS and RCS, we propose three mask schemes in this paper.

**Scheme (I)**: Enrollment Mask only with Largest Components Selection (EM-LCS). In the EM-LCS scheme, only the enrollment mask is applied. A fixed number of components are chosen based on LCS.

**Scheme (II)**: Enrollment Mask only with Reliable Components Selection (EM-RCS). In the EM-RCS scheme, only the enrollment mask is applied. A fixed number of components are chosen based on RCS.

**Scheme (III)**: Verification Mask only with Largest Components Selection (VM-LCS). In the VM-LCS scheme, only the verification mask is applied. A fixed number of components are chosen based on LCS. Since the enrollment mask need to be stored in the database as helper data in template protection based on the Helper Data scheme, the information from the enrollment mask may cause sensitive information leakage and lead to privacy risk. Using a verification-mask-only scheme can avoid this risk.

### 6.3.4   Multi-Sample Fusion of the spectral minutiae representations

In this paper, we will investigate the strategies of fusing multiple fingerprint samples (obtained from the same sensor) at three different levels: (1) feature-level; (2) score-level; (3) decision-level, respectively. In Figure 6.11, we show the various processing modules of the binary spectral minutiae fingerprint recognition system, together with the stages where the feature-, score- and decision-level fusions can be performed. The output after each processing modules are: (a) minutiae set; (b) real-valued complex spectral minutiae representations; (c) the minutiae spectra after the CPCA feature reduction; (d) the Spectral Bits representation; (e) comparison scores measured by fractional Hamming Distance.

#### 6.3.4.1   Fusion levels and their properties

For the fusion strategies at feature-, score- and decision-level, we summarize their properties in Table 6.2.

**Information available**. The information contained at the feature-level is richer than the one at the other two levels. In this sense, feature-level has the advantage.

**Storage and speed requirement**. When implementing score-level or decision-level fusion, all the templates derived from the multiple enrollment samples need to be stored in the database and compared with the test one during verification/identification. Therefore, the storage requirement is high and comparison (or matching) speed is slow. The feature-level fusion can be done in the enrollment stage and only a synthesized
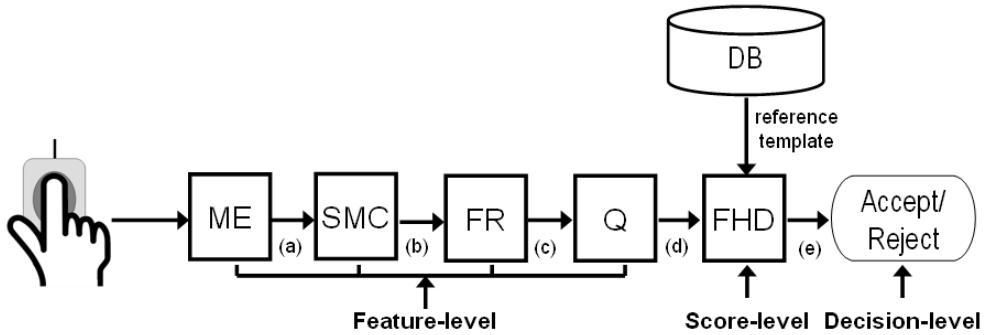
Fig. 6.11: The various processing modules of the binary spectral minutiae fingerprint recognition system together with the stages where the feature-, score- and decision-level fusions can be performed respectively. ME: Minutiae Extractor. SMC: Complex Spectral Minutiae representation. FR: Feature Reduction. Q: Quantization. FHD: Fractional Hamming Distance.

Table 6.2: A summary of fusion strategies at different information level

| Level⟍ Properties | Feature | Score | Decision |
|---|---|---|---|
| Information available | $+$ | $+/-$ | $-$ |
| Storage | $+$ | $-$ | $-$ |
| Speed | $+$ | $-$ | $-$ |
| Ease of design | $-$ | $+/-$ | $+$ |
| Template protection | $+$ | $-$ | $+/-$ |
| Robustness to overfitting | $+/-$ | $+$ | $+$ |

template need to be stored in the database. Therefore, the storage requirement and comparison speed will remain unchanged.

**Ease of design**. Compared with the feature-level fusion, the score-level and decision-level fusion are easier to study and implement.

**Template protection**. As with the 'Storage' and 'Speed' properties, if multiple enrollment templates need to be stored in the database, the template protection procedure also need to be applied to each of the templates (including error correction encoding/decoding), which will greatly reduce the speed. Moreover, because of the limited error-correcting capability of error correction code, fusion at score-level with template protection also needs to be implemented differently [80].

**Robustness to overfitting**. The complex spectral minutiae features are complicated in relation to the amount of examples available for training the statistical model. This overfitting problem may occur during the feature-level fusion. The score- and decision-level fusions are more robust to the overfitting problem.

### 6.3.4.2   Feature-level fusion

During the Feature-level fusion, the features from multiple samples are combined to produce a single enrollment template. This is also known as *template consolidation* [1]. As shown in Figure 6.11, the feature-level fusion can be performed at the modules "Minutiae Extractor (ME)", "Complex Spectral Minutiae representation (SMC)", "Feature Reduction (FR)"and "Quantization (Q)". At each module, the amount of information available is different (the information available decreases from left to right in the figure). Fusing at minutiae feature level involves several steps such as alignment and reliable minutiae selection. Several research works have been done on this topic [81, 82]. In this paper, we will focus on the fusion of the spectral minutiae features. This can be done after the SMC, FR and Q modules. Considering the information available, implementing fusion after the SMC or FR modules is preferable over after the module Q. If we choose a linear operation for the feature-level fusion (for example, an averaging operation), implementing this fusion after the module SMC or FR is equivalent. In this paper, we will perform the spectral minutiae features fusion after the CPCA feature reduction (module FR).

In the spectral minutiae representations, the translations between fingerprint samples become invariant, while the rotations become the circular shifts in the horizontal direction. Before the feature-level fusion, we need to first align the spectral minutiae features to compensate the rotation differences. After the rotation alignment, we average the aligned spectral minutiae features to generate the synthesized enrollment (or reference) template.

Assume we have $N_{\mathrm{E}}$ enrollment spectral minutiae representation samples $R_1, \ldots, R_{N_{\mathrm{E}}}$ available for fusion, the procedure of our spectral minutiae feature-level fusion is as follows.

Step 1: Denote $R_{i*}$ as the enrollment sample with the largest similarity to all the
other samples, that is,

$$i^* = \arg\max_i \sum_{\substack{k=1 \\ (k \neq i)}}^{N_{\mathrm{E}}} S^{(R_i, R_k)}, i = 1, \ldots, N_{\mathrm{E}}, \qquad (6.8)$$

with $S^{(R_i, R_k)}$ calculated following Equation (6.5).

Step 2: Take $R_{i*}$ as the reference, align all the other enrollment samples to $R_{i*}$ by
trying out different circular shifts following Equation (6.5). The aligned samples are
denoted as $\widetilde{R}_1, \ldots, \widetilde{R}_{N_{\mathrm{E}}}$.

Step 3: Generate the the synthesized enrollment template $R_{\mathrm{S}}$ by averaging $\widetilde{R}_1, \ldots, \widetilde{R}_{N_{\mathrm{E}}}$,
that is,

$$R_{\mathrm{S}} = \frac{1}{N_{\mathrm{E}}} \sum_{i=1}^{N_{\mathrm{E}}} \widetilde{R}_i. \qquad (6.9)$$

Finally, the synthesized enrollment template $R_{\mathrm{S}}$ will be stored in the database as the
reference template for verification/identification.

### 6.3.4.3   Score-level fusion

The score-level fusion is performed at the module "Fractional Hamming Distance
(FHD)", see Figure 6.11. At this module, the binary reference templates from multiple
enrollment samples are compared with the test binary template, and then multiple
comparison scores are fused. The commonly used score-level fusion techniques are
*Sum Rule*, *Max Rule* and *Min Rule* [50]. In Section 6.3.5, we will present the score-
level fusion result based on the Max Rule[1].

### 6.3.4.4   Decision-level fusion

The decision-level fusion is performed at the final decision making module, see Fig-
ure 6.11. The very straightforward decision-level fusion techniques are *AND Rule*,
*OR Rule* and *Majority Voting* [50]. The outliers in a fingerprint database can cause
*false rejection*. To reduce the recognition errors caused by the outliers, in this pa-
per, we show the performance of the decision-level fusion based on the OR Rule in
Section 6.3.5[2]. It should be noted that the decision-level fusion based on the OR

---

[1]We also tried other techniques such as the Sum Rule fusion. The Max Rule fusion gives best
results in our case.

[2]We also tried AND Rule and Majority Voting. The OR Rule fusion gives best results in our
case.

Table 6.3: Permutation setting: samples used for multi-sample enrollment and single-sample verification.

| Permutation | Enrollment | Genuine Verification |
|:---:|:---:|:---:|
| P1 | 1,2,3,4 | 5,6,7,8 |
| P2 | 1,3,5,7 | 2,4,6,8 |
| P3 | 1,2,7,8 | 3,4,5,6 |
| P4 | 1,5,6,7 | 2,3,4,8 |

Rule is equivalent as the score-level fusion based on the Max Rule and their recognition performance is the same. Therefore, we will show one performance curve in Section 6.3.5.

## 6.3.5　Results

The proposed algorithms have been evaluated on the FVC2000-DB2 [47] fingerprint database. We apply the same experimental protocol as in the FVC competition: the samples from finger ID 101 to 110 for the CPCA training and samples from person ID 1 to 100 for test. Each identity contributes 8 samples. The minutiae sets including the minutiae quality data are extracted by a proprietary method.

We test our algorithm in a verification setting. In the single-sample enrollment case, for genuine comparisons, we used all the possible combinations. For imposter comparisons, we chose the first sample from each identity. Therefore, we generate $100 \times \binom{8}{2} = 2800$ genuine comparisons and $\binom{100}{2} = 4950$ imposter comparisons in total.

### 6.3.5.1　Results of Multi-Sample Fusions

To test different multi-sample fusion schemes proposed in Section 6.3.4, we set up a multi-sample enrollment and single-sample verification system. We use the Fractional Hamming Distance shown in Equation (6.6) as the classifier. For generating more test cases, we implemented four permutations. In each permutation, $N_{\mathrm{E}} = 4$ enrollment samples are used for multi-sample fusions and the other four samples for genuine verification. For imposter verification, we chose the first sample from each identity to compare with the multiple enrollment samples (or the synthesized enrollment template in the feature-level fusion case). The permutation setting is shown in Table 6.3. In total, we will generate $100 \times 4 \times 4 = 1600$ genuine comparisons and $100 \times 99 \times 4 = 39600$ imposter comparisons.

For comparison, we also present the results of the single-enrollment scheme (both with and without incorporating minutiae quality data). The ROC curves of each scheme are shown in Figure 6.12. From the two single-enrollment results, we can see that
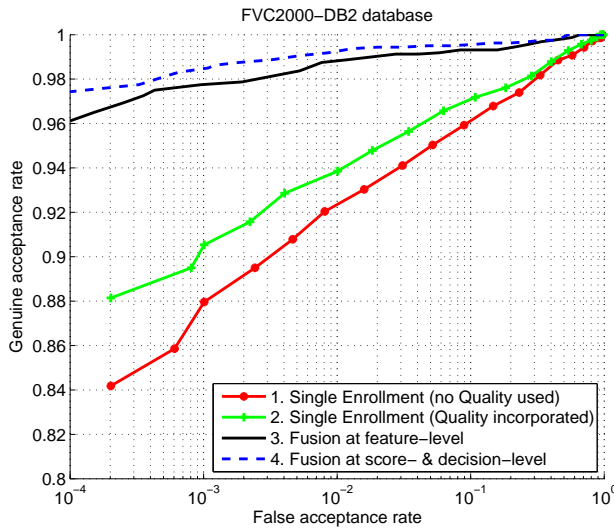
Fig. 6.12: ROC curves of different multi-sample fusion schemes.

the recognition performance improved about 20% in terms of the equal error rate by incorporating minutiae quality data. This improvement is consistent with the results shown in [57], where the minutiae quality data are incorporated in two other spectral minutiae representations. For the multi-sample fusion results, we can see that all the three multi-sample fusion schemes received significant improvements compared with the single-enrollment scheme. The OR Rule decision-level fusion and the Max Rule score-level fusion are equivalent and their performances are shown with one curve. They outperformed the feature-level fusion since they are more robust to outliers and the overfitting problem.

### 6.3.6 Results obtained with different Quantization Masking Schemes

The main reason to investigate the different masking schemes is for the integration of template protection schemes. As we discussed in Section 6.3.4, the feature-level fusion is most suitable for template protection schemes. In this paper, we evaluate the different masking schemes combined with the feature-level fusion algorithm. The results of four masking schemes are shown: 1. original masking schemes using both enrollment and verification masks; 2. EM-LCS; 3. EM-RCS; 4. VM-LCS. The number of masked out components are set as 5500 for EM-LCS and VM-LCS, and 5000 for EM-RCS. The ROC curves of each scheme are shown in Figure 6.13 (the curve of "Both masks" is the same as the "Fusion at feature-level" curve in Figure 6.12). We can see that the performance differences between the four schemes are not significant. For the privacy concerns as we discussed in Section 6.3.3, we recommend the VM-LCS
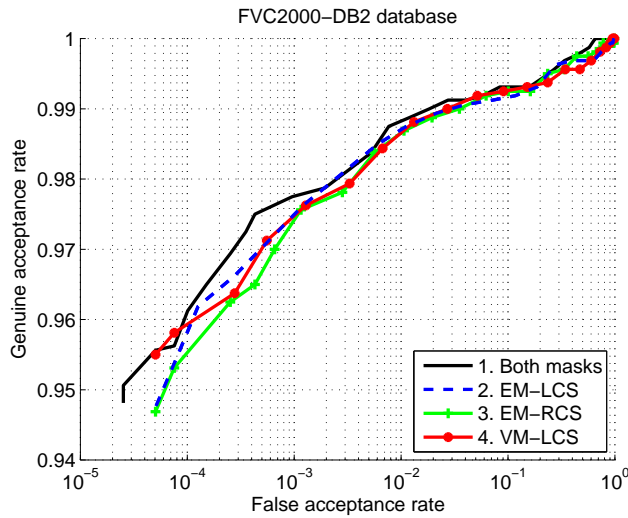
Fig. 6.13: ROC curves of different masking schemes.

scheme for template protection.

## 6.3.7   Discussion and Conclusion

In this paper, we investigated the multi-sample fusions of the spectral minutiae representations. We also proposed different mask schemes applied to the similarity measure of binary representations in context with template protection. Our main conclusions are: (1) Multiple enrollment samples can be used to train a statistical model of the biometric characteristics. By applying multi-sample fusions, we can obtain a more accurate representation of the biometric characteristics and improve the recognition accuracy. (2) The performance of the fusion at feature-level can be degraded due to outliers and the overfitting problem and its recognition performance can be lower than the one from score- or decision-level fusion. However, feature-level fusion has advantages on template storage requirement and comparison speed. It is also the most suitable solution when incorporating template protection. (3) When using fractional Hamming Distance, to incorporate template protection and error correction scheme, we can apply *one-mask* schemes (enrollment- or verification-mask only), which showed similar performances as the one using both masks. (4) To prevent the sensitive information leakage, using the verification-mask-only scheme will be the best choice.

To apply the spectral minutiae representation with a template protection scheme based on the Helper Data Scheme [53], an error correction scheme is needed. Furthermore, to enhance the recognition performance, we can incorporate other fingerprint features such as singular points. Investigating the possible error correcting codes and other methods to enhance recognition performance will be our future work.

## 6.4 Chapter Conclusions

This chapter presented several methods to quantize the real-valued spectral minutiae features into binary strings. In this chapter, we also applied several methods to enhancement the performance of the spectral minutiae representation scheme, including integrating minutiae quality data to the SMC feature, multi-sample fusion and different schemes to mask out unreliable bits.

The main contributions of this chapter are the two quantization methods: the *Spectral Bits* method, which quantizes the spectral minutiae features after the CPCA feature reduction, and the *Phase Bits* method, which quantizes the features after the LDFT feature reduction. The Spectral Bits representation consists of a long binary string, of around 10,000 bits, while the Phase Bits representation consists of a shorter binary string, of around 2,000 bits. Comparing the recognition performance of these two methods, the Spectral Bits representation has the advantages. These two methods can also be fused for a higher recognition performance.

Table 6.4: The contributions of Chapter 6 and their achieved targets.

| Contribution(s) | Target(s) |
|---|---|
| Spectral Bits | Target III: Binarization |
| Phase Bits | Target V: High comparison speed |
| Multi-Sample Fusion | Target IV: High recognition performance |

With regard to the research question and the targets of this thesis that are formulated in Section 1.3, this chapter addressed Target III, binarization, Target IV, high recognition performance and Target V, high comparison speed. By quantizing the real-valued spectral minutiae features into binary strings, we can not only achieve a binary input, which is required by the help data scheme, but also achieve a higher comparison speed. Furthermore, Target IV, high recognition performance, is achieved by multi-sample fusion. The contributions of this chapter together with their achieved targets are summarized in Table 6.4.

# Chapter 7

# Evaluation and Evolution

Until now, we have introduced several spectral minutiae representation techniques in Chapters 2-6. Since each of these chapters consists of one or more papers in their original published format, with the progress of our research, some techniques presented in the papers were evaluated on different fingerprint databases and/or using different minutiae extractors. In order to have a clear comparison of each technique and to make our progress explicit, we include this chapter to evaluate these techniques on the same database, using the same minutiae extractor. For giving a clear presentation of the progress of the spectral minutiae representation scheme, we select several relevant techniques and their combinations for evaluation in this chapter.

## 7.1 Experimental settings

In this chapter, we evaluate different techniques on the FVC2000-DB2 [47] fingerprint database. We apply the same experimental protocol as in the FVC competition: the samples from finger ID 101 to 110 for the relevant training purpose and samples from person ID 1 to 100 for test. Each identity contributes 8 samples. The minutiae sets including the minutiae quality data are extracted by a proprietary method.

We test our algorithms in a verification setting. In the single-sample enrollment case, for genuine comparisons, we used all the possible combinations. For imposter comparisons, we chose the first sample from each identity. The experimental protocol for single- and multi-sample enrolment is the same as in Chapter 6.

We divide the techniques to be evaluated into three categories: (i) basic spectral minutiae representations, including SML (Ch. 2), SMO (Ch. 2) and SMC (Ch. 5); (ii) enhancement techniques, including Enhancement by Quality (Ch. 3), Enhancement by SP (Ch. 2) and Minutiae Subsets (Ch. 3); (iii) binary representations, including

Spectral Bits (Ch. 6) and Multi-Sample Fusion (Ch. 6). It should be noted that we will not present the performances of the feature reduction techniques CPCA (Ch. 4) and LDFT (Ch. 4) in this chapter since their performances are equivalent to the ones without feature reduction.

## 7.2   Results

### 7.2.1   Basic spectral minutiae representations

First, we will evaluate the performances of the three basic spectral minutiae representation methods: SML (Ch. 2), SMO (Ch. 2) and SMC (Ch. 5). We show the results in Table 7.1 and the ROC curves are in Figure 7.1.

Table 7.1: Results of basic spectral minutiae representation methods.

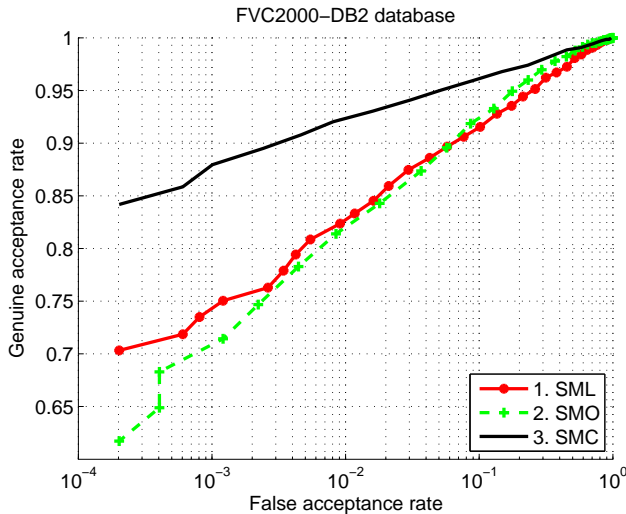| Methods | EER | GAR @ FAR=0.1% |
|---------|-----|----------------|
| SML | 8.8% | 74.3% |
| SMO | 8.3% | 71.0% |
| SMC | 5.0% | 88.2% |



Fig. 7.1: ROC curves (basic spectral minutiae representation methods).

As the performances shown in Chapter 5, SMC achieved the best results in this evaluation. In terms of the equal error rate, SMC has a recognition performance that is almost 2 times better than that of SML and SMO.

## 7.2.2   Enhancement techniques

Section 7.2.1 shows that SMC outperformes SML and SMO. Therefore, we evaluate the enhancement techniques on SMC features. We present the performances of Enhancement by Quality (Ch. 3), Enhancement by SP (Ch. 2), Minutiae Subsets (Ch. 3) and their combinations. We also present the performances of SMC as baseline for comparison. We show the results in Table 7.2 and the ROC curves are in Figure 7.2.

Table 7.2: Results of enhancement techniques (on SMC features).

| Methods | EER | GAR @ FAR=0.1% |
|---------|-----|----------------|
| SMC (baseline) | 5.0% | 88.2% |
| Enhancement by Quality | 4.0% | 90.6% |
| Enhancement by SP | 3.8% | 91.3% |
| Enhancement by SP + Quality | 3.1% | 93.9% |
| Minutiae Subsets | 3.3% | 93.2% |
| Minutiae Subsets + Quality | 2.8% | 95.2% |
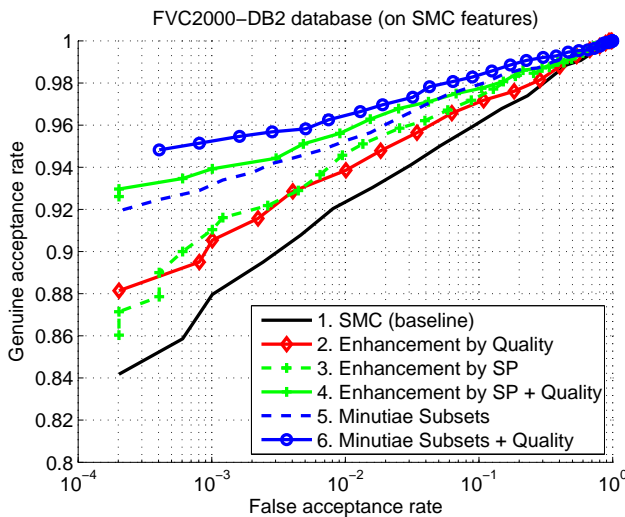


Fig. 7.2: ROC curves (enhancement techniques).

From the results, we can see that incorporating quality information gives an overall improvement in the recognition performance. The improvements achieved by using SP and minutiae subsets are comparable. By applying Enhancement by SP, the template size and the comparison time will be doubled. By applying Minutiae Subsets, the template size will be 4 times larger, and the comparison will be 16 times slower. Considering the template size and comparison speed, Enhancement by SP is more favorable for real time applications.

### 7.2.3    Binary representations

A binary representation is required for combining a fingerprint recognition system
with template protection schemes based on the helper data scheme. Section 7.2.2
shows that Enhancement by Quality gives an overall improvement under different
conditions. Therefore, for evaluating binary representations, we use the SMC features
combining Enhancement by Quality as the baseline. In Chapter 6, we presented two
binary representations: Spectral Bits and Phase Bits. Since Spectral Bits obtains a
better performance, in this subsection, we evaluate different enhancement techniques
on Spectral Bits as binary representation performances. For different masking schemes
(Ch. 6), we choose 'both masks' since it gives the best recognition performance. Since
the degradations when using the other masking schemes are small, the performance
we show in this subsection will give a reasonable prediction of the performances of
binary representations with different masks.

Table 7.3: Results of binary representations (on SMC features combining Enhancement by
Quality).

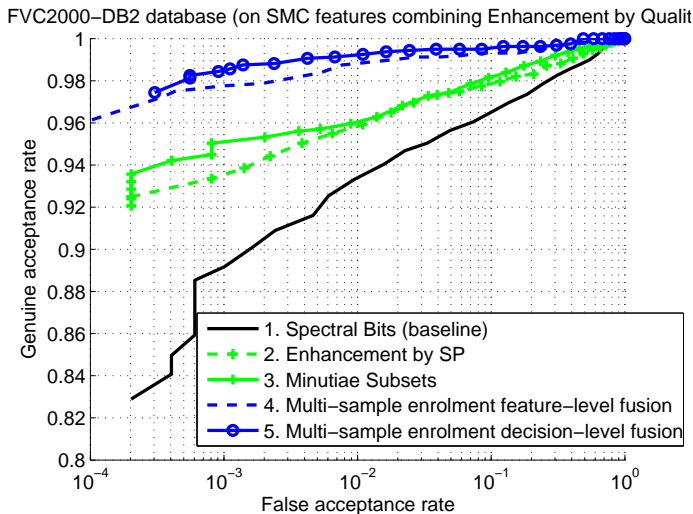| Methods | EER | GAR @ FAR=0.1% |
|---|---|---|
| Spectral Bits (baseline) | 4.4% | 89.3% |
| Enhancement by SP | 2.9% | 93.7% |
| Minutiae Subsets | 2.8% | 95.0% |
| Multi-sample enrolment feature-level fusion | 1.1% | 97.8% |
| Multi-sample enrolment decision-level fusion | 0.8% | 98.5% |



Fig. 7.3: ROC curves (binary representations).

We also present the results of the following enhancement methods applied to Spectral

Bits: Enhancement by SP (Ch. 2), Minutiae Subsets (Ch. 3), Multi-sample enrolment feature-level fusion (Ch. 6) and Multi-sample enrolment decision-level fusion (Ch. 6). We show the results in Table 7.3 and the ROC curves are in Figure 7.3.

The binary spectral minutiae representations show recognition performances that are similar to those of the real-valued representations. At the same time, they greatly compact the template size and increase the comparison speed. Applying multi-sample enrolment fusion can improve the recognition performance significantly. It is recommended for a high security system.

## 7.3  Chapter Conclusions

We showed how the performances of the spectral minutiae scheme improved as the result of several enhancements. In fact, the initial performance in terms of the equal error rate improved from 8.8% (SML) to 0.8% (quality enhanced SMC Spectral Bits with Multi-sample enrolment decision-level fusion). The binary representations greatly compact the template size, increase the comparison speed, and enable the combination of minutiae-based fingerprint recognition system with template protection schemes based on the helper data scheme, without degrading the recognition performance.

# Chapter 8

# Conclusions and Recommendations

In order to conclude this thesis, we will first address the research question formulated in Chapter 1 and summarize the contributions of this thesis. Furthermore, we will present possible applications of our proposed algorithms and give future research directions.

## 8.1   Conclusions

In Section 1.3, we formulated the research question of this thesis as:

**How can we combine a minutiae-based fingerprint recognition system with template protection based on the helper data scheme?**

The spectral minutiae representation scheme proposed in this thesis provides a feasible solution to our research question. The spectral minutiae representation and its quantization scheme transform an unordered, variant-length minutiae set into a fixed-length binary feature vector, which is required as an input to the helper data scheme. The feature vector output of the spectral minutiae representation is also translation and rotation invariant, which enables the comparison of minutiae sets in an encrypted domain. Furthermore, the feature reduction methods and the quantization schemes proposed in this thesis compact the spectral minutiae template and increase the comparison speed significantly.

In Section 1.3, we also specified five targets that had to be achieved in order to answer the research question. All these five targets have been achieved in this thesis. In Table 8.1, we list these targets and their solutions that are contributed by this thesis.

In this thesis, three spectral minutiae representation methods have been proposed: the

Table 8.1: Defined targets and solutions contributed by this thesis.

| Target | Solutions |
|---|---|
| Target I.<br>Fixed-length feature vector | SML (Ch. 2)<br>SMO (Ch. 2)<br>SMC (Ch. 5) |
| Target II.<br>Translation and rotation invariance | SML (Ch. 2)<br>SMO (Ch. 2)<br>SMC (Ch. 5) |
| Target III.<br>Binarization | Spectral Bits (Ch. 6)<br>Phase Bits (Ch. 6) |
| Target IV.<br>High recognition performance | SM Fusion (Ch. 2)<br>Enhancement by SP (Ch. 2)<br>Enhancement by Quality (Ch. 3)<br>Minutiae Subsets (Ch. 3)<br>SMC (Ch. 5)<br>Multi-Sample Fusion (Ch. 6) |
| Target V.<br>High comparison speed | CPCA (Ch. 4)<br>LDFT (Ch. 4)<br>Spectral Bits (Ch. 6)<br>Phase Bits (Ch. 6) |

location-based spectral minutiae representation (SML), the orientation-based spectral minutiae representation (SMO) and the complex spectral minutiae representation (SMC). SML encodes minutiae location information, while SMO and SMC encode both minutiae location and orientation information. From the experiments shown in this thesis, SMC achieved the best results. In terms of the equal error rate, SMC has a recognition performance that is about 2-4 times better than that of SML and SMO.

Furthermore, this thesis provided five methods to enhance the recognition performance: (1) SM Fusion; (2) Enhancement by using SP; (3) Enhancement by incorporating quality information; (4) Using Minutiae Subsets; (5) Multi-Sample Fusion. Considering the effectiveness and feasibility of all these methods, we recommend to apply methods (3) Enhancement by Quality, and (5) Multi-Sample Fusion, in real-life situations. Method (1) can be applied to SMC and SML. However, the template size will be doubled and the comparison speed will be slowed down. Method (2) showed an improvement of around 20% in recognition performance. However, this method relies on a reliable singular points detection, and it suffers from the same disadvantages as method (1), that the template size increases and the comparison

speed degrades. Method (4) is an effective way to cope with the limited overlap problem for applications in which only partial fingerprints are available. However, this method also has disadvantages on the template size and the comparison speed. For the target applications of this thesis that are described in Section 1.3.1, this method is not recommended.

With regard to feature reduction, both CPCA and LDFT can effectively reduce the feature dimensionality by 70%-80%, while maintaining the recognition performance. For a high reduction rate, we recommend to apply both CPCA and LDFT in combination.

With regard to quantization, the Spectral Bits representation is recommended because of its better recognition performance. This method quantizes the spectral minutiae features to a binary string of around 10,000 bits. The Phase Bits representation consists of a shorter binary string, of around 2,000 bits. In case that a shorter binary string is preferred, the Phase Bits representation can be the choice. The Spectral Bits and the Phase Bits can also be concatenated in order to achieve a higher recognition performance.

## 8.2 Recommendations

### 8.2.1 Applications

The spectral minutiae representation scheme proposed in this thesis can be used for the following applications:

- **Template protection based on the helper data scheme.**
  This is the main target application of this thesis. The spectral minutiae representation algorithm proposed in this thesis enables the combination of fingerprint recognition with template protection based on the helper data schemes. In Figure 8.1, we show our designed system in a helper data scheme. The block 'Spectral Minutiae' is our system. In this block, the quantization scheme (Spectral Bits or Phase Bits) is also included.
  When applying the helper data scheme, another important task is designing the error correcting codes (ECCs). When designing the ECC for the spectral minutiae binary outputs ($Z$ and $Z'$ in Figure 8.1), we need to consider the characteristics of these binary outputs, such as the error probability and binary string length. This is one of the future research directions.

- **Pre-selector.**
  Due to the fact that minutiae sets are unordered and the correspondence between individual minutia in two minutiae sets is unknown before minutiae sets comparison, it is difficult to find the geometric transformation (consisting of translation, rotation, scaling, and optionally non-linear deformations) that optimally align the two minutiae sets. For fingerprint identification systems with very large databases,
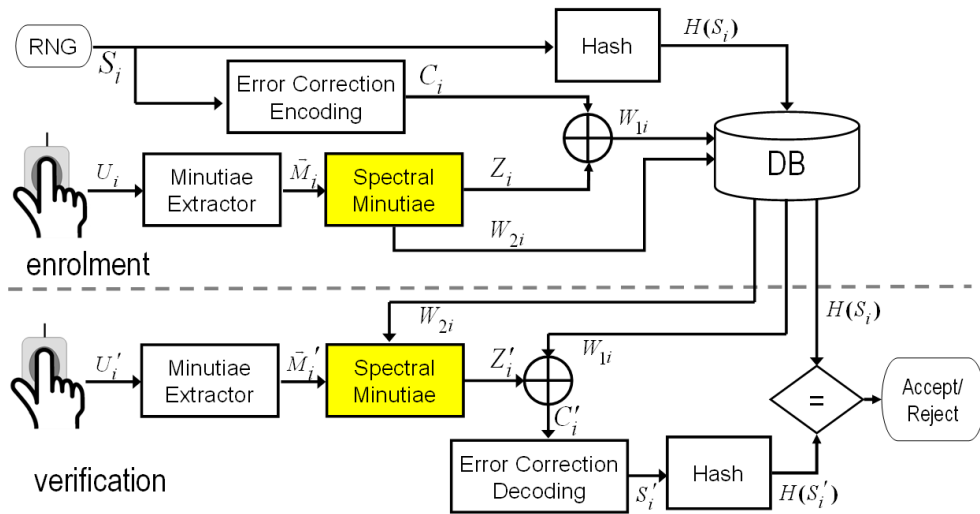
Fig. 8.1: *Diagram of applying our designed system 'Spectral Minutiae' for combining finger-print recognition with template protection.*

in which a fast comparison algorithm is necessary, most minutiae-based matching algorithms will fail to meet the high speed requirements. The spectral minutiae algorithm proposed in this thesis coped with the above disadvantages of the minutiae-based matching algorithms, thus, it greatly increased the comparison speed. For a large-scale Automated Fingerprint Identification System (AFIS), we might combine good identification performance and speed by using our designed scheme, the 'spectral minutiae', as a pre-selector (or pre-filter), see Figure 8.2. As a pre-selector, the 'spectral minutiae' scheme will find a number of best matches from a large amount of templates in the database, and then use a very accurate minutiae comparison for a good recognition performance.
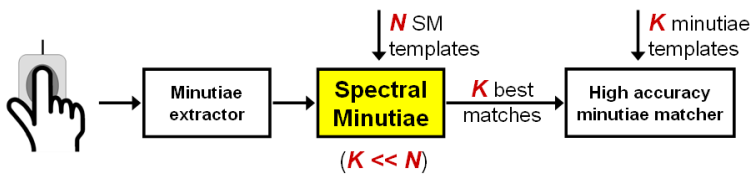


Fig. 8.2: *Diagram of applying our designed system 'Spectral Minutiae' as a pre-selector.*

As a pre-selector, the recognition performance in the area of high GAR is important. For fingerprints with good quality, the spectral minutiae algorithm can be used as pre-selector to speed up the minutiae sets comparison. However, the spectral minutiae algorithm is not robust to the low quality fingerprints. The fingerprint outliers will degrade the recognition performance, which limits the application of using the

spectral minutiae scheme as pre-selector. The solutions to such problem are incorporating minutiae quality and applying multi-sample fusion. Further investigation to make the spectral minutiae scheme more robust to fingerprint outliers is another future research direction.

Besides the target applications mentioned above, the contributions of this thesis can also be applied for other pattern recognition purposes. The basic principle of the spectral minutiae representation can be applied for point pattern recognition. The CPCA and LDFT methods can be applied to the patterns that have similar characteristics as the spectral minutiae features, for example, the iris pattern, for the feature reduction purpose.

### 8.2.2  Future research

In Section 8.2.1, we mentioned several possible applications of the spectral minutiae scheme, together with some future research directions on "error correcting codes" and "dealing with fingerprint outliers". Future research on the spectral minutiae representation can focus on:

- **Poor quality fingerprints.** Some research has shown that minutiae-based fingerprint recognition algorithms are less robust to the image quality degradation compared with image-based algorithms [64]. The spectral minutiae representation algorithm proposed in this thesis is based on the minutiae feature. However, in some applications, the quality of some fingerprints is so poor that even the experts cannot reliably manually extract minutiae. In such cases, we need to look for solutions based on the image-based features. The fusion of minutiae- and image-based fingerprint comparison algorithms is a robust solution against poor quality fingerprints and will have a better recognition performance.

- **Limited overlap.** In this thesis, we proposed the method "Using minutiae subsets" to cope with the limited overlap problem. However, this method has the disadvantages of increasing template size and degrading comparison speed. Moreover, it still needs to be optimized for real time applications. Further research on this topic is very important, especially for the applications where only partial fingerprints are available, e.g., forensic applications.

- **Large rotations.** The current spectral minutiae representation algorithm copes with fingerprint rotations within a certain range by testing a set of rotation possibilities. In case that a large rotation exists between two fingerprints, this rotation compensation will be time consuming and it will also increase the false acceptance rate. We may combine the spectral minutiae representation algorithm with rotation-invariant minutiae descriptors to solve this problem.

- **Elastic distortion.** When combining fingerprint recognition with template protection, the two fingerprints need to be compared in an encrypted domain. How

to deal with elastic distortion in such cases is still unknown. Furthermore, for applications where big elastic distortions are likely to exist, e.g., forensic applications where the fingerprints are obtained from the crime scenes, dealing with elastic distortions is a very important task to investigate.

- **Binary representation.** In this thesis, we introduced two binary representations: the Spectral Bits and the Phase Bits. Both representations consist of a considerable large number of bits with fairly high error probabilities. Further research can focus on other possibilities of extracting a smaller number of more reliable bits. This will be beneficial for the helper data scheme since it is easier to find a suitable ECC with lower error correcting capability. Generating more reliable bits also opens the possibility to combine the spectral minutiae representation algorithm with the key generation scheme [53, 83].

# Bibliography

[1] D. Maltoni, D. Maio, A. K. Jain, and S. Prabhakar, *Handbook of Fingerprint Recognition*. Springer Publishing Company, Incorporated, 2009.

[2] "Biometrics Market and Industry Report 2009-2014." `http://www.biometricgroup.com`.

[3] "Spotlight on Biometrics." `http://www.unisyssecurityindex.com`.

[4] A. Jain, S. Prabhakar, L. Hong, and S. Pankanti, "Filterbank-based fingerprint matching," *IEEE Trans. Image Processing*, vol. 9, pp. 846–859, May 2000.

[5] P. Tuyls, A. Akkermans, T. Kevenaar, G. Schrijen, A. Bazen, and R. Veldhuis, "Practical biometric authentication with template protection.," in *AVBPA*, pp. 436–446, 2005.

[6] D. Maio and D. Maltoni, "Direct gray-scale minutiae detection in fingerprints," *IEEE Trans. PAMI*, vol. 19, pp. 27–39, Jan. 1997.

[7] A. Jain, L. Hong, and R. Bolle, "On-line fingerprint verification," *IEEE Trans. PAMI*, vol. 19, pp. 302–314, Apr. 1997.

[8] X. Jiang, W. Yau, and W. Ser, "Detecting the fingerprint minutiae by adaptive tracing the gray-level ridge," *Pattern Recognition*, vol. 34, pp. 999–1013, May 2001.

[9] A. Bazen and S. Gerez, "Fingerprint matching by thin-plate spline modelling of elastic deformations," *Pattern Recognition*, vol. 36, pp. 1859–1867, Aug. 2003.

[10] X. Chen, J. Tian, X. Yang, and Y. Zhang, "An algorithm for distorted fingerprint matching based on local triangle feature set," *Information Forensics and Security, IEEE Transactions on*, vol. 1, pp. 169 – 177, june 2006.

[11] "VeriFinger SDK." `http://www.neurotechnologija.com/`.

[12] "Cogent Systems Incorporated." `http://www.cogentsystems.com/`.

[13] "Sagem Morpho Incorporated." `http://www.morpho.com/`.

[14] "Precise Biometrics." `http://www.precisebiometrics.com/`.

[15] "Dermalog Identification Systems GmbH." `http://www.dermalog.de/`.

[16] "NEC Corporation." `http://www.nec.com/`.

[17] "L-1 Identity Solutions, Inc.." `http://www.l1id.com/`.

[18] J. L. Wayman, A. K. Jain, D. Maltoni, and D. Maio, *Biometric Systems: Technology, Design and Performance Evaluation.* Secaucus, NJ, USA: Springer-Verlag New York, Inc., 2004.

[19] "ISO/IEC JTC 1/SC 37/WG 1 Harmonized biometric vocabulary," 2009.

[20] "ISO/IEC Standards on Biometrics." `http://www.iso.org`.

[21] "United States Visitor and Immigrant Status Indicator Technology Program (US-VISIT)." `http://www.dhs.gov/us-visit`.

[22] "ISO/IEC 19795-1, Information technology – Biometric performance testing and reporting – Part 1: Principles and framework," 2006.

[23] J. P. Aus, "Decision-making under pressure: The negotiation of the biometric passports regulation in the council," ARENA Working Papers 11, ARENA, Sept. 2006.

[24] C. Busch, "ISO 24745 - Biometric Template Protection.," in *The first International Biometric Performance Testing Conference*, Match 2010.

[25] J. Breebaart, B. Yang, I. Buhan, and C. Busch, "Biometric template protection - the need for open standards," *Datenschutz und Datensicherheit - DuD*, vol. 33, no. 5, pp. 299–304, 2009.

[26] P. Tuyls, B. Skoric, and Tom Kevenaar (Eds), *Security with Noisy Data - On Private Biometrics, Secure Key Storage and Anti-Counterfeiting.* Springer, 2007.

[27] A. K. Jain, K. Nandakumar, and A. Nagar, "Biometric template security," *EURASIP J. Adv. Signal Process*, vol. 2008, pp. 1–17, 2008.

[28] N. K. Ratha, S. Chikkerur, J. H. Connell, and R. M. Bolle, "Generating cancelable fingerprint templates," *IEEE Trans. Pattern Anal. Mach. Intell.*, vol. 29, no. 4, pp. 561–572, 2007.

[29] T. Boult, W. Schdrer, and R. Woodworth, "Revocable fingerprint biotokens: Accuracy and security analysis," in *Computer Vision and Pattern Recognition, 2007. CVPR '07. IEEE Conference on*, pp. 1–8, June 2007.

[30] A. Juels and M. Sudan, "A fuzzy vault scheme," in *Information Theory, 2002. Proceedings. 2002 IEEE International Symposium on*, p. 408, 2002.

[31] U. Uludag and A. Jain, "Securing fingerprint template: Fuzzy vault with helper data," in *Computer Vision and Pattern Recognition Workshop, 2006. CVPRW '06. Conference on*, pp. 163 – 163, 17-22 2006.

[32] K. Nandakumar, A. Jain, and S. Pankanti, "Fingerprint-based fuzzy vault: Implementation and performance," *Information Forensics and Security, IEEE Transactions on*, vol. 2, pp. 744–757, Dec. 2007.

[33] A. Juels, "Fuzzy commitment," in *Security with Noisy Data - On Private Biometrics, Secure Key Storage and Anti-Counterfeiting* (P. Tuyls, B. Skoric, and T. Kevenaar, eds.), ch. 3, pp. 45–56, Springer, 2007.

[34] H. Xu, R. Veldhuis, A. Bazen, T. Kevenaar, T. Akkermans, and B. Gokberk, "Fingerprint verification using spectral minutiae representations," *Information Forensics and Security, IEEE Transactions on*, vol. 4, pp. 397–409, Sept. 2009.

[35] D. Maltoni, D. Maio, A. Jain, and S. Prabhakar, *Handbook of Fingerprint Recognition*. Springer, New York, 2003.

[36] A. Bazen, R. Veldhuis, and S. Gerez, "Hybrid fingerprint matching using minutiae and shape," in *Computer Aided Intelligent Recognition Techniques and Applications*, John Wiley, 2004.

[37] D. Casasant and D. Psaltis, "Position, rotation, and scale invariant optical correlation," *Applied Optics*, vol. 15, pp. 1795–1799, July 1976.

[38] S. Derrode and F. Ghorbel, "Robust and efficient Fourier-Mellin transform approximations for gray-level image reconstruction and complete invariant description," *Computer Vision and Image Understanding: CVIU*, vol. 83, pp. 57–78, July 2001.

[39] Q.-S. Chen, M. Defrise, and F. Deconinck, "Symmetric phase-only matched filtering of fourier-mellin transforms for image registration and recognition," *Pattern Analysis and Machine Intelligence, IEEE Transactions on*, vol. 16, pp. 1156–1168, Dec 1994.

[40] Y. Sheng and H. Arsenault, "Experiments on pattern recognition using invariant Fourier-Mellin descriptors," *J. of the Optical Society of America A*, vol. 3, pp. 771–776, June 1986.

[41] F. Ghorbel, "A complete invariant description for gray-level images by the harmonic analysis approach," *Pattern Recogn. Lett.*, vol. 15, no. 10, pp. 1043–1051, 1994.

[42] R. Bolle, J. H. Connell, S. Pankanti, N. K. Ratha, and A. W. Senior, *Guide to Biometrics*. Springer Verlag, 2003.

[43] "ISO/IEC 19794-2, Information Technology - Biometric Data Interchange Format - Part 2: Finger Minutiae Data," 2005.

[44] R. Bracewell, *The Fourier Transform and Its Applications, 3rd ed.* New York: McGraw-Hill, 1999.

[45] Y. Sheng and J. Duvernoy, "Circular-fourier-radial-mellin transform descriptors for pattern recognition," *J. of the Optical Society of America A*, vol. 3, pp. 885–888, June 1986.

[46] Ortega-Garca, J., et al., "MCYT baseline corpus: a bimodal biometric database," in *IEE Proc. Vision, Image and Signal Processing 150(6)*, pp. 395–401, 2003.

[47] D. Maio, D. Maltoni, R. Cappelli, J. Wayman, and A. Jain, "FVC2000: Fingerprint verification competition," *IEEE Trans. PAMI*, vol. 24, pp. 402–412, Mar. 2002.

[48] D. Maio, D. Maltoni, R. Cappelli, J. Wayman, and A. Jain, "FVC2002: Second fingerprint verification competition," vol. 3, pp. 811–814, Aug. 2002.

[49] A. Bazen and S. Gerez, "Segmentation of fingerprint images," in *Proc. ProR-ISC2001, 12th Annual Workshop on Circuits, Systems and Signal Processing*, (Veldhoven, The Netherlands), Nov. 2001.

[50] A. A. Ross, K. Nandakumar, and A. K. Jain, *Handbook of Multibiometrics (International Series on Biometrics)*. Secaucus, NJ, USA: Springer-Verlag New York, Inc., 2006.

[51] A. Ross, A. K. Jain, and J.-Z. Qian, "Information fusion in biometrics," in *AVBPA '01: Proceedings of the Third International Conference on Audio- and Video-Based Biometric Person Authentication*, (London, UK), pp. 354–359, Springer-Verlag, 2001.

[52] E. Henry, *Classification and Uses of Finger Prints*. London: Routledge, 1900.

[53] Y. Dodis, L. Reyzin, and A. Smith, "Fuzzy extractors," in *Security with Noisy Data - On Private Biometrics, Secure Key Storage and Anti-Counterfeiting* (P. Tuyls, B. Skoric, and T. Kevenaar, eds.), ch. 3, pp. 45–56, Springer, 2007.

[54] J. Daugman, "How iris recognition works," *IEEE Transactions on Circuits and Systems for Video Technology*, vol. 14, pp. 21–30, January 2004.

[55] C. Chen, R. Veldhuis, A. Akkermans, and T. Kevenaar, "Biometric binary string generation with detection rate optimized bit allocation," in *Proceedings of the IEEE Computer Society Conference on Computer Vision and Pattern Recognition - Workshop on Biometrics*, (Anchorage, USA), 2008.

[56] H. Xu, R. Veldhuis, T. Kevenaar, A. Akkermans, and A. Bazen, "Spectral Minutiae: A Fixed-length Representation of a Minutiae Set," in *Proceedings of the IEEE Computer Society Conference on Computer Vision and Pattern Recognition - Workshop on Biometrics*, (Anchorage, USA), June 2008.

[57] H. Xu and R. Veldhuis, "Spectral minutiae representatoins of fingerprints enhanced by quality data," in *IEEE Third International Conference on Biometrics: Theory, Applications and Systems (BTAS '09)*, September 2009.

[58] H. Xu and R. Veldhuis, "Spectral representations of fingerprint minutiae sub-sets," in *Image and Signal Processing, 2009. CISP '09. 2nd International Congress on*, pp. 1–5, Oct. 2009.

[59] "United States Visitor and Immigrant Status Indicator Technology Program (US-VISIT)." http://www.dhs.gov/us-visit.

[60] A. Willis and L. Myers, "A cost-effective fingerprint recognition system for use with low-quality prints and damaged fingertips," *Pattern Recognition*, vol. 34, no. 2, pp. 255–270, 2001.

[61] C.-H. Park, M. J. T. Smith, M. Boutin, and J.-J. Lee, "Fingerprint matching using the distribution of the pairwise distances between minutiae," in *AVBPA*, pp. 693–701, 2005.

[62] H. van Trees, *Detection, Estimation and Modulation Theory, Part I*. New York: John Wiley and Sons, 1968.

[63] "Digital Persona." http://www.digitalpersona.com/.

[64] J. Fierrez-aguilar, J. Ortega-garcia, and A. K. Jain, "Incorporating image quality in multi-algorithm fingerprint verification," in *Proc. IAPR Intl. Conf. on Biometrics, ICB, Springer LNCS-3832*, pp. 213–220, Springer, 2006.

[65] S. Lee, H. Choi, K. Choi, and J. Kim, "Fingerprint-quality index using gradient components," *Information Forensics and Security, IEEE Transactions on*, vol. 3, pp. 792–800, Dec. 2008.

[66] H. Fronthaler, K. Kollreider, J. Bigun, J. Fierrez, F. Alonso-Fernandez, J. Ortega-Garcia, and J. Gonzalez-Rodriguez, "Fingerprint image-quality estimation and its application to multialgorithm verification," *Information Forensics and Security, IEEE Transactions on*, vol. 3, pp. 331–338, June 2008.

[67] H. Xu, R. Veldhuis, T. Kevenaar, and T. Akkermans, "A fast minutiae-based fingerprint recognition system," *Systems Journal, IEEE*, vol. 3, pp. 418 –427, dec. 2009.

[68] S. Raudys and A. Jain, "Small sample size effects in statistical pattern recognition: Recommendations for practitioners," vol. 13, pp. 252–264, March 1991.

[69] R. Duda, P. Hart, and D. Stork, *Pattern Classification*. Wiley-Interscience, 2nd edition ed., Oct. 2000.

[70] A. V. Oppenheim, A. S. Willsky, and S. H. Nawab, *Signals & systems (2nd ed.)*. Upper Saddle River, NJ, USA: Prentice-Hall, Inc., 1996.

[71] H. Xu and R. N. Veldhuis, "Complex spectral minutiae representation for fingerprint recognition," in *Computer Vision and Pattern Recognition Workshops (CVPRW), 2010 IEEE Computer Society Conference on*, pp. 1–8, 13-18 2010.

[72] A. Ross, J. Shah, and A. K. Jain, "From template to image: Reconstructing fingerprints from minutiae points," *IEEE Transactions on Pattern Analysis and Machine Intelligence*, vol. 29, no. 4, pp. 544–560, 2007.

[73] H. Xu and R. Veldhuis, "Binary representations of fingerprint spectral minutiae features," in *20th International Conference on Pattern Recognition (ICPR 2010)*, (Turkey), August 2010.

[74] H. Xu and R. Veldhuis, "Binary spectral minutiae representation with multi-sample fusion for fingerprint recognition," in *The 12th ACM Workshop on Multimedia and Security*, (Rome, Italy), September 2010.

[75] S. Prabhakar and A. K. Jain, "Decision-level fusion in fingerprint verification," *Pattern Recognition*, vol. 35, pp. 861–874, 2001.

[76] J. Daugman, "The importance of being random: Statistical principles of iris recognition," *Pattern Recognition*, vol. 36, no. 2, pp. 279–291, 2003.

[77] F. J. MacWilliams and N. J. A. Sloane, *The Theory of Error-Correcting Codes (North-Holland Mathematical Library)*. North Holland, June 1988.

[78] F. Hao, R. Anderson, and J. Daugman, "Combining crypto with biometrics effectively," *IEEE Trans. Comput.*, vol. 55, no. 9, pp. 1081–1088, 2006.

[79] J. Bringer, H. Chabanne, G. D. Cohen, B. Kindarji, and G. Zémor, "Theoretical and practical boundaries of binary secure sketches," *IEEE Transactions on Information Forensics and Security*, vol. 3, no. 4, pp. 673–683, 2008.

[80] E. J. C. Kelkboom, J. Breebaart, R. N. J. Veldhuis, X. Zhou, and C. Busch, "Multi-sample fusion with template protection," in *BIOSIG 2009 : Proceedings of the Special Interest Group on Biometrics and Electronic Signatures.*, pp. 55–67, 2009.

[81] X. Jiang and W. Ser, "Online fingerprint template improvement," *IEEE Trans. Pattern Anal. Mach. Intell.*, vol. 24, no. 8, pp. 1121–1126, 2002.

[82] H. Ramoser, B. Wachmann, and H. Bischof, "Efficient alignment of fingerprint images," in *ICPR '02: Proceedings of the 16 th International Conference on Pattern Recognition (ICPR'02) Volume 3*, (Washington, DC, USA), p. 30748, IEEE Computer Society, 2002.

[83] Y. Sutcu, Q. Li, and N. Memon, "Protecting biometric templates with sketch: Theory and practice," *Information Forensics and Security, IEEE Transactions on*, vol. 2, pp. 503–512, Sept. 2007.

# List of publications

[1] H. Xu, A. M. Bazen, R. N. J. Veldhuis, T. A. M. Kevenaar, and A. H. M. Akkermans. Spectral representation of fingerprints. In *Proceedings of the 28th Symposium on Information Theory in the Benelux, Enschede, The Netherlands*, pages 313–319, Eindhoven, June 2007. Werkgemeenschap voor Informatie- en Communicatietechniek.

[2] H. Xu, R. N. J. Veldhuis, T. A. M. Kevenaar, A. H. M. Akkermans, and A. M. Bazen. Spectral Minutiae: A Fixed-length Representation of a Minutiae Set. In *Proceedings of the IEEE Computer Society Conference on Computer Vision and Pattern Recognition - Workshop on Biometrics*, Anchorage, USA, 2008.

[3] H. Xu and R. N. J. Veldhuis. A quality integrated spectral minutiae fingerprint recognition system. In *Thirtieth Symposium on Information Theory in the Benelux*, Eindhoven, The Netherlands, 2009.

[4] H. Xu, R. N. J. Veldhuis, A. M. Bazen, T. A. M. Kevenaar, A. H. M. Akkermans, and B. Gokberk. Fingerprint verification using spectral minutiae representations. *Information Forensics and Security, IEEE Transactions on*, 4(3):397–409, Sept. 2009.

[5] H. Xu and R. N. J. Veldhuis. Spectral minutiae representatoins of fingerprints enhanced by quality data. In *IEEE Third International Conference on Biometrics: Theory, Applications and Systems (BTAS '09)*, September 2009.

[6] H. Xu and R. N. J. Veldhuis. Spectral representations of fingerprint minutiae subsets. In *Image and Signal Processing, 2009. CISP '09. 2nd International Congress on*, pages 1–5, Oct. 2009.

[7] H. Xu, R. N. J. Veldhuis, T. A. M. Kevenaar, and A. H. M. Akkermans. A fast minutiae-based fingerprint recognition system. *Systems Journal, IEEE*, 3(4):418 –427, dec. 2009.

[8] H. Xu and R. N. J. Veldhuis. Complex spectral minutiae representation for fingerprint recognition. In *Computer Vision and Pattern Recognition Workshops (CVPRW), 2010 IEEE Computer Society Conference on*, pp. 1–8, 13-18 2010.

[9] H. Xu and R. N. J. Veldhuis. Binary representations of fingerprint spectral minutiae features. In *20th International Conference on Pattern Recognition (ICPR 2010)*, Turkey, 2010.

[10] H. Xu and R. N. J. Veldhuis. Binary spectral minutiae representation with multi-sample fusion for fingerprint recognition. In *The 12th ACM Workshop on Multimedia and Security*, Rome, Italy, 2010.

[11] H. Xu and R. N. J. Veldhuis. Spectral Minutiae Representations for Fingerprint Recognition. In *The Sixth International Conference on Intelligent Information Hiding and Multimedia Signal Processing*, Darmstadt, Germany, 2010.

# Summary

The term biometrics refers to the technologies that measure and analyze human intrinsic physical (such as fingerprints, face, iris) or behavioral (such as signature, voice, gait) characteristics for authenticating individuals. Recognition of individuals by means of biometric characteristics is gaining importance because of several reasons: first, unlike passwords, PIN codes or tokens, biometric identifiers cannot be forgotten or lost, and they add user convenience since they are always at hand; second, a biometric identifier is tightly linked to an individual, therefore, it cannot easily be forged or shared.

Currently, fingerprint is the most commonly used biometric modality. Compared with various biometric characteristics, such as face, signature and voice, the fingerprint has high levels of distinctiveness, permanence and performance. At the same time it has the advantages of both ease of use and low cost. Nowadays, many fingerprint recognition systems are based on minutiae comparison. Minutiae are the endpoints and bifurcations of fingerprint ridges. They are known to remain unchanged over an individual's lifetime and allow a very discriminative classification of fingerprints.

Nowadays, biometric technology is increasingly deployed in civil and commercial applications. The growing use of biometrics is raising security and privacy concerns. Storing biometric data, known as biometric templates, in a database leads to several privacy risks such as identity fraud and cross matching. A solution is to apply *biometric template protection* techniques, which aim to make it impossible to recover the biometric data from the templates.

The research question addressed in this thesis is how to combine fingerprint recognition systems with template protection. Most fingerprint recognition systems are based on the comparison of minutiae sets, which are unordered collection of minutiae locations and orientations suffering from various deformations such as translation, rotation and scaling. Many template protection systems, however, require an ordered feature vector of fixed-length. The spectral minutiae representation introduced in this thesis is a novel method that, indeed, represents a minutiae set as a fixed-length feature vector, which is invariant to translation, and in which rotation and scaling

become translations that can be easily compensated for. These characteristics enable the combination of fingerprint recognition systems with template protection schemes based on fuzzy commitment or helper data schemes.

In this thesis, three spectral minutiae representation methods have been proposed: the *location-based spectral minutiae representation* (SML), the *orientation-based spectral minutiae representation* (SMO) and the *complex spectral minutiae representation* (SMC). SML encodes minutiae location information, while SMO and SMC encode both minutiae location and orientation information. From the experiments shown in this thesis, SMC achieved the best results. In terms of the equal error rate, SMC has a recognition performance that is about 2-4 times better than that of SML and SMO.

Based on the spectral minutiae features, this thesis further presented contributions in three research directions. First, this thesis recommends several ways to enhance the recognition performance of SMC. Examples are the incorporation of minutiae quality information and multi-sample fusion. Second, with regard to feature reduction, this thesis introduced two feature reduction methods, *Column-PCA* (CPCA) and *Line-DFT* (LDFT), which can effectively reduce the feature dimensionality by 70%-80%, while maintaining the recognition performance. For a high reduction rate, we recommend to apply both CPCA and LDFT in combination. Third, with regard to quantization, this thesis introduced the *Spectral Bits* and *Phase Bits* representations. We recommend the Spectral Bits representation because of its better recognition performance. This method quantizes the spectral minutiae features to a binary string of around 10,000 bits. The Phase Bits representation consists of a shorter binary string, of around 2,000 bits. In case that a shorter binary string is preferred, the Phase Bits method can be the choice. The Spectral Bits and the Phase Bits can also be concatenated in order to achieve a higher recognition performance.

The spectral minutiae representation scheme proposed in this thesis enables the combination of fingerprint recognition systems with template protection based on the helper data scheme. Furthermore, this scheme allows for a fast minutiae comparison, which renders this scheme suitable as a pre-selector for a large-scale fingerprint identification system, thus significantly reducing the time to perform matching. The binary spectral minutiae representation achieved an equal error rate of less than 1% on the FVC2000-DB2 database when applying multi-sample enrolment. The fast comparison speed together with the promising recognition performance makes this spectral minutiae scheme very applicable for real time applications.

# Samenvatting

De term biometrie verwijst naar de technologieën die unieke fysieke (zoals vingerafdrukken, gezicht, iris) of gedragsmatige (zoals de handtekening, stem, lichaamshouding) lichaamskenmerken van personen meten en analyseren met het doel individuen te identificeren of de geclaimde identiteit te verifiëren. Herkenning van individuen door middel van biometrische kenmerken wint aan belang vanwege verschillende redenen: ten eerste kunnen biometrische kenmerken, in tegenstelling tot wachtwoorden, pincodes of pasjes, niet worden vergeten of verloren en zijn ze praktisch in gebruik; ze zijn altijd voorhanden. Een tweede belangrijk voordeel is dat lichaamskenmerken goed gekoppeld zijn aan een individu, dus niet gemakkelijk vervalsbaar of overdraagbaar.

Op dit moment is de vingerafdruk de meest gebruikte biometrische modaliteit. Vergeleken met diverse biometrische technieken, zoals gebaseerd op het gezicht, handtekening en stem, heeft de vingerafdruk de hoogste niveaus van onderscheidend vermogen, duurzaamheid en prestaties. Vingerafdrukherkenningssystemen hebben tegelijkertijd de voordelen van zowel gebruiksvriendelijkheid als lage kosten. Tegenwoordig zijn veel vingerafdrukherkenningssystemen gebaseerd op het vergelijken van minutiae. Minutiae zijn de eindpunten en splitsingen in het lijnenspel van een vingerafdruk. Ze staan bekend om het ongewijzigd blijven tijdens de levensduur van een individu en staan een zeer discriminerende classificatie van vingerafdrukken toe.

Tegenwoordig wordt biometrische technologie in toenemende mate ingezet in civiele en commerciële toepassingen. Door het toenemende gebruik van biometrische gegevens groeit de bezorgdheid over veiligheid van biometrische technologie en aantasting van de individuele privacy. Door het opslaan van biometrische gegevens, die bekend staan als biometrische templates, in een database ontstaat in potentie de mogelijkheid tot koppeling met andere persoonlijke gegevens en zelfs identiteitsfraude. Een oplossing is de toepassing van *biometrische template bescherming* technieken, die beogen het terughalen van biometrische gegevens uit de templates onmogelijk te maken.

De onderzoeksvraag van dit proefschrift is hoe de vingerafdrukherkenningssystemen te combineren met template bescherming. De vingerafdrukherkenningssystemen zijn

gebaseerd op de vergelijking van de minutiae sets, de ongeordende verzameling van minutiae locaties en oriëntaties die onderhevig zijn aan verschillende vervormingen, zoals translatie, rotatie en schaal. Veel templatebeschermingssystemen vereisen echter een geordende kenmerk vector met vaste lengte. De spectral minutiae representation in dit proefschrift is een nieuwe methode die inderdaad de minutiae set representeert als een kenmerk vector met vaste lengte, die invariant is voor translatie en waarbij rotatie en schaal translaties worden, die gemakkelijk kunnen worden gecompenseerd. Deze kenmerken maken het mogelijk vingerafdrukherkenningssystemen te combineren met template bescherming gebaseerd op fuzzy commitment of helper data methoden.

In dit proefschrift worden drie spectral minutiae representation methoden voorgesteld: de *locatie-gebaseerde spectral minutiae representation* (SML), de *oriëntatie-gebaseerde spectral minutiae representation* (SMO) en de *complexe spectral minutiae representation* (SMC). SML encodeert minutiae locatie informatie, terwijl SMO en SMC zowel minutiae locatie als oriëntatie informatie coderen. Uit de experimenten in dit proefschrift blijkt dat SMC de beste resultaten behaalt. Met betrekking tot de equal error rate, heeft SMC een herkenningsprestatie welke 2 tot 4 keer beter is dan SML en SMO.

Gebaseerd op de spectral minutiae kenmerken, presenteert dit proefschrift verder bijdragen in drie onderzoeksrichtingen. In de eerste plaats geeft dit proefschrift verschillende aanbevelingen om de herkenningsprestaties van SMC te verbeteren. Voorbeelden hiervan zijn het gebruiken van minutiae kwaliteitsinformatie en multi-sample fusion. In de tweede plaats, met betrekking tot kenmerk reductie, introduceert dit proefschrift twee kenmerk reductie methoden, *Column-PCA* (CPCA) en *Line-DFT* (LDFT), die de kenmerk dimensionaliteit effectief kan reduceren met 70% -80%, met behoud van de herkenningsprestaties. Voor een grote reductie raden wij aan CPCA en LDFT in combinatie toe te passen. Ten derde, gericht op kwantisatie, introduceert dit proefschrift de *Spectral Bits* en *Phase Bits* representations. Wij bevelen de Spectral Bits representation aan vanwege de betere herkenningsprestatie. Deze methode kwantiseert de spectral minutiae kenmerken tot een binaire string van ongeveer 10,000 bits. De Phase Bits representatie genereert een kortere binaire string van ongeveer 2,000 bits. In het geval een kortere binaire string gewenst is, kan de Phase Bits methode worden gekozen. De Spectral Bits en de Phase Bits methoden kunnen ook aan elkaar gekoppeld worden om een betere herkenningsprestatie te bereiken.

De spectral minutiae representation methode voorgesteld in dit proefschrift maakt het mogelijk vingerafdrukherkenningssystemen te combineren met template beveiliging gebaseerd op helper data. Verder staat deze methode een snelle minutia vergelijking toe, waardoor deze methode geschikt is als voorselectie binnen een groot vingerafdruk identificatiesysteem, waarmee de tijd om een match te vinden sterk wordt gereduceerd. De binaire spectral minutiae representation behaalt een equal error rate van minder dan 1% met de FVC2000-DB2 database in het geval van multi-sample enrolment. De hoge vergelijkingssnelheid tezamen met veelbelovende prestaties maken de spectral minutiae erg geschikt voor real-time toepassingen.

# Acknowledgements

Five years ago, I came to the Netherlands from China to start my Ph.D. research at the chair of Signals and Systems of the University of Twente. The past five years are fruitful and joyful for me. I would like to take this opportunity to thank the people who have supported me during this unforgettable period.

First of all, I would like to express my sincere gratitude to my supervisor, Raymond Veldhuis. I respect him very much for both his strong professional skills and his cheerful attitude to life. I always enjoy discussing with him, not only on our research, but also on all kinds of topics like culture, philosophy, sport, food and tea. Working with him gives me a lot of pleasure.

I am grateful to my promotor, Kees Slump. Professor Kees Slump is an amiable person and an expert in solving misunderstandings. He maintains a perfect working environment for our group.

During my Ph.D. research, I had a very happy cooperation with our project members from Philips and priv-ID. I would like to first thank Tom Kevenaar, who has given me great support for my research work. I still remember his help on my first journal paper. Tom let me know how to write a scientific paper and his sincere attitude on research impressed me deeply. Further, I would also like to thank Ton Akkermans, Aweke Lemma, Michiel van der Veen, Koen de Groot, Ileana Buhan and Emile Kelkboom for all the support and interesting discussions during our cooperation. I would also like to thank our partners of the Turbine project for their great support.

I would like to thank Asker Bazen, who has introduced me to this research area on fingerprints. Asker impressed me very much for his knowledge on fingerprint recognition technologies. He is always open to share his experience and ideas. The discussions with him are cheerful and inspiring.

I would like to thank my colleagues from the Signals and Systems group. My thanks first goes to Anneke and Sandra for their friendship and accurate administration help. Johan, ik vond het heel leuk om het kantoor met je te delen en vaak samen te reizen in de trein. Luuk, je bent mijn beste leraar Nederlands van mijn collega's. Berk, I had

a nice time to share the office and work together on fingerprints with you. Xiaoying, thank you for sharing the experience on thesis and promotion preparation. And of course, I would like to say thanks to all my colleagues for creating such a cheerful (en gezellige) working atmosphere.

My thanks will now go to my family in China. Dad, mom en Lynn, thank you for all your great support in the past five years. Because of the distance between China and the Netherlands, most of the time I could only contact you via telephone. But I know that you are always there, ready for sharing my happiness and sadness. Whenever I have difficulties, you are there to comfort me and encourage me. Xie xie. Wo ai ni men.

Elly en Rijk, bedankt voor uw support en zorg voor de laatste vijf jaar. Jullie geven mij het gevoel dat ik ook in Nederland een hele familie heb. Jullie zijn ook graag bereid om ons gezin hulp te bieden wanneer dat nodig is.

Tenslotte, wil ik Marco, Leon en Rick bedanken. Jullie zijn de belangrijkste mannen in mijn leven. Marco, bedankt voor je ongelooflijke interesse en hulp bij mijn werk en je geduld. Door jou voel ik mij erg thuis in Nederland. Leon en Rick, jullie zien opgroeien geeft mij elke dag heel veel plezier. Ik hou van jullie!


Haiyun
Deventer, August 2010

# Curriculum vitae

Haiyun Xu was born in Shanghai, China on February 12, 1977. She received the B.E. and M.E. degrees in electrical engineering from Beijing University of Technology, China, in 2000 and 2003, respectively. In 2003 she worked at Sony in Beijing on the Chinese input method for Sony PlayStation 2. In 2004 she joined Siemens Ltd. China to work on mobile phone software development for one year.

From 2005, she began to pursue the Ph.D. degree with the Department of Electrical Engineering, University of Twente, the Netherlands. In the summer of 2010, she finished her Ph.D. thesis on the topic of the combination of fingerprint recognition system with template protection scheme. Her research interests include biometrics, template protection, pattern recognition, signal and image processing.